Engineering DNA Hydrogels for Programmable Mechanical Properties

Dissertation

zur Erlangung des Grades

„Doktorin der Naturwissenschaften”

im Promotionsfach Chemie

am Fachbereich Chemie, Pharmazie, Geographie und Geowissenschaften

der Johannes-Gutenberg-Universität Mainz

Cecilia Oluwadunsin Akintayo

geboren in Ado-Ekiti, Nigeria

Mainz, 2026

JOHANNES GUTENBERG UNIVERSITÄT MAINZ

JG|U

1st Reviewer:

2nd Reviewer:

Date of Oral examination:

The work presented in this thesis was carried out at the Institute of Macromolecular Chemistry, Albert-Ludwigs-University Freiburg from September 2019 to December 2020 and continued at Department of Chemistry, Johannes Gutenberg University of Mainz from January 2021 to January 2024 under the supervision of Prof. Dr. Andreas Walther. This period includes a maternity leave from September 2022 to June 2023, as well as a maternity leave after January 2024.

Key findings of this thesis have been published in the following scientific journals:

1. **Akintayo, C. O.**; Creusen, G.; Straub, P.; Walther, A., Tunable and Large-Scale Model Network Starpeg-DNA Hydrogels. *Macromolecules* **2021,** *54* (15), 7125-7133, doi: https://doi.org/10.1021/acs.macromol.1c00600
2. Lallemang, M.[†]; **Akintayo, C. O.**[†]; Wenzel, C.; Chen, W.; Sielaff, L.; Ripp, A.; Jessen, H. J.; Balzer, B. N.; Walther, A.; Hugel, T., Hierarchical Mechanical Transduction of Precision-Engineered DNA Hydrogels with Sacrificial Bonds. *ACS Appl. Mater. Interfaces* **2023,** *15* (51), 59714-59721, doi: https://doi.org/10.1021/acsami.3c15135, [†]These authors contributed equally.

The publications listed above including the supporting information (SI) contain essential parts of this thesis. The contributions of each author are described in detail at the start of each chapter. The manuscripts and SI were modified for clarity and to fit the format of this thesis.

Abstract

Materials found in nature are inherently adaptive, obtaining their mechanical and structural properties from dynamic, reversible molecular interactions. These systems achieve remarkable functional complexity through bottom-up assembly strategies. In contrast, synthetic materials are typically produced via top-down methods and lack the hierarchical, responsive characteristics of biological systems. As a result, they often fail to deliver the dynamic and adaptive functions needed for advanced material applications.

This thesis introduces a modular bottom-up strategy for engineering starPEG-DNA hydrogels, whose mechanical properties are precisely tuned through programmable DNA hybridization. By systematically varying crosslinking density, sequence design, and network topology, I investigate how control over connectivities and defects at the molecular level influences macroscopic mechanics. Following a general introduction, three research projects are presented.

In the first project, I prepared starPEG-DNA hydrogels crosslinked with divalent DNA duplex linkers and examine how the hydrogel mechanical properties are influenced by factors such as linker length, salt concentration, and building block composition. The hydrogels displayed a wide range of mechanical properties and self-healing behavior. The study presents a tunable mechanical phase space and shows the impact of both sequence and network topology on macroscopic behavior.

The second project presents some insights into programmable mechanical nonlinearity properties of the starPEG-DNA hydrogels by embedding sacrificial DNA hairpin motifs into them. The DNA hairpin unzips and function as force-responsive actuators within the hydrogel network. Single-molecule force spectroscopy combined with bulk rheology confirmed the translation of nanoscale mechanical behavior into macroscopic hydrogels with enhanced yield strain and tunable energy dissipation.

In the third project, a light-responsive moiety, DEACM, a coumarin derivative was incorporated into the DNA linker. This enabled spatiotemporal control over hydrogel assembly, disassembly, and mechanical strengthening through light irradiation. The system responds rapidly to light triggers and the changes in mechanical properties were confirmed by rheology and high-performance liquid chromatography (HPLC) analysis.

Kurzzusammenfassung

Biologische Materialen sind von Natur aus adaptiv. Sie gewinnen ihre mechanischen und strukturellen Eigenschaften aus dynamischen, reversiblen molekularen Wechselwirkungen. Solche Systeme erreichen eine bemerkenswerte funktionale Komplexität durch Bottom-up-Strategien. Im Gegensatz dazu werden synthetische Materialien in der Regel durch Top-down-Methoden hergestellt, die nicht über die hierarchische Reaktionsfähigkeit biologischer Systeme verfügen. Daher gelingt es synthetischen Materialien häufig nicht, die dynamischen und adaptiven Funktionen bereitzustellen, die für fortgeschrittene Materialanwendungen erforderlich sind.

Diese Dissertation stellt eine modulare Bottom-up-Strategie zur Entwicklung von starPEG-DNA-Hydrogelen vor, deren mechanische Eigenschaften durch programmierbare DNA-Hybridisierung präzise gesteuert werden. Variationen in der Vernetzungsdichte, im Sequenzdesign und in der Netzwerktopologie werden systematisch eingesetzt, um zu untersuchen, wie molekulare Kontrolle über Konnektivität und Defekte die makroskopische Mechanik beeinflusst. Nach einer allgemeinen Einführung werden drei Forschungsprojekte vorgestellt.

Im ersten Projekt werden starPEG-DNA Hydrogele mit divalenten DNA Duplex Linkern vernetzt, und es wird untersucht, wie Faktoren wie Linkerlänge, Salzkonzentration und Bausteinzusammensetzung die mechanischen Eigenschaften beeinflussen. Die Hydrogele zeigen eine große Bandbreite an mechanischen Eigenschaften sowie selbstheilendes Verhalten. Die Studie demonstriert einen steuerbaren mechanischen Phasenraum und verdeutlicht den Einfluss sowohl der Sequenz als auch der Netzwerktopologie auf das makroskopische Verhalten.

Das zweite Projekt führt eine programmierbare mechanische Nichtlinearität ein, indem opferbare DNA-Haarnadelmotive in die Hydrogele eingebettet werden. Diese Haarnadelstrukturen öffnen sich wie ein Zipper unter mechanischer Belastung und fungieren als kraftsensitive Aktuatoren innerhalb des Netzwerks. Einzelmolekül-Kraftspektroskopie in Kombination mit Bulkrheologie bestätigt die Übertragung nanoskaliger mechanischer Eigenschaften auf makroskopische Hydrogele mit erhöhter Bruchdehnung und steuerbarer Energiedissipation.

Im dritten Projekt wird ein lichtempfindliches Molekül, DEACM, in den DNA-Linker integriert. Dies ermöglicht eine raumzeitliche Kontrolle über die Assemblierung, Disassemblierung und mechanische

Verstärkung der Hydrogele durch Lichtbestrahlung. Das System reagiert schnell auf Lichtreize, und die Veränderungen der mechanischen Eigenschaften werden durch Rheologie und HPLC bestätigt.

Contents

Abbreviations

ACN	Acetonitrile
AGE	Agarose gel electrophoresis
γ	Amplitude
AFM	Atomic force microscopy
ATRP	Atom transfer radical polymerization
k_B	Boltzmann constant
τ	Bond relaxation time
c^*	Overlap concentration (for polymers)
CPG	Controlled pore glass
ΔL_{Cont}	Contour length
DBCO	Dibenzocyclooctyne
DCA	Dichloroacetic acid
DCM	Dichloromethane
DEACM	7-(Diethylamino)-4-(Hydroxymethyl)-Coumarin
DLS	Dynamic light scattering
DMAc	Dimethylacetamide
DMSO	Dimethyl sulfoxide
DNA	Deoxyribonucleic acid
DMT	4,4'-dimethoxytrityl
dsDNA	Double-stranded DNA
Eq.	Equivalent
EO	Ethylene Oxide
ETT	5-(Ethylthio)-1H-tetrazole
f	Frequency (rheology)
f_c	Crosover frequency (rheology)
FRET	Förster resonance energy transfer
G'	Storage modulus
G''	Loss modulus
GPC	Gel-permeation-Chromatography
H.E.L.P.	High Efficiency Liquid Phase
HEPES	4-(2-Hydroxyethyl)-1-piperazineethanesulfonic acid
3-HPA	3-Hydroxypicolinic acid
HPLC	High-performance liquid chromatography
invOLS	Inverse optical lever sensitivity
LPOS	Liquid phase oligonucleotide synthesis
LVE	Linear viscoelastic region
MALDI-ToF	Matrix-Assisted Laser Desorption/Ionization Time-of-Flight
mCPBA	Meta-chloroperoxybenzoic acid
ξ	Mesh size

MFE	Minimum free energy
M_n	Number average molecular weight
M_w	Weight average molecular weight
MWD	Molecular weight distribution
nbs	Nucleobases
NHS	*N*-Hydroxysuccinimide
NMR	Nuclear magnetic resonance spectroscopy
NPs	Nucleoside phosphoramidites
nts	Nucleotides
NB	Nitrobenzyl
ODNs	Oligonucleotides
OP-LPOS	One-pot Liquid-Phase DNA Synthesis
δ	Phase angle
pAAm	Polyacrylamide
PEG	Polyethylene glycol
PLL	Poly(L-lysine)
pNIPAM	Poly(N-isopropylacrylamide)
RAFT	Reversible addition–fragmentation chain-transfer polymerization
ROMP	Ring-opening metathesis polymerization
RT	Room temperature
SEC	Size exclusion Chromatography
SMFS	Single molecule force spectroscopy
SPOS	Solid-phase oligonucleotide synthesis
E	Stiffness
ε	Strain
σ	Stress
T_m	Melting temperature
T_{co}	Crossover temperature
TBPH	Tert-butyl hydroperoxide
TCA	Trichloroacetic acid
TEA	Triethylamine
TEAA	Triethylamine / acetic acid (buffer)
TES	Triethyl silane
TFA	Trifluoroacetic acid
THF	Tetrahydrofuran
UV-VIS	Ultraviolet–visible spectrophotometry
η	Viscosity
WLC	Wormlike Chain
V_e	Elution volume

Dedicated to my family.

1 Introduction

1.1 Engineering materials with life-like properties

Living organisms offer a rich source of inspiration for the design of intelligent materials that can sense, respond, and adapt to external stimuli with high spatiotemporal precision.[1] Octopuses, for example, possess the remarkable ability to dynamically alter the texture and color of their skin for camouflage and communication. Bacteria such as Escherichia coli respond to environmental changes through chemotaxis, moving in response to chemical gradients,[2] while plants like the Venus flytrap exhibit rapid mechanical responses by activating their snap-trap closure when sensory hairs are stimulated. These biological systems have inspired the development of synthetic materials with such advanced functionalities and behavior.[3] By studying how organisms respond to stimuli such as mechanical stress, temperature, pH, light, or enzyme activity, researchers have pioneered the field of smart materials and engineered systems designed to exhibit life-like responsiveness.[4] The ability of these materials to react to external stimuli is fundamentally governed by the intrinsic properties of their molecular and supramolecular structures, enabling controlled and sometimes programmable responses such as a change in shape or mechanical properties.[5] The development of responsive materials represents a significant advancement in materials science and in the design of switchable soft materials, characterized by the integration of stimulus-responsive functionalities that enable autonomous sensing, actuation, and adaptation within engineered systems.[6-7]

Responsive systems are typically in a thermodynamic equilibrium state denoted as state A. Upon application of an external trigger, the system's energy landscape is altered, driving it toward a new thermodynamic equilibrium state B. State B is relatively stable until a counter-trigger is applied and the energy landscape reverts, enabling the system to return to its original equilibrium state A. The alternation between state A and B is highly repeatable and reversible. In contrast to responsive materials, so-called adaptive materials not only respond upon exposure to stimulus but also modulate their response over time, often incorporating feedback mechanisms or exhibiting memory-like behavior. Adaptive systems not only alternate between state A and state B in response to a trigger and counter-trigger, but can also transition to a new thermodynamic state C upon repeated application of the same stimuli or evolve to resist further response to external stimuli by remaining in the initial equilibrium state A (**Figure 1.1.1**).[8]

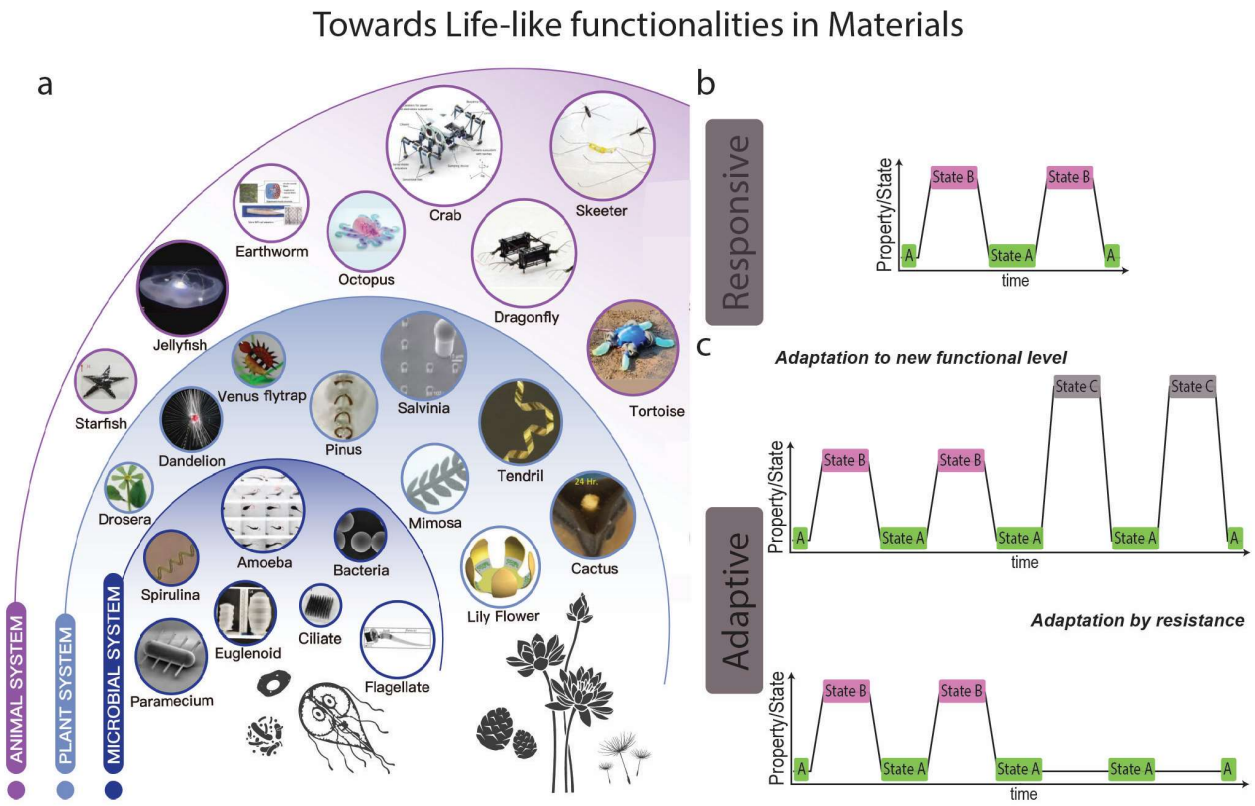

Figure 1.1. (a) Materials inspired by nature. Graphics adapted from Ref. ([3]) **(b)** Responsive **(c)** and adaptive materials. Adapted and modified from Ref. ([8])

Among the various molecular frameworks explored for implementing such life-like functionalities in materials, biomolecules such as Deoxyribonucleic acid, DNA, and peptides/proteins have emerged as highly versatile and programmable building blocks.[9-10]

1.1.1 DNA as a Structural Motif in Smart Materials

In the case of DNA, its structural predictability, programmability and molecular recognition capabilities makes DNA a promising candidate for engineering smart materials. DNA is particularly well-suited for the rational design of stimuli-responsive and information-encoded materials. DNA is a double helical molecule that serves as the carrier and store of genetic information in biological organisms, with its functionality encoded by four nucleobases, nbs, : adenine (A), thymine (T), guanine (G), and cytosine (C). These bases pair selectively through Watson-Crick hydrogen bonding, specifically A always pairs with T and G pairs with C, forming the basis for highly specific and programmable molecular interactions (**Figure 1.2**). While relatively weak hydrogen bonds stabilize individual base pairs, the cumulative effect of multiple complementary base

interactions results in stable DNA duplexes capable of hybridizing at temperatures significantly above ambient conditions.[11-12]

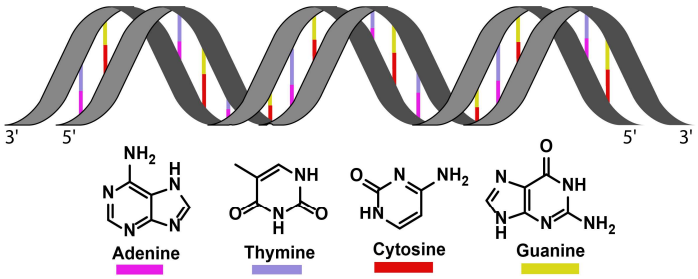

Figure 1.2. Schematic representation of DNA.

DNA has many unique properties that make it exceptionally promising for designing life-like materials. These include its indispensable genetic function, broad biocompatibility, precise molecular recognition capability and programmability.[13] The programmability of DNA refers to the ability to design and engineer DNA molecules with precise sequences and structures to perform specific functions. However, despite its unique features for material design, the widespread use of DNA in constructing all DNA-based materials has been primarily limited by challenges in scalability and cost. Furthermore, the susceptibility of single-stranded DNA to enzymatic degradation (e.g., by DNases) and chemical hydrolysis has further discouraged the use of DNA in material science.[14-16] The development of DNA-polymer conjugates circumvents these limitations and has enabled the fabrication of responsive hybrid materials that leverage the programmability of DNA with the chemical versatility and scalability of synthetic polymers.

1.1.2 Model Network Hydrogels

Hydrogels bridge synthetic materials and life-like systems due to their ability to mimic soft, hydrated, and mechanically dynamic environments like those in biological tissues.[17-20] The term hydrogel is used to define cross-linked water-swelling polymer networks. The properties of a hydrogel are determined by the type of polymer and the type and degree of crosslinks. Structurally, hydrogels are classified into three network types namely - classic, double, and ideal network hydrogels.[21] Classic networks, typically formed via free radical polymerization, are structurally heterogeneous, resulting in variability in tensile strength and higher susceptibility to fracture.[22-23] Double networks combine a highly crosslinked rigid network with a loosely crosslinked elastic one and offers advantages such as exceptional toughness and tear resistance, although it exhibits pronounced hysteresis under cyclic loading.[24-25] Ideal networks or near-ideal networks, in contrast,

feature perfectly uniform crosslinking and chain length, enabling highly resilient and elastic behavior with minimal hysteresis.[26-27]

Ideal networks feature defined polymer chain lengths, a controlled network architecture and are a powerful toolbox in the rational design of stimuli responsive materials. Its precise topology guarantees minimal defects while uniform distance between crosslinks allows easier study of the connectivities on a molecular level. Furthermore a direct correlation can be made between molecular-scale architecture and macroscopic mechanical properties and viscoelastic behaviour.[28-29] Such networks can also reversibly store energy and result in a material with structurally and mechanical tunability and reproducible mechanical properties.[21, 30] Among the various strategies previously employed for the synthesis of ideal polymer networks,[31-33] a significant breakthrough was achieved by Sakai et. al., who successfully developed a uniform and well-defined hydrogel based on tetra-functional polyethylene glycol (PEG) precursors. In their approach, tetra-amine functionalized polyethylene glycol, PEG (A_4) and tetra-N-hydroxysuccinimide, NHS functionalized PEG (B_4) were homogeneously mixed at overlap concentration to yield a precisely crosslinked $A_4 + B_4$ network that is mostly free of loop defects and most inhomogeneities.[34] The structure of these so called Tetra-PEG gels, also commonly referred as star-PEG gels, can be controlled by tuning the molecular weights and concentrations of the star-PEG prepolymers. Star-PEG gels are referred to as near-"ideal" polymer networks with very small fractions of defects. This class of near-ideal polymer network gels have revolutionized the field for their potential applications and feature a (nearly) perfect network structure, uniform crosslinking density and a remarkably high mechanical strength.[35-37]

1.1.3 Hydrogel Network Connectivity and Architecture

Designing hydrogels with precisely defined mechanical properties remains a challenge in materials science research.[38] The relationship between molecular-scale crosslinker design and material performance is highly complex, spanning multiple hierarchical levels. Addressing this challenge requires a focus on hydrogel network architecture, which is primarily governed by crosslinkers. Crosslinkers are molecular entities that establish connectivities between polymer chains, thereby generating a cohesive three-dimensional network structure.[39] Crosslinkers define network connectivity and create a versatile design space where parameters such as composition, molecular weight and dynamic properties can be varied to modulate mechanical properties.[40-43] Approaches such as sequence-defined linkers offer new opportunities for the rational design of hydrogels with programmable, application-specific mechanical properties.[44-46] PEG can for example be end-functionalized with a biologically active sequence, resulting in a partly synthetic and partly biological

system.[47] These systems show how architectural flexibility and chemical modularity can be combined to achieve hydrogels with tunable mechanics, stability, and responsiveness. In such systems, the polymer contributes to a predictable structure and robust mechanics, while the biological element introduces biochemical specificity or hierarchical function. PEG-DNA hybrid network merges the structural versatility and modularity of PEG with the programmability and molecular recognition properties of DNA, creating dynamic and highly tunable hydrogel networks. This class of materials opens new opportunities to precisely engineer network connectivity and mechanical response.

1.1.4 PEG-DNA Hybrid Networks as a Programmable Material Platform for Hydrogel design

Although star-PEG gels have set a new standard for structural uniformity and mechanical robustness among (near) ideal polymer networks, they lack the ability to store biochemical information or respond to molecular cues. DNA-based polymer hybrids address these shortcomings. They integrate the durability, scalability and cost-effectiveness of synthetic polymers with the molecular recognition, information storage, and programmable properties of DNA to create materials with predictable properties.[14] Nagahara and Matsuda laid the foundation in the field of polymer-DNA hybrids and designed thermoresponsive hydrogels constructed via DNA hybridization between oligonucleotide, ODNs, modified with water-soluble copolymers. The authors synthesized copolymers of N,N-dimethylacrylamide and N-acryloyloxysuccinimide, functionalized with amino-terminated ODNs (oligo-T and oligo-A). Hybridization of complementary ODNs on different copolymer chains induced physical crosslinking, resulting in hydrogel formation. The gels exhibit thermal reversibility, swelling at lower temperatures and dissociating at higher temperatures, thereby enabling thermally controlled gel-sol transitions. The system demonstrates the use of nucleic acid hybridization as a molecular switch for creating stimuli-responsive, reversible hydrogel networks.[48] Since then, researchers like Schulman, Tan, Willner and many others have significantly advanced this field, further expanding the possibilities for material applications that require precise, predictable interactions and facilitate complex functions such as targeted cell interactions or controlled release.[49-54] Polymer-DNA hybrids are promising as a tool to bridge the gap between DNA nanotechnology and macro-scale mechanical materials.

Unlike polyacrylamide, pAAm, and poly(N-isopropylacrylamide), pNIPAM, which have traditionally been used in the fabrication of polymer–DNA networks,[55-57] PEG offers several advantages and is a particularly attractive building block for conjugation with DNA due to its biological inertness, flexible polymer backbone, and high hydrophilicity.[58] The Kuzuya group prepared starPEG-DNA hybrids with few oligoG or oligoC at their

termini to form stimuli-responsive hydrogels through non-canonical DNA interactions. The oligoC modified constructs formed pH-reversible hydrogels via i-motif formation, while the oligoG variants exhibited salt-induced gelation through G-quadruplex structures. These systems relied on short ODNs sequences, which, although insufficient for Watson–Crick duplex hybridization under physiological conditions, could still assemble into higher-order DNA architectures in response to environmental triggers. Although these interactions enabled reversible gelation, the short length of the DNA strands inherently limited the ability to leverage DNA's full programmability and molecular recognition potential.[59-61] Towards these hybrid systems, Creusen in our lab introduced scalable starPEG–DNA building blocks that reversibly self-assemble into supramolecular model network hydrogel. The resulting hydrogels exhibit stable mechanical properties at room temperature, with melting transitions around 44 °C, thereby demonstrating the feasibility of using DNA duplexes as dynamic, reversible crosslinks for macroscale material applications.[62]

1.2 Methods for accessing Polymer-DNA Hybrids

Having outlined the advantages of Polymer-DNA hybrids, I now present the synthetic strategies used to construct them. DNA can be conjugated to synthetic polymers with varying degrees of efficiency. These methods include covalently bound systems such as solid-phase synthesis, liquid-phase methods and post-polymerization conjugation methods or non-covalently bound systems such as templating of polymers by DNA**.** Each method enables attachment of ODNs to polymer backbones while maintaining control over sequence orientation and polymer architecture. Overall, the choice of conjugation strategy is guided by factors such as the targeted structure and application, the nature of the polymer and its functional group. In the following sections, I examine these synthetic methods in detail, starting with the chemistry of DNA and DNA–polymer hybrid synthesis. I also discuss their respective advantages and limitations, which have enabled the transition of DNA from a purely biological molecule to a structural and functional component in smart materials.

1.2.1 Solid-Phase Oligonucleotide Synthesis, SPOS

Over the years, numerous strategies have been developed for the chemical synthesis of DNA ODNs.[63] Early techniques include the phosphotriester strategy introduced by Michelson and Todd in 1955[64] and Khorana's phosphodiester approach.[65] The phosphodiester approach involves coupling a 5'-activated phosphoester nucleotide with the 3'-hydroxyl group of another nucleotide, mimicking natural nucleotide biosynthesis. This breakthrough significantly advanced oligonucleotide synthesis and contributed to the foundational

understanding of the genetic code, earning Khorana the Nobel Prize in Physiology or Medicine in 1968. Letsinger[66] and Reese[67] independently built on the groundwork by Khorana and advanced the phosphotriester method for ODNs synthesis. Their key innovation was the use of 2-cyanoethyl and other labile protecting groups on the phosphate moiety, which significantly stabilized reactive intermediates and minimized side reactions such as hydrolysis or cleavage. Despite significant advancements in phosphotriester chemistry, the method has certain limitations. Stepwise coupling efficiencies are below 97%, hindering reliable synthesis of oligonucleotides longer than 20 bases. Additionally, the prolonged reaction times, > 1.5 hours per step, limits its practicality for routine applications. In 1965, Letsinger introduced the use of a styrene-divinylbenzene resin ("popcorn polymer") as a solid support for oligonucleotide synthesis via the phosphotriester approach, laying the groundwork for solid-phase oligonucleotide synthesis, SPOS methods.[68] Since then, SPOS has evolved significantly, with the phosphoramidite method, pioneered by Marvin Caruthers in the early 1980s, emerging as the current gold standard. This technique utilizes a reactive phosphorus–nitrogen bond and a protected 5'-hydroxyl group, enabling high-efficiency, high-fidelity coupling on solid supports.[69] Over time, numerous modifications and optimizations have further enhanced the scalability and reliability of this method, making it the most widely used approach for synthetic DNA production today.[70]

The phosphoramidite method proceeds in the 3'→5' direction on a solid support such as controlled-pore glass, CPG, polystyrene or functionalized PEG. Each nucleotide addition cycle consists of four main steps namely detritylation, coupling, capping, and oxidation and typically takes only a few minutes to complete on an automated synthesizer (**Figure 1.3**). **Detritylation** is the first step and involves the acid-catalyzed removal of the 5' - 4,4-dimethoxytrityl, DMT, protecting group, using trichloroacetic acid, TCA, or dichloroacetic acid, DCA, in an organic chlorinated solvent like dichloromethane, DCM. This exposes the 5'-OH for subsequent coupling. The release of the orange-colored DMT carbocation is monitored spectroscopically to assess efficiency. Although the reaction is reversible, continuous flushing shifts the equilibrium toward complete deprotection. **Coupling** is the next step wherein the exposed 5'-OH reacts with the incoming nucleoside phosphoramidite. The phosphoramidite, which contains a 2-cyanoethyloxy group and a di-isopropylamino phosphate at the 3' position, is activated by tetrazole-based catalysts like 5-(Ethylthio)-1H-tetrazole, ETT. The catalyst protonates the diisopropylamino leaving group, enabling substitution with the tetrazole to form a reactive phosphite triester (P(III)) intermediate. This is followed by the **oxidation** of the unstable phosphite triester to a more robust phosphate triester (P(V)). The oxidation is

performed using iodine in water and pyridine. **Capping** is the final step where any unreacted 5'-OH groups from the previous coupling step is acetylated, preventing the formation of truncated oligonucleotide chains and thus ensuring sequence fidelity. After synthesis, the oligonucleotide is cleaved from the solid support and deprotected under basic conditions, commonly with ammonia, methylamine, or ethylenediamine, EDA, to remove protecting groups from the nucleobases and phosphate backbone.

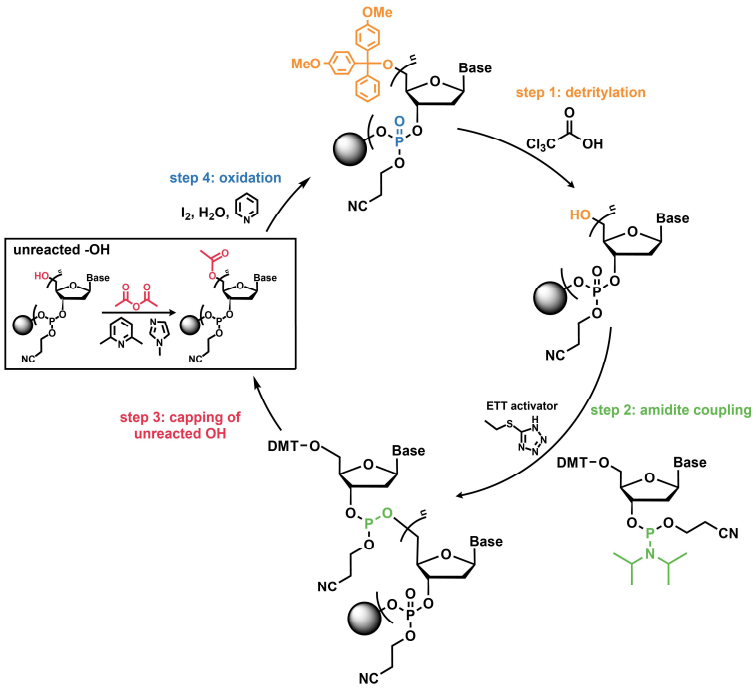

Figure 1.3. SPOS using the phosphoramidite technique. The four steps of the phosphoramidite oligonucleotide synthesis cycle, including the reagents used in all steps.

ODNs are predominantly synthesized today via automated SPOS using phosphoramidite chemistry, which enables high-quality production at gram scales. However, this approach still faces significant scalability challenges due to the high cost of solid supports and the excessive use of hazardous reagents. Furthermore, each cycle generates substantial chemical waste through repetitive protection and deprotection steps. To address these limitations, other strategies like the liquid-phase synthesis approach, which employs soluble polymer supports instead of insoluble resins, have been explored.[71-72] This method combines the scalability of liquid-phase synthesis with the modular control of solid-phase methods, offering a more sustainable and efficient pathway for large-scale oligonucleotide production.

1.2.2 Polymer-DNA Conjugate strategies

There are several strategies to achieve polymer-DNA conjugate synthesis. Although SPOS is a well-established and highly efficient method for producing oligonucleotides, the construction of highly defined polymer-DNA conjugates remains challenging due to factors such as scalability, high cost of modifiers, difficulties in post-synthetic conjugation and limited functional group compatibility. The first reports of DNA-polymer conjugates emerged in the late 1980s, when antisense ODNs were conjugated to a poly(L-lysine), PLL backbone and employed as antiviral agents.[73] These early systems marked the beginning of a rapidly expanding field. Since then, DNA-polymer conjugates have been explored not only for gene regulation and ODN delivery, but also for a wide range of applications, including nucleic acid sensing and bio-targeting.[74-79] There are currently two strategies often employed to generate DNA-polymer hybrid materials. The first involves post-synthetic conjugation, in which pre-synthesized, functionalized DNA strands are covalently linked to polymers using bio-orthogonal coupling chemistries, while the second strategy is in-situ polymerization, which occurs when DNA strands are first modified with polymerization initiators, enabling the growth of polymer chains directly from the DNA backbone. Some of the most common conjugation approaches depicted in **Figure 1.4** include: (i) Amine-NHS ester coupling, which is one of the most straightforward and widely used approaches for DNA-polymer conjugation, due to the availability of amine-functionalized oligonucleotides and commercial activated esters.[80] NHS esters are however hydrolytically labile, particularly at high pH, and reaction efficiency is sensitive to pH due to amine protonation in acidic environments. The Sleiman group presented a block copolymer synthesized via ring-opening metathesis polymerization, ROMP, containing PEG segments and NHS-activated carboxylic acids, which was reacted with amine-modified DNA strands to form stable amide-linked conjugates. These hybrids retained their hybridization functionality and self-assembled into defined polymer domains along DNA nanotubes. The resulting striped nanostructures can be selectively disassembled via strand displacement, demonstrating reversible, programmable polymer patterning on DNA templates.[75] In another example, Stayton et al. successfully conjugated pNIPAM monofunctionalized with an NHS ester to an amine-terminated ODN. Given the thermoresponsive nature of pNIPAM and its tendency to precipitate near its lower critical solution temperature (LCST), the reaction was conducted at 4 °C to maintain polymer solubility and ensure efficient coupling under aqueous conditions.[81] (ii) Another coupling techniques is the azide-alkyne Huisgen [3 + 2] cycloaddition (“click chemistry”). While the classical copper(I)-catalyzed version offers high specificity and tolerance to aqueous conditions, as demonstrated by Matyjaszewski and Das, who successfully conjugated

azide-terminated star polymers to alkyne-ODNs with high efficiency, [82] the field has increasingly shifted toward Strain-Promoted Azide-Alkyne Cycloaddition. By utilizing highly strained cyclooctyne derivatives (such as dibenzocyclooctyne, DBCO), the reaction proceeds spontaneously without the need for a toxic metal catalyst. This eliminates the risk of oxidative damage to the DNA backbone.[83] Azide-alkyne cycloaddition has been instrumental in the synthesis of DNA block copolymers incorporating various polymer segments, such as pNIPAM. The DNA component retained its sequence-specific hybridization capability, allowing the resulting block copolymers to participate in the assembly of nanostructures, including the formation of DNA tetrahedral decorated with pNIPAM side chains.[84] (iii) Thiol-Michael addition reactions, such as thiol-maleimide or thiol-vinyl sulfone coupling, have been employed for the conjugation of ODNs to polymers.[85] In one example, Kataoka and co-workers synthesized a DNA-polymer conjugate via thiol-Michael addition, coupling thiol-modified ODNs to acrylate-terminated PEG in aqueous Tris buffer.[86] Although thiol groups are highly reactive and stable in aqueous solution, they are prone to oxidation to disulfides, especially at low concentrations, complicating reaction control.

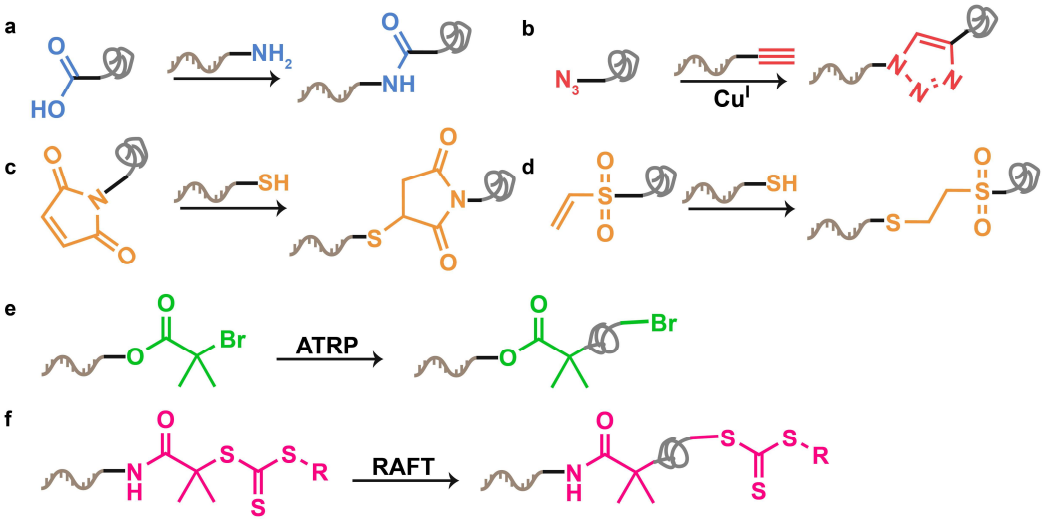

Figure 1.4. Accessing defined DNA–Polymer conjugates via common conjugation chemistries (a) Amine/NHS Ester substitution **(b)** Alkyne/Azide cycloaddition **(c)** Thiol/Maleimide addition **(d)** Thiol/Vinyl sulfone addition **(e)** on-DNA ATRP and **(f)** RAFT polymerization.

An alternative approach that allows more architectural control uses grafting-from techniques, where DNA is pre-functionalized with polymerization initiators, enabling controlled/living radical polymerizations such as atom transfer radical polymerization, ATRP and reversible addition-fragmentation chain-transfer polymerization, RAFT.[87-89] These methods provide precise control over polymer length, composition, and architecture, and allow for the direct synthesis of block copolymers and stimuli-responsive polymers

tethered to DNA. Importantly, initiating polymer growth from DNA simplifies downstream processing by circumventing the need to separate polymer and DNA precursors, a common bottleneck in post-conjugation approaches.

The Bonora group introduced a new approach in 1993 synthesizing DNA directly on polymer backbones. This method, known as High-Efficiency Liquid Phase, H.E.L.P., synthesis[90-91] was initially developed for the synthesis of short ODNs on PEG supports via a cleavable succinic ester linkage. Over time, it has become one of the most efficient strategies for preparing DNA-polymer conjugates. Bonora´s team showed it is possible to obtain oligonucleotides at the hundred-milligram scale, offering a significant advantage over traditional solid-phase synthesis for large-scale applications. Liquid-phase oligonucleotide synthesis, LPOS, provides key benefits, such as reduced waste and scalable reaction conditions owing to the homogeneous reaction environment. Each synthetic cycle—comprising coupling, capping, oxidation, and detritylation—is followed by precipitation of the polymer-bound intermediate, enabling efficient purification and continuation of the synthesis. The H.E.L.P. method merges the efficiency of solid-phase protocols with the scalability and cost-effectiveness of liquid-phase chemistry, making it highly attractive for the large-scale production of DNA-polymer hybrids. Synthesizing PEG-DNA conjugates using LPOS is primarily hindered by its extremely tedious, labor-intensive, multistep process which requires multiple precipitation workups per nucleotide addition cycle.[92] Additionally, the acid-catalyzed detritylation step is slow, partially reversible, and often incomplete in a homogeneous liquid environment. Unlike SPOS where the cleaved DMT group is continuously removed, LPOS involves prolonged acid exposure. This extended exposure increases the risk of backbone cleavage, particularly through depurination of adenine-rich (A) sequences,[93] thereby complicating the efficient synthesis of such oligonucleotides via LPOS.

To address these limitations of LPOS, in 2019 our group pioneered a one-pot liquid-phase synthesis technique, OP-LPOS, which enables scalable synthesis of long ssDNA sequences tethered to 4-arm PEG at multigram scale.[62] Our approach allows nucleotide addition through coupling, oxidation, and deprotection in a single reaction pot, followed by a precipitation step using 2-propanol, which minimizes losses and depurination during adenine addition. Key advantages of the OP-LPOS method include:

1. Integrated One-Pot Synthesis: The OP-LPOS method streamlines the synthetic process by merging the coupling, oxidation, and detritylation steps in a single reaction vessel. This eliminates the need for intermediate isolation, substantially simplifying the workflow and minimizing material loss.

2. Tailored Reagent System: Our approach employs optimized reagents and precisely controlled reaction conditions, including a specialized oxidizing agent and a DMT cation scavenger. This system effectively mitigates undesirable side reactions, such as depurination, thereby enhancing reaction specificity and yield.
3. Precipitation-Based Purification: OP-LPOS incorporates a precipitation-based purification strategy, thereby eliminating the need for extensive purification steps.
4. Enhanced Scalability: The OP-LPOS methodology has demonstrated robust scalability, enabling the efficient production of polymer-DNA conjugates at multigram-scale. This makes it suitable for applications requiring larger quantities of material.
5. Minimised Oligonucleotide Degradation: Another critical advantage of OP-LPOS is its capacity to significantly reduce oligonucleotide degradation. This enables the high-fidelity synthesis of even purine-rich oligonucleotides, which are often challenging to produce with conventional methods.

Overall, this synthesis strategy represents a significant advancement in the scalable and robust fabrication of DNA-based functional materials for applications in biomedicine, soft robotics, and nanotechnology. In the context of this thesis, we specifically leveraged this OP-LPOS strategy to synthesize starPEG-A_{20} and starPEG-T_{20} building blocks. This approach was instrumental in preparing the PEG-DNA conjugate hydrogel systems presented in the following chapters.

1.3 Rheology as a Tool for probing DNA-Polymer Hydrogels

The phrase Panta Rhei, meaning “everything flows”, symbolizes the importance of rheological measurements in modern materials research. Rheology is defined as the study of the viscoelasticity of materials and it aims to describe the temporal relationships between applied forces and the resulting deformation of materials using so-called constitutive equations. It is often one of the few techniques capable of offering detailed information about internal structure and connectivity, especially in soft, viscoelastic systems such as hydrogels. In the context of DNA-polymer hydrogels, rheology is a window into the hierarchical dynamics, bond lifetimes and connectivity of the network. While traditional mechanical models provide a conceptual foundation, the unique programmability of DNA hybridization introduces complex viscoelastic phenomena, such as frequency-dependent stress relaxation and non-linear strain stiffening, which are inaccessible to simple polymer networks.

Rheology, at its core, explores the elastic and viscous responses of materials under deformation, providing insight into the molecular dynamics of polymer chains and their segments. This makes rheological analysis

vital not only for understanding the flow and deformation behavior of polymeric materials but also for optimizing processing conditions and enhancing final mechanical properties. Traditional mechanical models, such as combinations of ideal elastic Hookean springs and the Newtonian dampers, are commonly used to conceptually describe the viscoelastic properties of systems like polymer hydrogels. A spring represents purely elastic behavior, responding instantly to stress with deformation and returning immediately to its original shape upon stress release, equation (1):

$$\sigma = E \cdot \varepsilon \tag{1}$$

where σ is the stress, E is the stiffness and ε is the strain. In contrast, a damper models purely viscous behavior, where strain accumulates over time under stress and only ceases when the stress is removed, equation (2):

$$\sigma(t) = \eta \cdot \frac{\partial \varepsilon}{\partial t} \tag{2}$$

where σ is the stress, η is the viscosity, t is the time and ε is the strain. By combining these elements into mechanical models, the complex responses of viscoelastic materials can be better understood and quantified through simplified mathematical frameworks. This combination has led to two different models, illustrated in **Figure 1.5**. **Figure 1.5a** schematically depicts the Maxwell model, which consists of a spring with the spring constant G connected in series with a damper representing a viscous fluid with viscosity η while the damper and the spring are connected in parallel in the Kelvin-Voigt model shown in **Figure 1.5b**.[94-96]

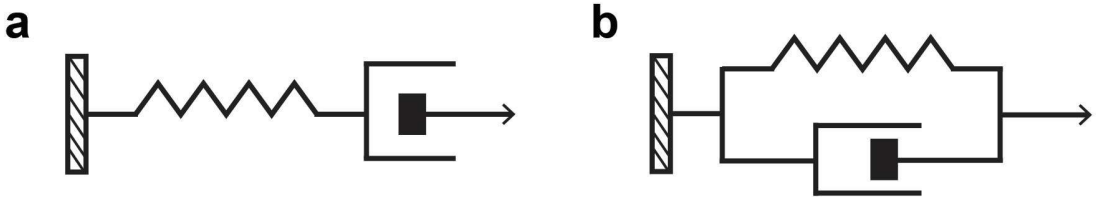

Figure 1.5. Rheological Models (a) Maxwell Model **(b)** Kelvin-Voigt Model.

In viscoelastic materials, the interplay between elastic energy stored and viscous energy dissipated is described by the phase angle, δ, which quantifies the lag between applied stress and resulting strain in oscillatory rheology. In a purely elastic solid, like a Hookean spring, stress and strain are perfectly in phase, giving a phase angle of $\delta = 0°$. In contrast, purely viscous liquids, like Newtonian dampers exhibit a complete

phase lag, where stress peaks at the point of maximum strain rate, corresponding to $\delta = 90°$. Most real-world materials lie between these two extremes, displaying viscoelastic behavior with $0° < \delta < 90°$.[97] Two key parameters in oscillatory rheology, storage moduli G' and loss moduli G'' quantify these elastic and viscous components, respectively. G' measures the in-phase response (elastic), indicating how much mechanical energy is stored and recovered per deformation cycle while G'' measures the out-of-phase response (viscous), representing the energy lost.[95]

The transition point where $G' = G''$ is commonly used to define the gel point which is the onset of percolated network formation in polymer systems, such as DNA-polymer hydrogels. This makes oscillatory rheology an indispensable and non-destructive technique for probing complex, responsive materials like DNA hydrogels. Unlike covalently crosslinked gels, DNA hydrogels are dynamic covalent or associative networks. The frequency at which G'' peaks or G' begins to drop is directly related to the dissociation rate of the DNA duplexes. By varying the DNA sequence length, one can tune the relaxation time of the bulk material across several orders of magnitude. Finally, rheology enables access to nonlinear phenomena such as strain stiffening, stress relaxation, and self-healing and remains a foundational and indispensable method for probing the viscoelastic and structural properties of smart, biomimetic materials.

1.4 Motivation and Outline of the Thesis

Inspired by natural systems where mechanical properties are governed by dynamic and reversible molecular interactions, researchers have long attempted to emulate this level of programmability in synthetic materials. This thesis presents a modular design strategy for engineering hydrogels from starPEG-DNA building blocks. I investigate how parameters such as connecting motifs and defects in the starPEG-DNA hydrogels translate into their macroscopic mechanical properties. DNA offers a powerful molecular building block for mechanical programmability. By exploiting the sequence-specific binding and predictable thermodynamics of DNA duplex formation, I present a strategy to finely tune hydrogel mechanics. Hydrogels assembled from these building blocks exhibit control over network architecture and connectivity. Over the course of this work, the architectural complexity of the hydrogel networks is increased, from starPEG-DNA assemblies connected by a simple DNA-duplex linker, to more complex systems incorporating switch on or off linker interactions. The incorporation of DNA not only introduces molecular recognition and programmability, but also provides a scalable, chemically defined route toward responsive and adaptive hydrogel materials.

Through rational variation of DNA sequence, I investigate how crosslinking topologies influence not only the macroscopic mechanical properties, but also parameters such as strain response and failure behavior of the hydrogels. In **Chapter 2**, I begin by thoroughly investigating hydrogels constructed from starPEG-DNA conjugates crosslinked by programmable, divalent DNA linkers. By varying linker length, salinity, and building block concentration, we access a broad mechanical phase space with G' tunable from ~20 Pa to 3.1 kPa. This modular and scalable approach allows for the formation of robust hydrogels with predictable and programmable properties, including tunable sol-gel transition temperatures and relaxation dynamics. Mechanical properties and relaxation dynamics are shown to depend not only on DNA duplex stability but also on network topology, with surprising nonlinearities observed in sequence-property relationships. These findings provide key design insights for programmable, mechano-responsive starPEG-DNA hydrogels.

In **Chapter 3**, we increase the complexity of these starPEG-DNA hydrogel as a step toward adaptive macromolecular materials by introducing programmable nonlinearity through embedded DNA hairpin motifs. These sacrificial structures, designed to unfold under mechanical stress, serve as molecular actuators that modulate the hydrogel's strain response. Using single-molecule force spectroscopy, SMFS, we first quantify the force-extension behavior of individual DNA hairpins, and then embed them into starPEG-DNA hydrogels to study their impact at both microscopic and macroscopic scales. Our findings demonstrate that the nonlinear mechanical characteristics of these hairpin loops such as stretchability, relaxation time, and energy dissipation are successfully transduced to the bulk material, resulting in hydrogels with increased yield strain and tunable mechanical adaptation. This work highlights the potential of using precision molecular design to engineer smart, strain-responsive hydrogels and lays the foundation for the development of mechano-adaptive soft materials.

Finally **in Chapter 4**, I introduce light-responsive control into the starPEG-DNA hydrogels by incorporating 7-(Diethylamino)-4-(Hydroxymethyl)-Coumarin, DEACM, -caged DNA linkers. This strategy enables hydrogel assembly, disassembly, and mechanical stiffening through light irradiation. Upon DEACM uncaging, DNA hybridization is triggered, allowing for the precise tuning of network connectivity within minutes. Rheological measurements reveal shifts in modulus while HPLC confirms efficient photouncaging kinetics. This light-driven approach offers a simple, biocompatible, and scalable method for engineering responsive DNA-polymer hydrogels, expanding their potential for smart material applications.

1.5 References

(1) Giuseppone, N.; Walther, A., Out‐of‐Equilibrium (Supra) Molecular Systems and Materials: An Introduction. *Out‐of‐Equilibrium (Supra) molecular Systems and Materials* **2021**, 1-19.

(2) Peterson, C. N.; Carabetta, V. J.; Chowdhury, T.; Silhavy, T. J., Lrha Regulates Rpos Translation in Response to the Rcs Phosphorelay System in Escherichia Coli. *Journal of Bacteriology* **2006,** *188*, 3175-3181.

(3) Chen, Z.; Chen, J.; Jung, S.; Kim, H.-Y.; Preti, M. L.; Laschi, C.; Ren, Z.; Sitti, M.; Full, R. J.; Yang, G.-Z., Bioinspired and Biohybrid Soft Robots: Principles and Emerging Technologies. *Matter* **2025,** *8*.

(4) Rivera-Tarazona, L. K.; Campbell, Z. T.; Ware, T. H., Stimuli-Responsive Engineered Living Materials. *Soft Matter* **2021,** *17*, 785-809.

(5) Bril, M.; Fredrich, S.; Kurniawan, N. A., Stimuli-Responsive Materials: A Smart Way to Study Dynamic Cell Responses. *Smart Materials in Medicine* **2022,** *3*, 257-273.

(6) Khizar, S.; Zine, N.; Errachid, A.; Elaissari, A., Introduction to Stimuli-Responsive Materials and Their Biomedical Applications. *Stimuli-Responsive Materials for Biomedical Applications* **2023**, 1-30.

(7) Stuart, M. A. C.; Huck, W. T.; Genzer, J.; Müller, M.; Ober, C.; Stamm, M.; Sukhorukov, G. B.; Szleifer, I.; Tsukruk, V. V.; Urban, M., Emerging Applications of Stimuli-Responsive Polymer Materials. *Nature materials* **2010,** *9*, 101-113.

(8) Walther, A., From Responsive to Adaptive and Interactive Materials and Materials Systems: A Roadmap. *Advanced Materials* **2020,** *32*, 1905111.

(9) Liu, J.; Ding, B., Stimuli-Responsive DNA Nanostructures for Biomedical Applications. *Handbook of Chemical Biology of Nucleic Acids* **2022**, 1-28.

(10) Kushner, A. M.; Guan, Z., Modular Design in Natural and Biomimetic Soft Materials. *Angewandte Chemie International Edition* **2011,** *50*, 9026-9057.

(11) Seeman, N. C.; Sleiman, H. F., DNA Nanotechnology. *Nature Reviews Materials* **2017,** *3*, 1-23.

(12) Aldaye, F. A.; Palmer, A. L.; Sleiman, H. F., Assembling Materials with DNA as the Guide. *Science* **2008,** *321*, 1795-1799.

(13) Roh, Y. H.; Ruiz, R. C.; Peng, S.; Lee, J. B.; Luo, D., Engineering DNA-Based Functional Materials. *Chemical Society Reviews* **2011,** *40*, 5730-5744.

(14) Whitfield, C. J.; Zhang, M.; Winterwerber, P.; Wu, Y.; Ng, D. Y.; Weil, T., Functional DNA–Polymer Conjugates. *Chemical reviews* **2021,** *121*, 11030-11084.

(15) Speed, S. K.; Gupta, K.; Peng, Y. H.; Hsiao, S. K.; Krieg, E., Programmable Polymer Materials Empowered by DNA Nanotechnology. *Journal of Polymer Science* **2023,** *61*, 1713-1729.

(16) Wang, D.; Liu, P.; Luo, D., Putting DNA to Work as Generic Polymeric Materials. *Angewandte Chemie* **2022,** *134*, e202110666.

(17) Zhang, C. W.; Si, M.; Chen, C.; He, P.; Fei, Z.; Xu, N.; He, X., Hierarchical Engineering for Biopolymer‐Based Hydrogels with Tailored Property and Functionality. *Advanced Materials* **2025**, 2414897.

(18) Dutta, A.; Pandit, S.; Panda, P.; Das, R. K., Competitive (Spatiotemporal) Techniques to Fabricate (Ultra) Stiff Polymer Hydrogels and Their Potential Applications. *ACS Applied Polymer Materials* **2025,** *7*, 3466-3497.

(19) Kopecek, J., Hydrogels: From Soft Contact Lenses and Implants to Self‐Assembled Nanomaterials. *Journal of Polymer Science Part A: Polymer Chemistry* **2009,** *47*, 5929-5946.

(20) Zhao, X.; Chen, X.; Yuk, H.; Lin, S.; Liu, X.; Parada, G., Soft Materials by Design: Unconventional Polymer Networks Give Extreme Properties. *Chemical reviews* **2021,** *121* (8), 4309-4372.

(21) Gu, Y.; Zhao, J.; Johnson, J. A., Polymer Networks: From Plastics and Gels to Porous Frameworks. *Angewandte Chemie International Edition* **2020,** *59*, 5022-5049.

(22) Tanaka, Y.; Fukao, K.; Miyamoto, Y., Fracture Energy of Gels. *The European Physical Journal E* **2000,** *3*, 395-401.

(23) Li, X.; Gong, J. P., Design Principles for Strong and Tough Hydrogels. *Nature Reviews Materials* **2024,** *9*, 380-398.

(24) Sun, J.-Y.; Zhao, X.; Illeperuma, W. R.; Chaudhuri, O.; Oh, K. H.; Mooney, D. J.; Vlassak, J. J.; Suo, Z., Highly Stretchable and Tough Hydrogels. *Nature* **2012,** *489*, 133-136.

(25) Gong, J. P.; Katsuyama, Y.; Kurokawa, T.; Osada, Y., Double‐Network Hydrogels with Extremely High Mechanical Strength. *Advanced Materials* **2003,** *15*, 1155-1158.

(26) Kamata, H.; Akagi, Y.; Kayasuga-Kariya, Y.; Chung, U.-i.; Sakai, T., "Nonswellable" Hydrogel without Mechanical Hysteresis. *Science* **2014,** *343*, 873-875.
(27) Parada, G. A.; Zhao, X., Ideal Reversible Polymer Networks. *Soft Matter* **2018,** *14*, 5186-5196.
(28) Shibayama, M.; Li, X.; Sakai, T., Precision Polymer Network Science with Tetra-Peg Gels—a Decade History and Future. *Colloid and Polymer Science* **2019,** *297*, 1-12.
(29) Khare, E.; de Alcântara, A. C.; Lee, N.; Skaf, M. S.; Buehler, M. J., Crosslinker Energy Landscape Effects on Dynamic Mechanical Properties of Ideal Polymer Hydrogels. *Materials Advances* **2024,** *5*, 1991-1997.
(30) Hild, G., Model Networks Based on Endlinking Processes: Synthesis, Structure and Properties. *Progress in Polymer Science* **1998,** *23*, 1019-1149.
(31) Rempp, P.; Herz, J. E., Model Networks—Synthesis and Structure. *Die Angewandte Makromolekulare Chemie: Applied Macromolecular Chemistry and Physics* **1979,** *76*, 373-391.
(32) Mark, J.; Rahalkar, R.; Sullivan, J., Model Networks of End‐Linked Polydimethylsiloxane Chains. Iii. Effect of the Functionality of the Cross‐Links. *The Journal of Chemical Physics* **1979,** *70*, 1794-1797.
(33) Wallace, D.; Cruise, G.; Rhee, W.; Schroeder, J.; Prior, J.; Ju, J.; Maroney, M.; Duronio, J.; Ngo, M.; Estridge, T., A Tissue Sealant Based on Reactive Multifunctional Polyethylene Glycol. *Journal of Biomedical Materials Research* **2001,** *58*, 545-555.
(34) Sakai, T.; Matsunaga, T.; Yamamoto, Y.; Ito, C.; Yoshida, R.; Suzuki, S.; Sasaki, N.; Shibayama, M.; Chung, U.-i., Design and Fabrication of a High-Strength Hydrogel with Ideally Homogeneous Network Structure from Tetrahedron-Like Macromonomers. *Macromolecules* **2008,** *41*, 5379-5384.
(35) Matsunaga, T.; Sakai, T.; Akagi, Y.; Chung, U.-i.; Shibayama, M., Structure Characterization of Tetra-Peg Gel by Small-Angle Neutron Scattering. *Macromolecules* **2009,** *42*, 1344-1351.
(36) Hiroi, T.; Ohl, M.; Sakai, T.; Shibayama, M., Multiscale Dynamics of Inhomogeneity-Free Polymer Gels. *Macromolecules* **2014,** *47*, 763-770.
(37) Shibayama, M., Exploration of Ideal Polymer Networks. *Macromolecular Symposia* **2017,** *372*, 7-13.
(38) Zhang, Y. S.; Khademhosseini, A., Advances in Engineering Hydrogels. *Science* **2017,** *356* (6337), eaaf3627.
(39) Salimi-Kenari, H.; Mollaie, F.; Dashtimoghadam, E.; Imani, M.; Nyström, B., Effects of Chain Length of the Cross-Linking Agent on Rheological and Swelling Characteristics of Dextran Hydrogels. *Carbohydrate polymers* **2018,** *181*, 141-149.
(40) Roca-Arroyo, A. F.; Gutierrez-Rivera, J. A.; Morton, L. D.; Castilla-Casadiego, D. A., Hydrogel Network Architecture Design Space: Impact on Mechanical and Viscoelastic Properties. *Gels* **2025,** *11*, 588.
(41) Previtera, M. L.; Chippada, U.; Schloss, R. S.; Yurke, B.; Langrana, N. A., Mechanical Properties of DNA-Crosslinked Polyacrylamide Hydrogels with Increasing Crosslinker Density. *BioResearch Open Access* **2012,** *1*, 256-259.
(42) Cauich-Rodriguez, J.; Deb, S.; Smith, R., Effect of Cross-Linking Agents on the Dynamic Mechanical Properties of Hydrogel Blends of Poly (Acrylic Acid)-Poly (Vinyl Alcohol-Vinyl Acetate). *Biomaterials* **1996,** *17*, 2259-2264.
(43) Morton, L. D.; Castilla-Casadiego, D. A.; Palmer, A. C.; Rosales, A. M., Crosslinker Structure Modulates Bulk Mechanical Properties and Dictates Hmsc Behavior on Hyaluronic Acid Hydrogels. *Acta Biomaterialia* **2023,** *155*, 258-270.
(44) Peng, Y.-H.; Hsiao, S.-K.; Gupta, K.; Ruland, A.; Auernhammer, G. K.; Maitz, M. F.; Boye, S.; Lattner, J.; Gerri, C.; Honigmann, A., Dynamic Matrices with DNA-Encoded Viscoelasticity for Cell and Organoid Culture. *Nature nanotechnology* **2023,** *18*, 1463-1473.
(45) Soliman, B. G.; Nguyen, A. K.; Gooding, J. J.; Kilian, K. A., Advancing Synthetic Hydrogels through Nature‐Inspired Materials Chemistry. *Advanced Materials* **2024,** *36*, 2404235.
(46) Lin, D. C.; Yurke, B.; Langrana, N. A., Mechanical Properties of a Reversible, DNA-Crosslinked Polyacrylamide Hydrogel. *Journal of Biomechanical Engineering* **2004,** *126* (1), 104-110.
(47) Morton, L. D.; Hillsley, A.; Austin, M. J.; Rosales, A. M., Tuning Hydrogel Properties with Sequence-Defined, Non-Natural Peptoid Crosslinkers. *Journal of materials chemistry B* **2020,** *8*, 6925-6933.
(48) Nagahara, S.; Matsuda, T., Hydrogel Formation Via Hybridization of Oligonucleotides Derivatized in Water-Soluble Vinyl Polymers. *Polymer Gels and Networks* **1996,** *4*, 111-127.

(49) Dorsey, P. J.; Rubanov, M.; Wang, W.; Schulman, R., Digital Maskless Photolithographic Patterning of DNA-Functionalized Poly (Ethylene Glycol) Diacrylate Hydrogels with Visible Light Enabling Photodirected Release of Oligonucleotides. *ACS Macro Letters* **2019,** *8*, 1133-1140.
(50) Cangialosi, A.; Yoon, C.; Liu, J.; Huang, Q.; Guo, J.; Nguyen, T. D.; Gracias, D. H.; Schulman, R., DNA Sequence–Directed Shape Change of Photopatterned Hydrogels Via High-Degree Swelling. *Science* **2017,** *357*, 1126-1130.
(51) Peng, L.; Wu, C. S.; You, M.; Han, D.; Chen, Y.; Fu, T.; Ye, M.; Tan, W., Engineering and Applications of DNA-Grafted Polymer Materials. *Chemical science* **2013,** *4*, 1928-1938.
(52) Huang, F.; Chen, M.; Zhou, Z.; Duan, R.; Xia, F.; Willner, I., Spatiotemporal Patterning of Photoresponsive DNA-Based Hydrogels to Tune Local Cell Responses. *Nature communications* **2021,** *12*, 2364.
(53) Kahn, J. S.; Hu, Y.; Willner, I., Stimuli-Responsive DNA-Based Hydrogels: From Basic Principles to Applications. *Accounts of chemical research* **2017,** *50*, 680-690.
(54) Wu, J.; Liyarita, B. R.; Zhu, H.; Liu, M.; Hu, X.; Shao, F., Self-Assembly of Dendritic DNA into a Hydrogel: Application in Three-Dimensional Cell Culture. *ACS applied materials & interfaces* **2021,** *13*, 49705-49712.
(55) Alemdaroglu, F. E.; Herrmann, A., DNA Meets Synthetic Polymers—Highly Versatile Hybrid Materials. *Organic & Biomolecular Chemistry* **2007,** *5*, 1311-1320.
(56) Li, F.; Tang, J.; Geng, J.; Luo, D.; Yang, D., Polymeric DNA Hydrogel: Design, Synthesis and Applications. *Progress in Polymer Science* **2019,** *98*, 101163.
(57) Xiong, X.; Wu, C.; Zhou, C.; Zhu, G.; Chen, Z.; Tan, W., Responsive DNA-Based Hydrogels and Their Applications. *Macromolecular Rapid Communications* **2013,** *34*, 1271-1283.
(58) Heyes, C. D.; Groll, J.; Möller, M.; Nienhaus, G. U., Synthesis, Patterning and Applications of Star-Shaped Poly (Ethylene Glycol) Biofunctionalized Surfaces. *Molecular BioSystems* **2007,** *3*, 419-430.
(59) Tanaka, S.; Wakabayashi, K.; Fukushima, K.; Yukami, S.; Maezawa, R.; Takeda, Y.; Tatsumi, K.; Ohya, Y.; Kuzuya, A., Intelligent, Biodegradable, and Self‐Healing Hydrogels Utilizing DNA Quadruplexes. *Chemistry–An Asian Journal* **2017,** *12*, 2388-2392.
(60) Tanaka, S.; Yukami, S.; Fukushima, K.; Wakabayashi, K.; Ohya, Y.; Kuzuya, A., Bulk Ph-Responsive DNA Quadruplex Hydrogels Prepared by Liquid-Phase, Large-Scale DNA Synthesis. *ACS Macro Letters* **2018,** *7*, 295-299.
(61) Kuzuya, A., Hydrogels Utilizing G-Quadruplexes. *MOJ Polymer Science* **2017,** *1*.
(62) Creusen, G.; Akintayo, C. O.; Schumann, K.; Walther, A., Scalable One-Pot-Liquid-Phase Oligonucleotide Synthesis for Model Network Hydrogels. *Journal of the American Chemical Society* **2020,** *142*, 16610-16621.
(63) Mohammed, A. A.; AlShaer, D.; Al Musaimi, O., Oligonucleotides: Evolution and Innovation. *Medicinal Chemistry Research* **2024**, 1-17.
(64) Michelson, A.; Todd, A. R., Nucleotides Part Xxxii. Synthesis of a Dithymidine Dinucleotide Containing a 3′ : 5′ -Internucleotidic Linkage. *Journal of the Chemical Society (Resumed)* **1955**, 2632-2638.
(65) Schaller, H.; Weimann, G.; Lerch, B.; Khorana, H., Studies on Polynucleotides. Xxiv. 1 the Stepwise Synthesis of Specific Deoxyribopolynucleotides (4). 2 Protected Derivatives of Deoxyribonucleosides and New Syntheses of Deoxyribonucleoside-3 ″ Phosphates 3. *Journal of the American Chemical Society* **1963,** *85*, 3821-3827.
(66) Letsinger, R. L.; Ogilvie, K. K., Nucleotide Chemistry. Xiii. Synthesis of Oligothymidylates Via Phosphotriester Intermediates. *Journal of the American Chemical Society* **1969,** *91*, 3350-3355.
(67) Reese, C. B., The Chemical Synthesis of Oligo-and Poly-Nucleotides by the Phosphotriester Approach. *Tetrahedron* **1978,** *34*, 3143-3179.
(68) Letsinger, R. L.; Mahadevan, V., Oligonucleotide Synthesis on a Polymer Support. *Journal of the American Chemical Society* **1965,** *87*, 3526-3527.
(69) Beaucage, S.; Caruthers, M. H., Deoxynucleoside Phosphoramidites—a New Class of Key Intermediates for Deoxypolynucleotide Synthesis. *Tetrahedron letters* **1981,** *22*, 1859-1862.
(70) Caruthers, M. H., The Chemical Synthesis of DNA/Rna: Our Gift to Science. *Journal of biological chemistry* **2013,** *288*, 1420-1427.
(71) Virta, P., From Liquid-Phase Synthesis to Chemical Ligation: Preparation of Oligonucleotides and Their Backbone Analogs in Solution. *Nucleic Acids Research* **2025,** *53*, gkaf1084.
(72) Brzezinska, J.; Trzciński, S.; Strzelec, J.; Chmielewski, M. K., From Cpg to Hybrid Support: Review on the Approaches in Nucleic Acids Synthesis in Various Media. *Bioorganic Chemistry* **2023,** *140*, 106806.

(73) Lemaitre, M.; Bayard, B.; Lebleu, B., Specific Antiviral Activity of a Poly (L-Lysine)-Conjugated Oligodeoxyribonucleotide Sequence Complementary to Vesicular Stomatitis Virus N Protein Mrna Initiation Site. *Proceedings of the National Academy of Sciences* **1987,** *84* (3), 648-652.
(74) Das, R. K.; Gocheva, V.; Hammink, R.; Zouani, O. F.; Rowan, A. E., Stress-Stiffening-Mediated Stem-Cell Commitment Switch in Soft Responsive Hydrogels. *Nature materials* **2016,** *15*, 318-325.
(75) Carneiro, K. M.; Hamblin, G. D.; Hänni, K. D.; Fakhoury, J.; Nayak, M. K.; Rizis, G.; McLaughlin, C. K.; Bazzi, H. S.; Sleiman, H. F., Stimuli-Responsive Organization of Block Copolymers on DNA Nanotubes. *Chemical science* **2012,** *3*, 1980-1986.
(76) Zimmermann, J.; Kwak, M.; Musser, A. J.; Herrmann, A., Amphiphilic DNA Block Copolymers: Nucleic Acid-Polymer Hybrid Materials for Diagnostics and Biomedicine. *Bioconjugation protocols: strategies and methods* **2011**, 239-266.
(77) Alemdaroglu, F. E.; Alemdaroglu, N. C.; Langguth, P.; Herrmann, A., DNA Block Copolymer Micelles–a Combinatorial Tool for Cancer Nanotechnology. *Advanced Materials* **2008,** *20*, 899-902.
(78) Gerrits, L.; Hammink, R.; Kouwer, P. H., Semiflexible Polymer Scaffolds: An Overview of Conjugation Strategies. *Polymer Chemistry* **2021,** *12*, 1362-1392.
(79) Vieira, S.; Silva‐Correia, J.; Reis, R. L.; Oliveira, J. M., Engineering Hydrogels for Modulation of Material‐Cell Interactions. *Macromolecular Bioscience* **2022,** *22*, 2200091.
(80) Liu, K.; Zheng, L.; Liu, Q.; de Vries, J. W.; Gerasimov, J. Y.; Herrmann, A., Nucleic Acid Chemistry in the Organic Phase: From Functionalized Oligonucleotides to DNA Side Chain Polymers. *Journal of the American Chemical Society* **2014,** *136*, 14255-14262.
(81) Fong, R. B.; Ding, Z.; Long, C. J.; Hoffman, A. S.; Stayton, P. S., Thermoprecipitation of Streptavidin Via Oligonucleotide-Mediated Self-Assembly with Poly (N-Isopropylacrylamide). *Bioconjugate chemistry* **1999,** *10*, 720-725.
(82) Averick, S.; Paredes, E.; Li, W.; Matyjaszewski, K.; Das, S. R., Direct DNA Conjugation to Star Polymers for Controlled Reversible Assemblies. *Bioconjugate chemistry* **2011,** *22*, 2030-2037.
(83) Agard, N. J.; Prescher, J. A.; Bertozzi, C. R., A Strain-Promoted [3+ 2] Azide− Alkyne Cycloaddition for Covalent Modification of Biomolecules in Living Systems. *Journal of the American Chemical Society* **2004,** *126*, 15046-15047.
(84) Wilks, T. R.; Bath, J.; de Vries, J. W.; Raymond, J. E.; Herrmann, A.; Turberfield, A. J.; O'Reilly, R. K., "Giant Surfactants" Created by the Fast and Efficient Functionalization of a DNA Tetrahedron with a Temperature-Responsive Polymer. *ACS Nano* **2013,** *7*, 8561-8572.
(85) Chrisnandy, A.; Blondel, D.; Rezakhani, S.; Broguiere, N.; Lutolf, M. P., Synthetic Dynamic Hydrogels Promote Degradation-Independent in Vitro Organogenesis. *Nature materials* **2022,** *21*, 479-487.
(86) Oishi, M.; Sasaki, S.; Nagasaki, Y.; Kataoka, K., Ph-Responsive Oligodeoxynucleotide (Odn)− Poly (Ethylene Glycol) Conjugate through Acid-Labile B-Thiopropionate Linkage: Preparation and Polyion Complex Micelle Formation. *Biomacromolecules* **2003,** *4*, 1426-1432.
(87) Lueckerath, T.; Strauch, T.; Koynov, K.; Barner-Kowollik, C.; Ng, D. Y.; Weil, T., DNA–Polymer Conjugates by Photoinduced Raft Polymerization. *Biomacromolecules* **2018,** *20*, 212-221.
(88) Lückerath, T.; Koynov, K.; Loescher, S.; Whitfield, C. J.; Nuhn, L.; Walther, A.; Barner‐Kowollik, C.; Ng, D. Y.; Weil, T., DNA‐Polymer Nanostructures by Raft Polymerization and Polymerization‐Induced Self‐Assembly. *Angewandte Chemie International Edition* **2020,** *59*, 15474-15479.
(89) Miura, Y., Glycopolymer Conjugates: Preparation and Functions. *Comprehensive Glycoscience* **2021**, 250-262.
(90) Bonora, G. M.; Biancotto, G.; Maffini, M.; Scremin, C. L., Large Scale, Liquid Phase Synthesis of Oligonucleotides by the Phosphoramidite Approach. *Nucleic Acids Research* **1993,** *21*, 1213-1217.
(91) Bonora, G.; Zaramella, S.; Veronese, F., Synthesis by High-Efficiency Liquid-Phase (Help) Method of Oligonucleotides Conjugated with High-Molecular Weight Polyethylene Glycols (Pegs). *Biological procedures online* **1998,** *1*, 59-69.
(92) Molina, A. G.; Sanghvi, Y. S., Liquid‐Phase Oligonucleotide Synthesis: Past, Present, and Future Predictions. *Current protocols in nucleic acid chemistry* **2019,** *77*, e82.
(93) Septak, M., Kinetic Studies on Depurination and Detritylation of Cpg-Bound Intermediates During Oligonucleotide Synthesis. *Nucleic Acids Research* **1996,** *24*, 3053-3058.

(94) Rudolph, N.; Osswald, T. A., Polymer Rheology: Fundamentals and Applications. **2014**.
(95) Ramli, H.; Zainal, N. F. A.; Hess, M.; Chan, C. H., Basic Principle and Good Practices of Rheology for Polymers for Teachers and Beginners. *Chemistry Teacher International* **2022,** *4*, 307-326.
(96) Goodwin, J. W.; Hughes, R. W., Rheology for Chemists: An Introduction. **2008**.
(97) Roberto, C.; Véronique, T., Introduction to Viscoelasticity and Plasticity, and Their Relation to the Underlying Microscopic Dynamics in Soft Matter Systems. *Physica A: Statistical Mechanics and its Applications* **2023,** *631*, 128653.

2 Tunable and Large-Scale Model Network StarPEG-DNA Hydrogels

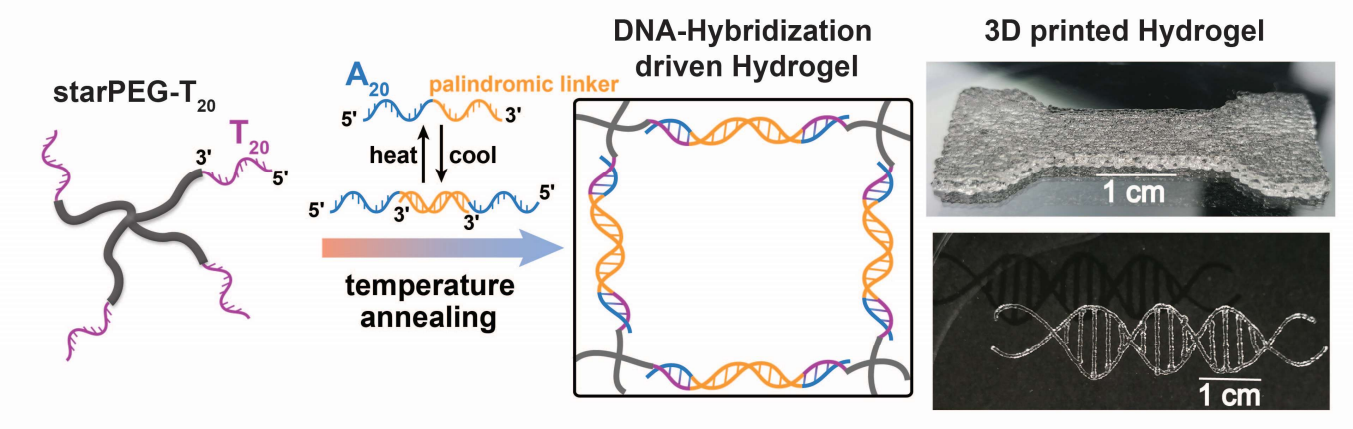

Figure 2.1. Table of contents graphic.

Preliminary note: This chapter is based on the journal article "Tunable and Large-Scale Model Network StarPEG-DNA Hydrogels. *Macromolecules*, **2021**, *54* (15), 7125-7133. DOI: 10.1021/acs.macromol.1c00600" by **Cecilia Oluwadunsin Akintayo (COA)**, Guido Creusen (GC), Paula Straub (PS), and Andreas Walther (AW)*. Minor changes in the text and formatting style have been made.

*Corresponding author

Author´s contribution: COA, GC and AW conceptualized the project. **COA** designed and performed the experiments and analyzed the data. GC and AW supervised the project. PS conducted polarized optical microscopy experiments.

COA wrote the manuscript, which was improved by GC and finalized by AW.

2.1 Abstract

The use of DNA as building block in synthetic polymer hydrogels promises high levels of programmability regarding sol/gel temperatures, tunable bond lifetimes, biocompatibility and interaction with biological components (e.g. enzymes, cells, growth factors). However, scalability and quantitative structure-property relationships for large scale materials are still challenging to achieve. Building on our recently introduced and scalable one pot liquid phase oligonucleotide synthesis of DNA onto star-shaped poly(ethylene glycol) (starPEG), we here report hydrogels based on starPEG-DNA conjugates together with divalent DNA linkers of tunable duplex hybridization length. By systematically varying parameters such as the duplex melting temperature, salinity and building block concentrations, we establish the mechanical phase space of such hydrogels. We elucidate tunable mechanical properties ranging from a few Pa to the kPa regime, discuss time-scales of self-healing and bond exchange, as well as tunable sol/gel transition temperatures. These comprehensive investigations shed some light on the future design principles for DNA hydrogel materials based on scalable building blocks and allowing for the formation of quasi-ideal networks due to their star-shaped and flexible building block topologies. Such materials can be useful in the field of biomedicine and cell culture.

2.2 Introduction

Hydrogels are water-swollen networks of cross-linked polymers. These soft materials are important model systems for fundamental soft matter research and are employed in diverse applications such as drug delivery, cell culture, tissue engineering and soft robotics.[1-4] Traditionally hydrogels have been constructed by chemically crosslinked polymers, which only offer a limited response regarding for instance full sol/gel transitions. In contrast, hydrogels formed by physically crosslinked polymers or by self-assembly of small molecules (supramolecular gels) can exhibit a more dynamic nature.[5-9] In recent years, peptide and DNA-based hydrogels have gained more attention as they offer high levels of programmability.[10-13] DNA motifs are especially attractive for constructing hydrogels with programmable properties because of the flexibility of DNA hybridization, the high predictability of bond formation, manipulation by enzymes and chemical signals, the possibility to build up complex architectures, and because of the possibility to interface them with reaction cascades and chemical reaction networks.[14-24] Reversible shape memory materials, force-programmable mechanosensing hydrogels, programmable soft robotics and transient hydrogels may serve as some examples.[25-32] Despite their unique features for materials design, limitations in the functionalization

of all-DNA hydrogel materials and the often inherent scalability limitations prevent extensive and broader application of DNA hydrogel materials.

Hydrogels can be classified according to their topology into random and model networks. Model networks are based on defined building blocks (e.g. 4-arm star polymers[33]) and can be highly regular, rather free of network defects and entanglements, and feature defined connectivity and mesh size, as for instance important for cell culture.[7, 33-35] The precise topology leads to a simultaneous rather than consecutive chain stretching, allowing for a high resilience.[36-38] Model networks cross-linked by DNA motifs may offer an interesting perspective for fundamental understanding and for applications due to their programmable bond strength and directionality. One common approach towards traditional DNA hydrogels is to use methacrylamide-functionalized ssDNA and subsequent radical co-polymerization (e.g. with acrylamide) followed by hybridization of incorporated DNA motifs.[15, 27, 39] This approach cannot lead to defined model networks, but it is material-efficient as the DNA is only present as functional linker. More defined network topologies can be achieved by using all-DNA nanostars, which assemble during cooling from mixture of single-stranded DNAs (ssDNAs).[28, 40-42] Although defined star-shaped building blocks crucial for model networks are obtained as intermediates, their stiff, shape-persistent nature can lead to topological frustration and the approach is not material-efficient due to scalability restrictions in an all-DNA network. Recently, Kuzuya *et al.* developed salt- and pH-responsive hydrogels based on starPEG functionalized with short ssDNA oligonucleotides of four dG-bases (PEG = polyethylene glycol). Hydrogel formation was obtained for instance by G-quadruplex formation. Although this non-canonical DNA binding by G-quadruplex formation can occur already for very short sequences, it does not offer the same programmability and features as canonical DNA binding based on programmable hybridization.[43]

In our recent work, we reported a simplified synthetic strategy (One-Pot – Liquid-Phase Oligonucleotide Synthesis (OP-LPOS)) towards different starPEG-DNA building blocks with long oligonucleotide homo-repeats on multi-gram scale.[44] This opens perspectives to use both the programmable nature of the DNA linkages and the flexibility of the starPEG core to construct new types of programmable hydrogels based on scalable building blocks. Herein, we report the mechanical properties of model starPEG-DNA network hydrogels based on starPEG-DNA building blocks carrying oligo-T sequences of varying length and hybridized with oligo-A linkers as connecting motifs. We investigate in detail how the linker binding strength, duplex length, salinity, temperature and concentration control the mechanical properties. We believe that these

detailed investigations on the mechanical space will lay important groundwork to push such polymer/DNA conjugate materials further into application, as e.g. programmable extracellular matrix for cell culture.

2.3 Results and Discussion

Scheme 2.1 describes the concept behind the starPEG-DNA hydrogels. The building blocks for the construction of the hydrogels are: (1) starPEG-DNA conjugates based on a 4-arm starPEG core with a total molecular weight of 41000 g·mol^{-1} (arm length = 233 Ethylene Oxide, EO units) containing a (T = thymine, T_{20} or T_{10}) single-stranded DNA (ssDNA) sequence as terminal block. Details of the synthesis and characterization can be found in our previous publication.[44] (2) Bivalent DNA linkers with single-stranded oligo-A overhangs of different length (A = adenine, A_5, A_{10}, A_{15}, A_{20}) to hybridize with the starPEG-T_x components and to provide a varying strength of interaction. Besides the defined oligo-A overhang, the bivalent linker contains a self-complementary (palindromic) segment for the formation of the double-stranded DNA (dsDNA) segment (L/L*) to furnish the bivalent linker A_x-L/L*-A_x. The bivalent linkers are synthesized via automated solid-phase oligonucleotide synthesis. We employ rheology to characterize the mechanical properties of the hydrogels formed by hybridization of both components. Strictly speaking quasi-ideal model networks are formed, as compared to fully ideal model networks formed by mixing two starPEGs with A_x and T_x terminal blocks.[7, 33] The linear viscoelastic regime of the hydrogel is investigated with an oscillatory temperature sweep and a frequency sweep. The dynamics of the DNA bonds and lifetimes of the crosslinks are derived during oscillatory frequency sweeps, and the nonlinear viscoelastic behavior of the hydrogel is examined via amplitude sweeps.

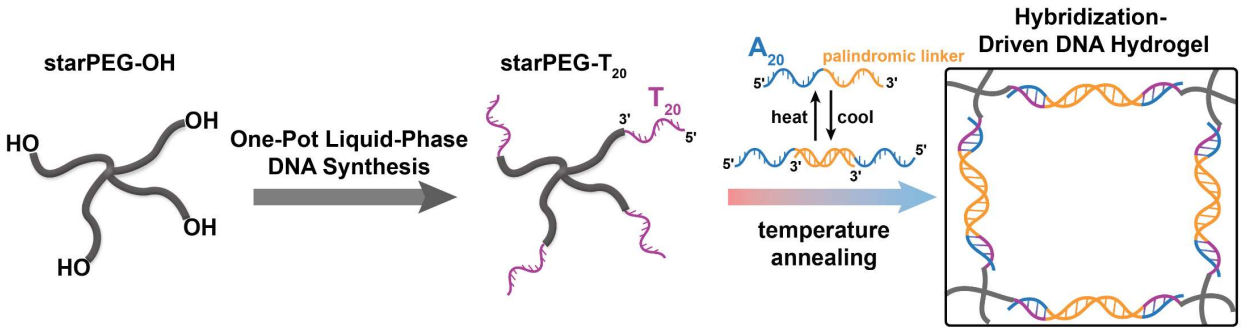

Scheme 2.1. Schematic Overview of the starPEG-DNA hydrogel formation. The first building block starPEG-T_{20} is synthesized in a one-pot liquid phase DNA Synthesis (OP-LPOS) as we previously reported.[44] This is followed by synthesis of the second linker building block via automated solid phase oligonucleotide synthesis. The starPEG-DNA hydrogel formation is triggered by duplex hybridization of the T_{20} and A_{20} overhangs in the two building blocks.

2.3.1 Design and synthesis of the self-complementary linker

The self-complimentary linker was designed to feature a higher melting point, T_m, in the inner palindromic area as compared to the A_{20}/T_{20} duplex to ensure formation of the linker at higher temperatures in annealing ramps. This is enabled by using a GC-rich ssDNA part with a palindromic L/L* sequence "GCAGCTGCAGCTGC" (**Table 2.1** and SI **Table 2.2**). Nupack simulations[45] of the melting curves based on 150 mM NaCl + variable $MgCl_2$ salt concentrations yield a T_m of 58 °C for the A_{20}/T_{20} pairing without $MgCl_2$ and a T_m of 67 °C with 50 mM $MgCl_2$. The L/L* linker already has a T_m of 77 °C in absence of $MgCl_2$ and a binding property of over 90% at 50 °C (**Figure 2.2b**).

Table 2.1. Melting temperatures of the A/T duplexes used in this work

Nucleobase pair	T_m (°C)[a]	
	0 mM $MgCl_2$	50 mM $MgCl_2$
A_5/T_5	5.7	22.8
A_{10}/T_{10}	41.6	53.2
A_{15}/T_{15}	52.7	62.1
A_{20}/T_{20}	58.3	66.7
L/L*	77.4	80.6

[a] The melting points are determined with the Oligo Analyzer tool from Integrated DNA technologies (IDT).[46] 1 mM DNA, 150 mM NaCl, variable $MgCl_2$ concentration.

The all-DNA linker was synthesized via automated solid phase oligonucleotide synthesis. **Figure 2.2** summarizes the characterization of the linker strands after HPLC purification. As expected for longer DNA strands, a shift to later elution times with increasing length of the ssDNA oligo-A extension is observed (**Figure 2.2d**). Similarly, Agarose Gel Electrophoresis (AGE) displays a single band for each linker complex, featuring a decrease in the band migration distance as the oligo-A segment increases in length (**Figure 2.2c**). The single bands indicate that all the strands self-assemble to form the linker with a dsDNA middle segment and ssDNA A-overhangs. The molecular weights of the synthesized linkers were determined via Matrix-Assisted Laser-Desorption-Ionization Time-of-Flight mass spectrometry (MALDI-TOF) and closely match the theoretical molecular weights of the strands (**SI Figure 2.8, Table 2.2**). HPLC, AGE, and MALDI-TOF results thus confirm that the synthesized DNA linkers are present in high purity and suitable for the build-up of defined hydrogels.

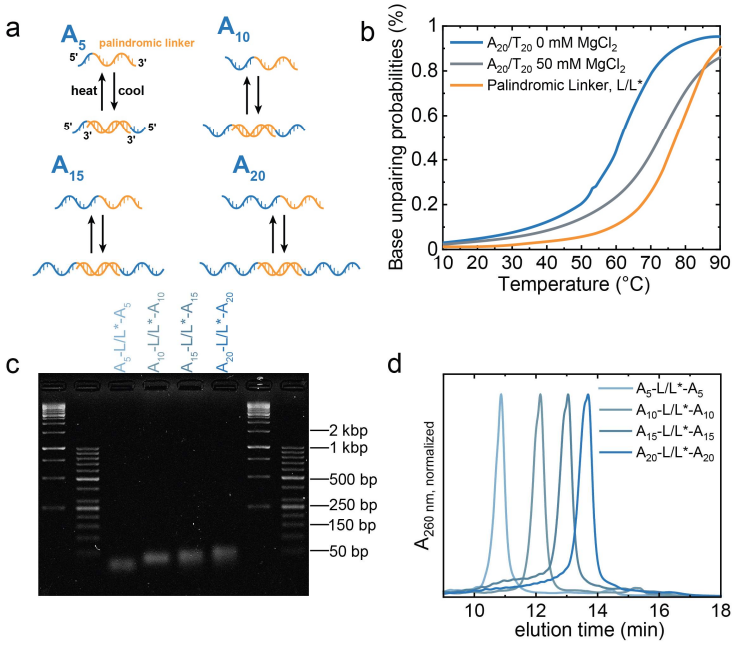

Figure 2.2. Design and analysis of the self-complementary DNA linker. (a) Schematic representation of the self-complementary DNA linker with 5 to 20 oligo-A extensions. **(b)** Melting curves of oligo-T_{20}/A_{20} and palindromic DNA linker strand L/L* at 150 mM NaCl + variable $MgCl_2$ salt concentrations simulated with the NUPACK software package.[45] **(c)** Agarose gel electrophoresis (AGE) of the purified DNA linkers with 50 bp and 1 kbp DNA ladders on both sides. The loaded 2 wt% agarose gel was stained with Roti-Gelstain and separated at 80 V for 75 minutes. **(d)** Analytical HPLC chromatograms of the purified DNA linker strands after deprotection and preparative HPLC purification.

2.3.2 Hydrogel formation and influence of salinity on mechanical properties

All hydrogels were prepared by mixing the starPEG-T_x and the respective linkers at stoichiometric ratios regarding the binding DNA segments in the presence of various salt concentrations, followed by an annealing ramp from 60 °C to 20 °C for hydrogels at 0 mM Mg^{2+} and a ramp from 70 °C to 20 °C for hydrogels containing Mg^{2+}. In order to facilitate an ideal network topology and to understand the presence of entanglements during hydrogel assembly, we first determined the overlap concentration *c** of the starPEG-OH and starPEG-T_{20} by concentration-dependent viscosity measurements[47-48] to ca. 3 wt% and ca. 2.7 wt%, respectively (**SI Figure 2.9**). The overlap concentration of the starPEG-T_{20} building block is slightly lower due to the extension with the T_{20} segments.

Salinity is next to the binder overlap length (T_x/A_x) an important parameter for the mechanical properties of DNA hydrogels. Monovalent and divalent cations electrostatically shield the negatively charged phosphates during DNA duplex formation, making the duplex binding stronger. Mg^{2+} ions are able to cluster around DNA phosphate backbones and provide significantly more stabilization beyond simple electrostatic screening considerations.[49] Although Mg^{2+} stabilize nucleic acid duplexes more effectively even in the absence of monovalent ions, Mg^{2+} combined with Na^+ has a higher ionic strength and is more effective for duplex

stabilization than Mg^{2+} alone.[49-50] All hydrogels studied in this work were formed in phosphate buffer containing 150 mM Na^+, while the concentration of Mg^{2+} was varied from 0 – 50 mM.

For a basic characterization of the influence of the salinity, we first focus on understanding starPEG-T_{20} with the A_{20}-L/L*-A_{20} linker as a function of the $MgCl_2$ concentration. **Figure 2.3a** depicts a schematic overview of hydrogel formation. The effect of $MgCl_2$ is evident in rheological temperature sweeps of the hydrogels (**Figure 2.3b**). The hydrogel without $MgCl_2$ shows a sol-gel transition temperature, as defined by the G'/G'' crossover temperature, T_{co}, of 26 °C and is barely a self-supporting gel at room temperature, RT. However, T_{co} increases by almost 20 degrees to 45 °C for the highest concentration of 50 mM $MgCl_2$. Importantly, T_{co} already increases to T_{co} = 39 °C with only 1 mM $MgCl_2$ in the hydrogel, due to the Mg^{2+}-specific effect on dsDNA stabilization.[49] This places the T_{co} already above typical cell culture experiment temperatures (**Figure 2.3c**). While the experimental T_{co} of the hydrogels cannot be directly compared to the theoretical T_m of the A_{20}/T_{20} pair, the observed trend of an increasing T_{co} with increasing $MgCl_2$ content follows the theoretical expectation (see **SI Figure 2.10** for calculated values).

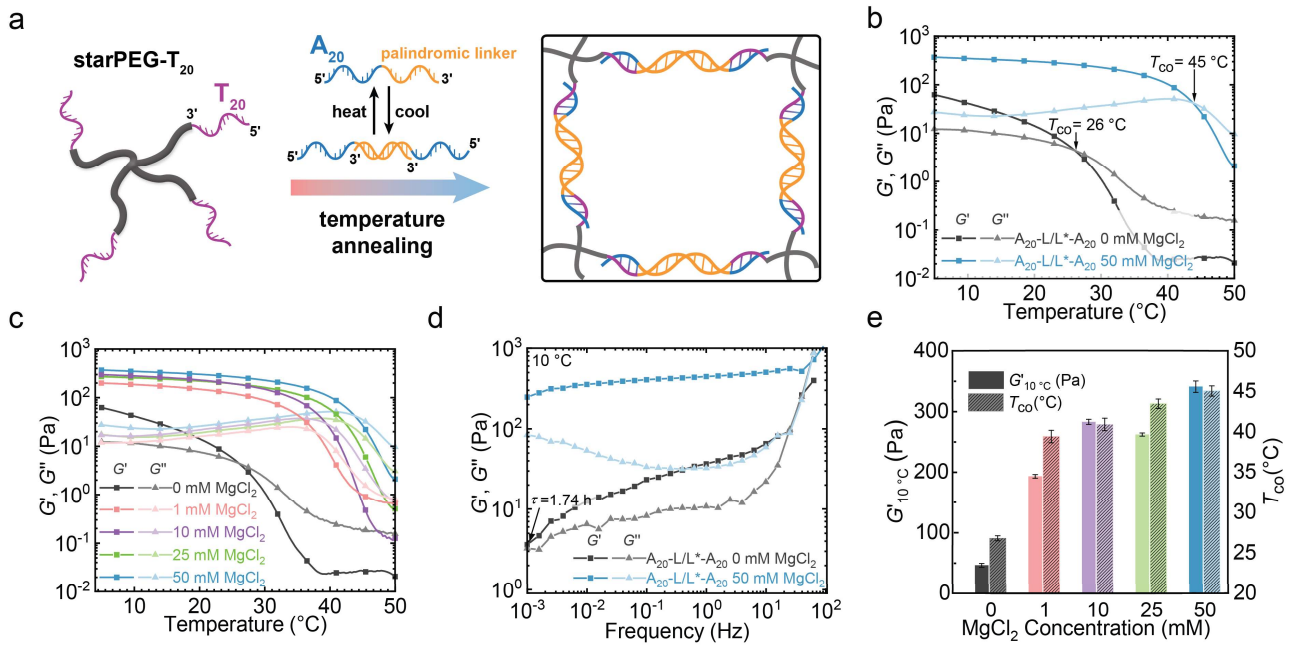

Figure 2.3. Influence of salinity on the rheological properties of the starPEG-T_{20}/A_{20}-L/L*-A_{20} hydrogel at $c^* \approx 0.75$ mM. Mg^{2+} concentration is varied from 0 mM - 50 mM while Na^+ concentration is held constant at 150 mM. **(a)** Schematic overview of hydrogel formation with starPEG-T_{20} and A_{20}-L/L*-A_{20}. **(b)** Temperature sweep of the hydrogel with 0 and 50 mM $MgCl_2$ (f = 1 Hz, γ = 6%, from 50 °C to 5 °C, temperature rate = 0.4 °C/min). The sol-to-gel crossover temperature, T_{co}, is denoted with arrows in the graphs. **(c)** Temperature sweep of the hydrogels at different $MgCl_2$ concentrations. **(d)** Frequency sweep of the hydrogels with 0 and 50 mM $MgCl_2$ (f = 0.001 - 100 Hz, γ = 0.1%, 10 °C). While the bond relaxation time τ, for the hydrogel containing 0 mM $MgCl_2$ is depicted by the arrow in the graph (gray curve), the hydrogel containing 50 mM $MgCl_2$ does not relax within the measured frequency range (blue curve). **(e)** Bar chart showing the evolution of the storage moduli at 10 °C, $G'_{10\ °C}$, and T_{co} for the hydrogels at different $MgCl_2$ concentrations. The error bar is the standard deviation from averaging duplicate measurements.

Next to the changes in the T_{co}, it is also relevant to compare the changes in the mechanical properties regarding the storage modulus, G' (for instance at 10 °C, hence significantly below the T_{co} of the Mg^{2+}-free system). Similar to the influence of $MgCl_2$ on the T_{co}, the mechanical properties can be divided into a Mg^{2+}-free and a Mg^{2+}-rich regime, whereby the changes in the Mg^{2+}-rich regime are less pronounced (**Figure 2.3c**). The $G'_{10\,°C}$ at 0 mM Mg^{2+} is 46 Pa, corresponding to a very soft gel. It amplifies to 200 Pa upon addition of 1 mM Mg^{2+} and then increases steadily to 350 Pa at 50 mM Mg^{2+} (**Figure 2.3e**). This salt-induced strengthening of the network can in principle originate from either an increase of the amount of load-bearing crosslinks (G' ~ network linkage per unit volume)[51] or an increase of the effective time scale of association of the crosslinks with respect to the rheological experiment. Since the amount of bound A_{20}/T_{20} duplexes is expected to be similar already at 20 °C (see **Figure 2.2b** for NUPACK simulations), we surmised that rather the dynamics of the crosslinks play an important role. To investigate the dynamics of the load-bearing A_{20}/T_{20} DNA duplex crosslinkers, we conducted oscillatory frequency sweeps at 10 °C (**Figure 2.3d**). Based upon these measurements, we calculated the relaxation time from the inverse of the crossover frequency f_c, which indicates the transition from "viscous fluid" to "elastic solid" region, and depicts the bond lifetimes within the hydrogels. The starPEG-T_{20}/A_{20}-L/L*-A_{20} hydrogel without $MgCl_2$ shows indeed a relaxation time, located at 1.74 h, while the same hydrogel with 50 mM $MgCl_2$ does not relax within the measured frequency range (relaxation time > 2 h) and represents a quasi-static, near covalent system. As expected, further frequency-dependent sweeps of this hydrogel at different temperatures show shorter relaxation times with increasing temperature (**SI Figure 2.11c**). A crossover starts to appear even for Mg^{2+} samples at higher temperatures (**SI Figure 2.12**). This can be explained by faster exchange dynamics at elevated temperatures. This is consistent also for other A_x linkers as discussed in the Supporting Information (**SI Figure 2.11a-c**). Therefore we conclude that rather the insufficient bond lifetimes of the Mg^{2+}-free systems lead to the lower G' values and that this is not an effect of incomplete hybridization.

In a general material perspective, the Mg^{2+}-containing hydrogels are very stable without visible flow at ambient temperature compared to other DNA cross-linked hydrogels previously reported.[40, 52-53] This is evident in the T_{co} of the hydrogels (above room temperature for all examined Mg^{2+} concentrations) and the frequency-dependent viscoelastic behavior of the hydrogels with long relaxation times at room temperature.

2.3.3 Programming the hydrogel response using the strength of the A_x/T_x linker

An orthogonal way of tuning the mechanical properties regarding gel strength and dynamics, and omitting salinity adjustments that may not be very desirable in specific application settings, is to exploit the strength of the DNA linker by varying the A_x/T_{20} overlap length. Since one specific aspect of this work is to understand the tunability of the dynamics of the load-bearing network chains, we here focus majorly on Mg^{2+}-free environments (yet 150 mM NaCl background salinity) to assure that crossovers in the rheological frequency sweeps are in fact accessible and can be judged regarding their programmability as a function of the linker overlap. In addition, we here also discuss changes in concentrations of the building blocks – while keeping perfect stoichiometry between the starPEG-T_{20} and the bivalent linker – surrounding the previously discussed overlap concentration of 0.75 mM.

Figure 2.4a-b depicts a schematic overview of the starPEG-T_{20}/A_{20}-L/L*-A_{20} and starPEG-T_{20}/A_{10}-L/L*-A_{10} hydrogel assembly**.** Looking first at the influence of the concentration, it is evident that both hydrogels containing either an A_{20} or an A_{10} overlap behave in a similar way. The temperature sweeps show an expected increase in $G'_{10\,°C}$ as a function of concentration due to a higher density of crosslinks per volume element (**Figure 2.4c-e**). The trend is close to linear. More interestingly, the sol-gel transition points, T_{co}, also display a clear trend towards higher T_{co} with increasing concentrations. For instance, the T_{co} of the A_{20}-L/L*-A_{20} hydrogel increases from 24 °C at 0.38 mM starPEG-T_{20} to 33 °C with 1.52 mM starPEG-T_{20}. This increase in the T_{co} can be best explained by the additional ionic strength added to the system by increasing the DNA concentration. Since every phosphate ester backbone group carries its own counterion, such as Na^+, the ionic strength added by increasing the concentration of the DNA is significant.

Secondly, when comparing the bond relaxation time scales (**Figure 2.4f-h**), an increase in the concentration leads to a shift to longer bond relaxation times in both hydrogel systems. τ of the A_{10}-L/L*-A_{10} hydrogel for example increases from 6 seconds at 0.38 mM starPEG-T_{20} to ~7 minutes with 1.52 mM starPEG-T_{20}. We suggest that this is due to an increasing amount of entanglements or crosslinks at concentrations substantially above the overlap concentration, but also, as seen above (**Figure 2.3, Figure 2.4c-e**), the additional influence of salt on the stabilization of the duplex due to higher DNA concentrations plays a role. Further temperature and frequency sweeps of hydrogels assembled from the A_5-L/L*-A_5 and the A_{15}-L/L*-A_{15} linker can be found in the Supporting Information (**SI Figure 2.13, Figure 2.14**), where a similar trend in shifts to longer τ and higher T_{co} is observed.

As an additional comparison, upon the addition of 50 mM Mg^{2+}, an increase in $G'_{10\,°C}$ as a function of concentration is observed (**SI Figure 2.15a-b**). Furthermore, all bond relaxation time scales are pushed beyond 3 h and a G'/G'' crossover does no longer occur in the measurable frequency window (**SI Figure 2.15d-e**). Similar to what is seen in **Figure 2.3**, the addition of Mg^{2+} also increases the $G'_{10\,°C}$ and the T_{co} at the various concentrations (**SI Figure 2.15c**). Overall it becomes clear that increasing the concentration of the DNA content in the hydrogels leads to a subtle interplay between presence of additional salt, increase in crosslinking density, lower bond relaxation dynamics, plus the formation of entanglements.

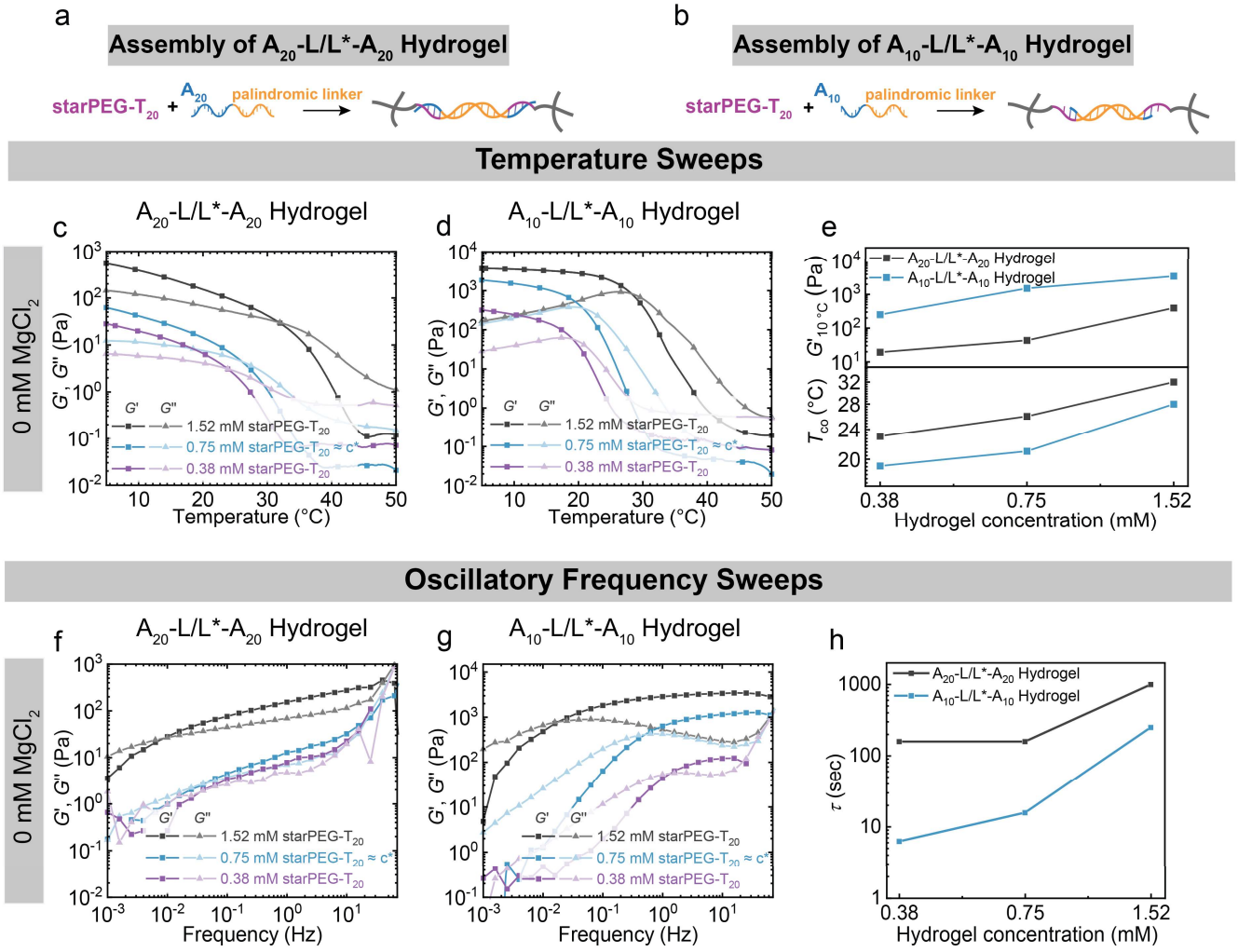

Figure 2.4. Influence of DNA linker strength and building block concentrations on the mechanical properties of the hydrogels. The starPEG-T_{20}/A_{20}-L/L*-A_{20} and starPEG-T_{20}/A_{10}-L/L*-A_{10} hydrogels were formed at different starPEG-T_{20} concentrations, above, below and at the c^* (0 mM $MgCl_2$, 150 mM NaCl). **(a-b)** Schematic overview of hydrogel formation with starPEG-T_{20} and an **(a)** A_{20}-L/L*-A_{20} and an **(b)** A_{10}-L/L*-A_{10} linker. **(c-d)** Temperature sweeps (f = 1 Hz, γ = 6%, from 50 °C to 5 °C, temperature rate = 0.4 °C/min) at 1.5 mM, 0.75 mM and 0.38 mM starPEG-T_{20} concentration. **(e)** Correlation of $G'_{10\,°C}$ and T_{co} at different starPEG-T_{20} concentrations. **(f-g)** Frequency sweeps (f = 0.001 - 100 Hz, γ = 0.1%, 20 °C) at 1.5 mM, 0.75 mM and 0.38 mM starPEG-T_{20} concentration. **(h)** τ at different starPEG-T_{20} concentrations.

The most striking and unexpected observation is the consistently lower G' values for the A_{20}-L/L*-A_{20} hydrogels as compared to the A_{10}-L/L*-A_{10} hydrogels (**Figure 2.4e, top part**). For instance, the $G'_{10\,°C}$ for the

A_{10}-L/L*-A_{10} hydrogel at *c** is at 1.5 kPa, whereas it is 0.050 kPa for the A_{20}-L/L*-A_{20} hydrogel. A similar order of magnitude difference, yet on a higher modulus level, is also found in presence of 50 mM Mg^{2+} (**SI Figure 2.15a-b**). This discrepancy is intuitively unexpected as A_{20}/T_{20} has a higher binding strength compared to an A_{10}/T_{20} segment. Nonetheless at 10 °C both DNA duplexes should be very tightly bound (**Figure 2.2b**) and the influence of the binding strength or binding propensity, hence degree of crosslinking, should not be a decisive factor.

As an explanation, one needs to look in detail at the molecular structure of these networks. Hybridization of starPEG-T_{20} with the A_{20}-L/L*-A_{20} linker leads to a complete dsDNA crosslinking motif that is in total 20 nucleobases (nbs) longer in its stiff dsDNA conformation, while hybridization with the A_{10}-L/L*-A_{10} linker would lead to a crosslink that contains some flexible ssDNA (at the T_{20} part) and the hybridized rigid dsDNA (**Figure 2.4a-b**). Additionally, the hybridization on the T_{20} part is more flexible for an A_{10}-L/L*-A_{10} linker in terms of the spatial position, which may lead to some self-correction of local stress. The built up of local stress can be understood considering the persistence length of dsDNA of ca. 50 nm, while that of ssDNA is lower than 2 nm.[54] With an approximate distance of ~3.4 Å between two neighboring nbs, the number of nb pairs in the persistence length of dsDNA is 147. This relates to the total linker sequence of 14 nbs in the core palindromic L/L* linker domain plus either 20 nbs in the A_{10} linker or 40 nbs in the A_{20} linker. Consequently, the linkers are essentially rigid rods, that only contain two flexible points at the transition from the A_x/T_{20} sequence to the L/L* sequence (dsDNA is discontinuous at this point). The presence of linear rigid linkers in the A_{20}-L/L*-A_{20} hydrogel system is observed in the appearance of slight birefringence under crossed polarizers and shearing. Polarized optical micrographs are presented in the supporting information (**SI Figure 2.16**).

Since the hydrogels are made at the overlap concentration of the starPEG-OH, the addition of the stiff rigid rod-like linkers may in fact lead to some degree of supercoiling of the PEG chains and hence to a network with lower elastic behavior. The very presence of flexible unbound oligo-T in the A_{10}-L/L*-A_{10} hydrogel system is another explanation for increased *G'* values in the A_{10}-L/L*-A_{10} hydrogels. As previously mentioned, the persistence length of dsDNA is up to 50 times larger than that of ssDNA. A linker containing ssDNA would lead to more DNA bonds being formed due to less topological frustration during network formation while a system with long, rigid and inflexible crosslinks such as dsDNA, would result in lower crosslinking density. The former is the case in the A_{10}-L/L*-A_{10} hydrogel system, as flexibility is introduced in form of shorter A_{10}-L/L*-A_{10} linker. Additionally, the A_{10}-L/L*-A_{10} linkers do have the possibility to hybridize in a 2 x A_{10} on one

T_{20} end block on the starPEG-T_{20}. This would lead to a network with crosslinks of higher connectivity and hence also to an increase in *G*'. To better probe for these effect, we investigated a starPEG-T_{10} system together with the A_{10}-linker (**Figure 2.5**). This system prevents any kind of topological defects with two A_{10} linkers binding on one T_{20} block. Indeed we find a significantly lower $G'_{10\,°C}$ value in this systems of 0.5 kPa for the starPEG-T_{10}/A_{10}-L/L*-A_{10}, which is ca. 33% of the 1.5 kPa of the previous starPEG-T_{20}/A_{10}-L/L*-A_{10} at *c**. This is indicative of the fact that the double linkage of 2 A_{10} segments on one T_{20} end block may in fact contribute to some extent to the observed higher *G*' values in the starPEG-T_{20} system. Nonetheless the frequency sweeps, which show near-perfect Maxwellian behavior, are rather self-similar with only slight offsets. Below the crossover frequency, the viscous modulus *G*'' dominates and shows linear scaling with frequency ~*f*, while *G*' scales as ~f^2. The Maxwellian behavior is indicative of a good network structure with limited defects.[48, 55] Hence, we conclude that it is a combination of the discussed effects. Overall this data shows that subtle changes in the molecular composition and network topology with a mixture of flexible and rigid DNA segments is an important aspect to deduce design principle for tuning the viscoelastic properties of such DNA based materials.

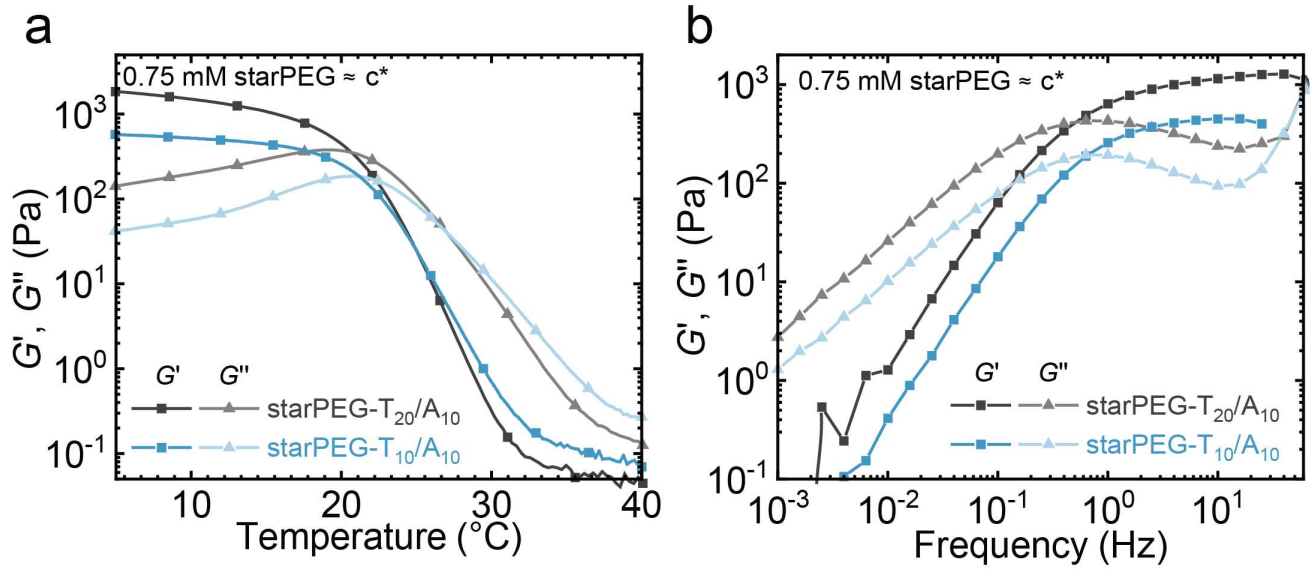

Figure 2.5. Investigation of the mechanical properties of hydrogels formed from starPEG-T_{20}/A_{10}-L/L*-A_{10} and starPEG-T_{10}/A_{10}-L/L*-A_{10} at *c ≈ 0.75 mM, 0 mM $MgCl_2$. (a)** Temperature sweep (*f* = 1 Hz, *γ* = 6%, at *c**≈ 0.75 mM, 0 mM $MgCl_2$, from 40 °C to 5 °C, temperature rate = 0.4 °C/min). **(b)** Frequency sweep (*f* = 0.001 - 100 Hz, *γ* = 0.1%, 20 °C).

2.3.4 Self-healing Property and 3D printing of the starPEG-DNA Hydrogel

The reversible nature of the DNA duplex gives DNA-cross-linked hydrogels excellent reversible thixotropic and self-healing properties.[56-57] The self-healing character of our DNA hydrogel is examined using the A_{20}-L/L*-A_{20} hydrogel in its strong conditions (at 50 mM $MgCl_2$). We characterized the hydrogel strain sweeps in oscillatory rheology (γ = 0.1–1000%) to determine the linear viscoelastic region (LVE). The yield point of the hydrogel is determined in a strain sweep and is the value of the shear strain at the limit of the LVE, $\gamma_c \approx 300\%$ (**Figure 2.6a**). In order to show the recovery/self-healing after mechanical disruption of the network, hydrogel samples were subjected to oscillatory deformation alternating between low (6%) and high (500%) deformation in 60 minute intervals multiple times (**Figure 2.6b**). Results for the hydrogel show that they have the ability to fully recover in very short timescales (< 4 minutes), even after multiple deformation cycles, performing better than existing DNA hydrogel systems with DNA as a responsive crosslinker.[43, 58-59] This property is attributed to the reversibility of the DNA duplex hybridization, leading to full recovery even at RT. Macroscopically, cut pieces of the A_{20}-hydrogel placed in contact with each other fully join at the interface to one uniform piece after few minutes (**Figure 2.6c**).

Furthermore, to detect possible changes in mechanical properties and probe hydrogel durability, rheological measurements were repeated for the same A_{20}-L/L*-A_{20} hydrogel sample after 85 days (~3 months), showing only very minor differences in mechanical behavior and bond relaxation time scales (**Figure 2.6d-e**). This underscores a high shelf-life and a robust structure formation with very limited temporal rearrangements. Additional compression test performed on the A_{20}-L/L*-A_{20} hydrogel indicates some onset of fracture of the hydrogel at about 60% strain (**SI Figure 2.17**).

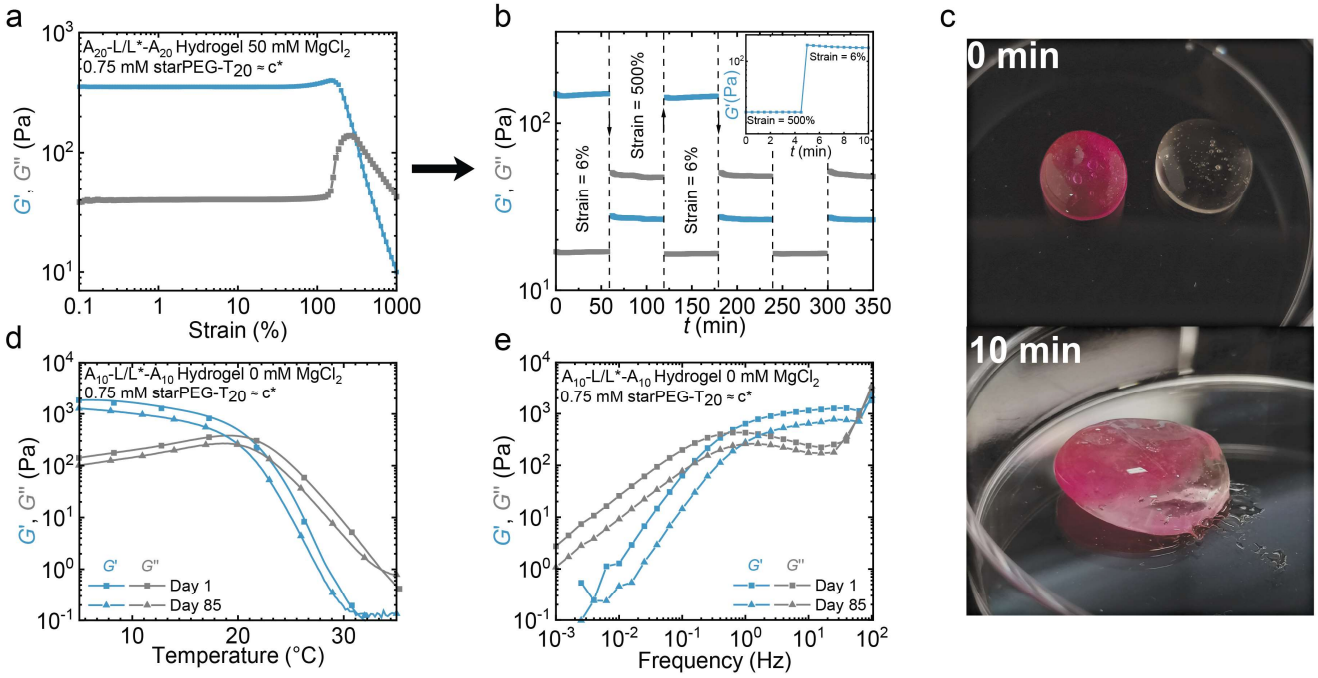

Figure 2.6. Self-healing properties and gel stability. (a) Amplitude sweep of starPEG-T_{20}/A_{20}-L/L*-A_{20} (γ = 0.1 – 1000%, f = 1 Hz, 25 °C, 50 mM $MgCl_2$, 150 mM NaCl). **(b)** Rheological properties of the A_{20}-L/L*-A_{20} hydrogel with alternating strain cycles of 6 and 500% at a fixed frequency, f = 1 Hz at 25 °C plotted against time. The hydrogel shows full recovery after several rounds of deformation. **(c)** Visual representation of self-healing of one dyed and one undyed A_{20}-hydrogel. After about 10 minutes, the two hydrogel pieces are fused into a defect free single piece. **(d-e)** Analysis of hydrogel durability over time of starPEG-T_{20}/A_{10}-L/L*-A_{10}. **(d)** Temperature and **(e)** frequency sweeps at day 1 and at day 85.

Due to the shear-thinning nature of the hydrogels and thermally induced gel-sol transitions, the hydrogels are amendable for 3D printing using bioprinters (**Figure 2.7**). Printing a starPEG-T_{20}/A_{20}-L/L*-A_{20}-hydrogel from a heated cartridge (55 °C) delivers self-supporting stable gel structures at room temperature.

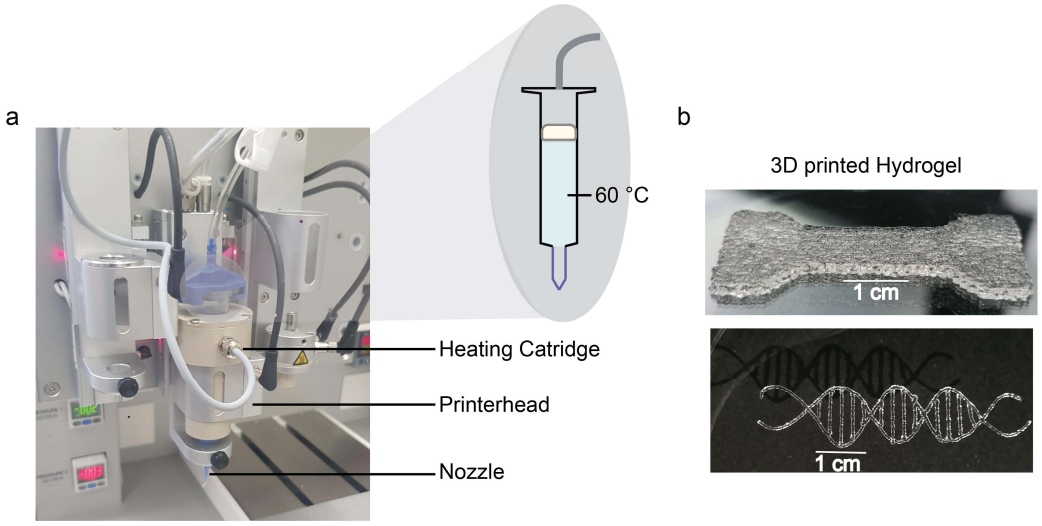

Figure 2.7. 3D printing of the starPEG-T_{20}/A_{20}-L/L*-A_{20} hydrogel. (a) 3D printing set up showing cartridge, nozzle and piston required for bioprinting. **(b)** 3D printing of hydrogels in a dogbone and a DNA double helix structure. The photographs show the printability and the self-supporting nature of the gel at room temperature (RT).

2.4 Conclusions

This chapter reported a first detailed investigation on the characterization of quasi-ideal model network hydrogels based on starPEG-DNA building blocks with duplex linkers. The material design builds on our recently developed OP-LPOS synthesis strategy, which opens up pathways to large scale polymer/DNA hybrid materials. A wide property space can be accessed by varying the linker length and by changing the salinity and the concentration of the building blocks. The gel G' values are tunable from 20 Pa to 3.1 kPa and therefore in the range where mechanosensing of cells occurs.[60-62] Relaxation time scales are also particularly tunable by salinity. All hydrogels assembled in the presence of a divalent cation (Mg^{2+}) show no relaxation time in the measured frequency range (f = 0.001 - 100 Hz) at 10 °C, but change accordingly along a wide spectrum in other conditions. The hydrogel formation is robust and the mechanical properties of such starPEG-DNA hydrogels can withstand repeated heating and cooling cycles, and properties such as T_{co} and τ are maintained several months after hydrogel assembly.

On the fundamental side, detailed investigations reveal non-linearities, as seen in the difference between G' values for starPEG-T_{20}/A_{10}-L/L*-A_{10} and starPEG-T_{20}/A_{20}-L/L*-A_{20} hydrogels. Surprisingly, the A_{10}-L/L*-A_{10} hydrogel shows higher G' than its A_{20}-L/L*-A_{20} counterpart. These differences could be reconciled partly by comparing to a starPEG-T_{10}/A_{10}-L/L*-A_{10} system, that displays intermediate properties. This allows to conclude that the mechanical properties of such hydrogels result from an interplay of network topology and molecular composition, and that despite the high programmability of DNA and the highly defined building blocks employed here, a more detailed understanding on the network structure is still needed. Further investigations using e.g. scattering techniques or NMR spectroscopy will be valuable, and will be addressed in future publications.

The ease and scalability of synthesis of the building blocks needed for hydrogel assembly, starPEG-T_{20} via OP-LPOS and DNA linker via automated solid phase synthesis should facilitate the application of this hydrogel as a biomaterial in a wide variety of applications. This work therefore lays the groundwork, but ample possibilities to include higher levels of response using aptamers, enzymatically responsive segments or targeting e.g. strain stiffening hydrogels using more complex DNA linkers appear feasible.

2.5 Experimental

2.5.1 Materials

All reagents and solvents were used as received from the following suppliers: Ac-dC Synbase CPG 1000/110 (Link Technology), DMT-dA(bz) phosphoramidite, DMT-dG(iBU) phosphoramidite, DMT-dG(dmf) phosphoramidite DMT-dC(ac) phosphoramidite, DMT-dC(bz) phosphoramidite, DMT-dT phosphoramidite (Sigma-Aldrich, 99%, was dissolved 50mM in anhydrous acetonitrile), CAP A (Sigma Aldrich, tetrahydrofuran/pyridine/acetic anhydride, 8:1:1), CAP B (Sigma Aldrich, 10% methylimidazole in tetrahydrofuran), Trichloroacetic acid Deblock (TCA Deblock, Sigma-Aldrich, 3% in DCM), 5-(Ethylthio)-1H tetrazole (ETT Activator, Sigma Aldrich, 3% in ACN), Oxidizer (Sigma Aldrich, Pyridine / Water / Iodine, 9:1:12.7), Dichloromethane (DCM, Fischer Scientific U.K., CH_2Cl_2, analytical reagent grade), Acetonitrile (ACN, Sigma-Aldrich, C_2H_3N), Acetonitrile anhydrous (ACN, 99.8%, abcr GmbH), Sodium chloride (NaCl, 99%, Sigma Aldrich), Sodium hydroxide (NaOH, VWR), Magnesium chloride ($MgCl_2$, 1M, Fischer Scientific), Sodium dihydrogen phosphate (NaH_2PO_4, Sigma Aldrich), Silicon oil (350cSt, Carl Roth GmbH).

StarPEG-T_{20} was synthesized as described previously in detail.[44]

2.5.2 Instrumentation

High-performance liquid chromatography (HPLC) was performed on a Thermo Fischer Scientific Dionex Ultimate 3000 HPLC system and chromatograms were processed using the Chromeleon data system. The sample was dissolved in milli-Q water and measured using a gradient from 100% A to 90% B with solvent A being 0.1 M TEAA buffer (1/1) in 95/5 water/acetonitrile, and solvent B being acetonitrile.

Ultraviolet-visible spectrophotometry (UV-VIS) measurements were conducted on an Analytik Jena ScanDrop 250 Spectrophotometer using a Tray cell cuvette from Hellma with a path length of 1.0 mm.

Agarose gel electrophoresis (AGE): 2wt% Agarose solutions were prepared in tris-acetate EDTA buffer (TAE, containing 40 mM Tris, 20 mM acetic acid and 1 mM EDTA; pH 8.0) and the gel was stained with Roti-GelStain with a mixing ratio of 25 µL per 150 mL agarose solution. AGE was performed using a 20-sample gel chamber at a voltage of 80 V for 75 min. Images were captured with an Intas Chemostar ECL & Fluorescence Imager in UV transilluminator mode.

Matrix-assisted laser-desorption-ionization time-of-flight mass spectrometry (MALDI-ToF MS) measurements were performed using 3-HPA (3-Hydroxypicolinic acid) as matrix. The measurements were conducted on an AUTOFLEX III from BRUKER.

Rheological Characterization was performed on an Anton Paar Modular Compact Rheometer MCR 302 equipped with a 25 mm plate-plate geometry. *G*' and *G*'' were measured in oscillation mode with a constant strain amplitude of 6%. This value was found to be in the linear viscoelastic range based on the results of an amplitude sweep at 1 Hz. Analysis of the data was done with the Rheocompass software. Frequency sweeps were carried out on mixtures between 100 Hz and 0.001 Hz at a fixed strain of 0.1%. Temperature ramps were performed at a fixed frequency and strain of 1 Hz and 6%, respectively. The ramping rate of the temperature was 0.4 °C/min. Amplitude strain sweeps were performed at room temperature and a fixed frequency of 1 Hz. The gap between the plates was fixed at 0.2 mm and a thin layer of silicon oil was added around the measuring system to prevent evaporation.

For starPEG-OH and starPEG-T_{20} critical overlap concentration measurements, the average viscosity for different concentrations was measured over 2 min at a shear rate of 100 s^{-1}.

Compression tests were performed using a MCR702 MultiDrive from Anton Paar.

Polarized optical microscopy was done with a Nikon SMZ25 microscope fitted with an optical cross polarizer at the base.

3D Bioprinting of the hydrogel was done using 3DDiscovery™ Evolution 3D bio printer from RegenHU, Switzerland. The Bioprinter was fitted with a heating jacket for thermal printing and the obtained G-codes of the printed designs were generated with the 3D bioCAD software. The hydrogel solution was loaded into a 10 mL syringe and heated up to 60 °C during printing. The hydrogel was extruded through a plastic conical tip with a diameter of 0.4 mm.

2.5.3 Procedures and Synthesis

Synthesis and purification of oligonucleotide sequences

Automated synthesis. The oligonucleotides were synthesized on a H-8 custom LNA, DNA/RNA automatic synthesizer from K&A Laborgeräte at 10 µmol scale employing the standard solid phase β-cyanoethyl-phosphoramidite chemistry in trityl-on mode. The DNA phosphoramidites (DMT-dT, DMT-dA(bz), DMT-

dG(dmf) and DMT-dC(ac)) were diluted to 50 mM with dry acetonitrile and synthesis occurred from the 3' towards the 5' end of the oligonucleotides on packed solid phase columns.

Deprotection and purification (general procedure for 10 µmol scale synthesis). Cleavage of the oligonucleotides from the solid support and base deprotection was achieved in one step to ensure optimal yields. The 34 µmol/g controlled pore glass (CPG) solid support was treated with 10 mL of a 50:50 wt% mixture of ethylenediamine:toluene for 2 hours at room temperature. The deprotection solution is removed and the column is rinsed twice with 10 mL toluene to detach synthesized DNA from the support. The synthesized DNA sequence was then extracted with 6 mL milliQ water and purified by reverse phase-HPLC (RP-HPLC). The solvent was removed by freeze drying. After purification, the DMT group was cleaved by making a 2 wt% solution of the dry DNA in pH 4.0 (200 mM) NaOAc/HOAc buffer containing 200 mM NaCl at and stirring at 50 °C for one hour. Precipitation of the sample into a 5 fold excess of 2-propanol removes contaminants and exchanges counterions to sodium. The solvent was removed by freeze drying and the synthesized strands were stored at -20 °C until further use. The purity of the obtained oligonucleotides were confirmed with analytical HPLC and MALDI-TOF.

StarPEG-DNA hydrogel preparation

The dry starPEG-T_{20} and synthesized linker DNA were dissolved separately at desired concentration in a 25 mM Diphosphate EDTA buffer + 100 mM NaCl (pH = 7.9) and the DNA concentration in the starPEG-T_{20} conjugate and in the linker DNA was determined by UV Vis. StarPEG-DNA hydrogels were hybridized by mixing equimolar quantities of starPEG-T_{20} and linker-DNA in the same buffer, but potentially also containing Mg^{2+}, to assist the DNA hybridization process. The sample was heated (up to 60 °C for hydrogels at 0 mM Mg^{2+} and to 70 °C for hydrogels containing Mg^{2+}) for about 15 min and cooled to room temperature at about 1 °C/min. Samples were kept in the fridge at 4 °C until use.

2.6 Supplementary Information

Linker data

Table 2.2. Overview of the synthesized linkers and its corresponding molecular weight.

Linker Abbreviation	Full seqence 5'→3'	Calculated Molecular weight[a] ($gmol^{-1}$)
A_5-L/L*-A_5	5' AAA AA GCA GCT GCA GCT GC	5831
A_{10}-L/L*-A_{10}	5' AAA AAA AAA A GCA GCT GCA GCT GC	7397
A_{15}-L/L*-A_{15}	5' AAA AAA AAA AAA AAA GCA GCT GCA GCT GC	8963
A_{20}-L/L*-A_{20}	5' AAA AAA AAA AAA AAA AAA AA GCA GCT GCA GCT GC	10529

[a]The calculated molecular weights are determined with the Oligo Analyzer package from Integrated DNA technologies (IDT).

Molecular weight determination of DNA duplex linkers

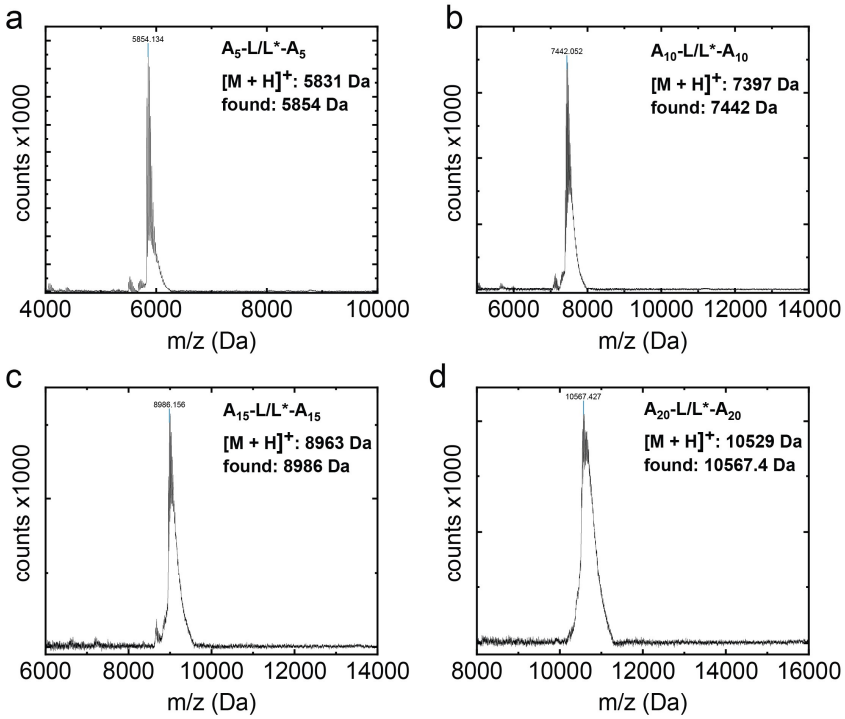

Figure 2.8. MALDI-TOF analysis of synthesized DNA linkers showing **(a)** A_5-L/L*-A_5 linker **(b)** A_{10}-L/L*-A_{10} linker **(c)** A_{15}-L/L*-A_{15} linker **(d)** A_{20}-L/L*-A_{20} linker.

Determination of the overlap concentration, *c**

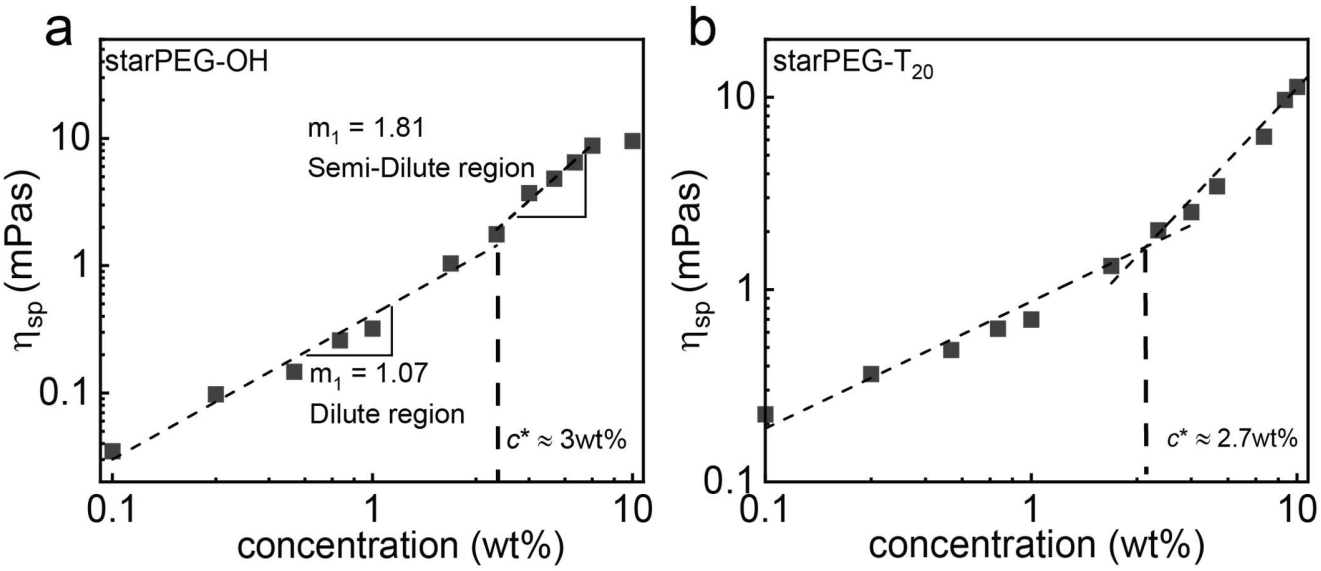

Figure 2.9. Determination of overlap concentration, *c of (a) starPEG-OH and (b) starPEG-T_{20}.** Specific viscosity plotted against concentration in wt%. The specific viscosity is calculated using **Equation 4**. *C** is determined as the crossover between the two slopes of the plot.

$$\eta_{sp} = \frac{\eta_{solution} - \eta_{solvent}}{\eta_{solution}} \quad (4)$$

Influence of salinity on the melting temperature of the A_{20}/T_{20} base pair

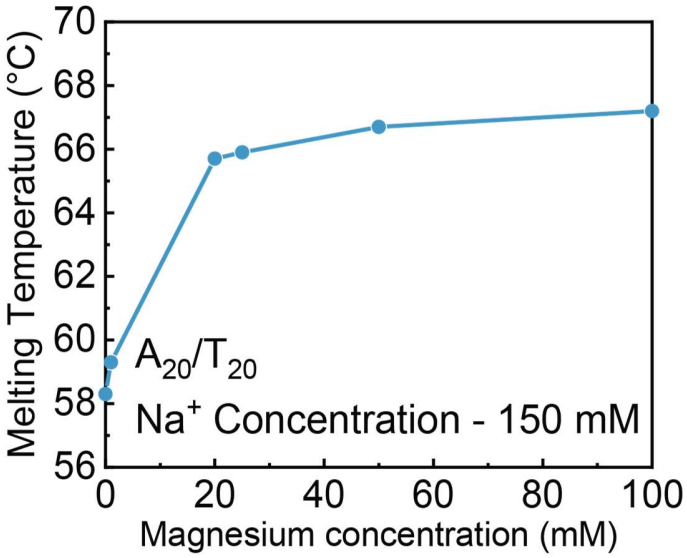

Figure 2.10. Calculated melting temperatures of the equivalent A_{20}/T_{20} base pair in the synthesized DNA linkers at different $MgCl_2$ concentrations. The melting points for the A_{20}/T_{20} base pair is determined with the Oligo Analyzer tool from Integrated DNA technologies (IDT).[46] DNA concentration set to 1 mM. NaCl concentration is set to 150 mM for all samples while Mg^{2+} concentration is varied.

Rheological characterization - Frequency dependent behavior of hydrogels with different duplex linker length at 0 mM and 50 mM $MgCl_2$ concentration

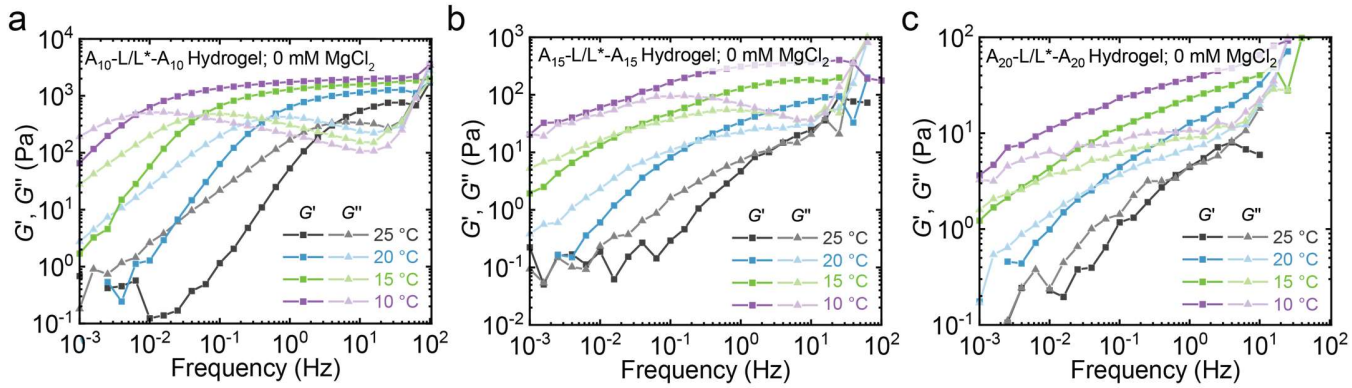

Figure 2.11. Frequency sweeps (f = 0.001 - 100 Hz, γ = 0.1%) of the hydrogels (at 0.75 mM ≈ c^*, 0 mM $MgCl_2$) at different temperatures. (a) A_{10}-L/L*-A_{10} hydrogel (b) A_{15}-L/L*-A_{15} hydrogel (c) A_{20}-L/L*-A_{20} hydrogel. The crossover frequency f_{co}, is indicated by the G'/G'' crossover.

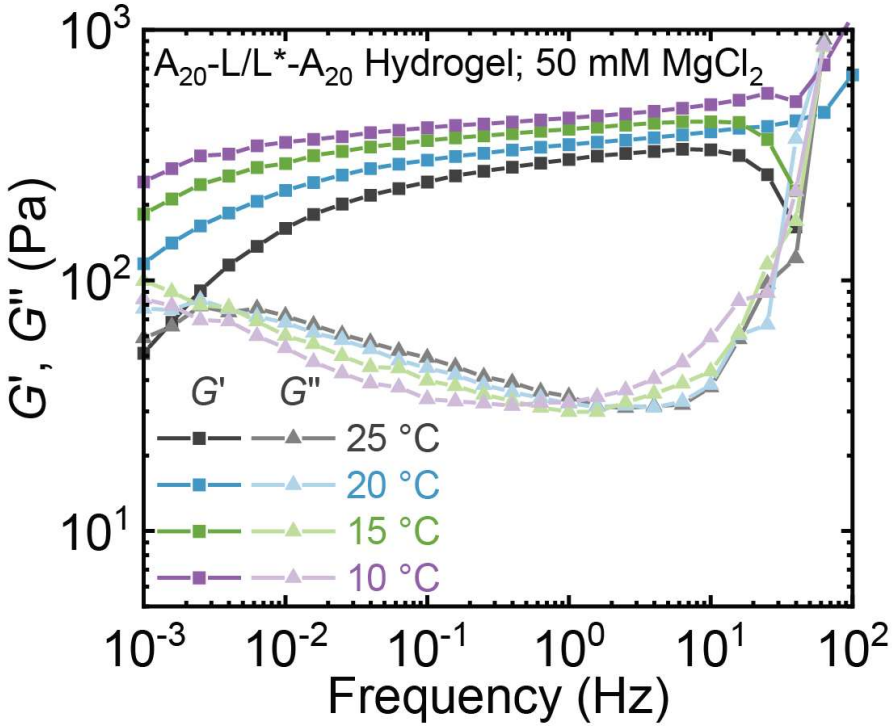

Figure 2.12. Frequency sweep (f = 0.001 - 100 Hz, γ = 0.1%) of the A_{20}-L/L*-A_{20} hydrogel (at 0.75 mM ≈ c^*, 50 mM $MgCl_2$) at different temperatures.

Rheological characterization – Mechanical properties of the hydrogels with different duplex linker length at different starPEG-T_{20} concentrations

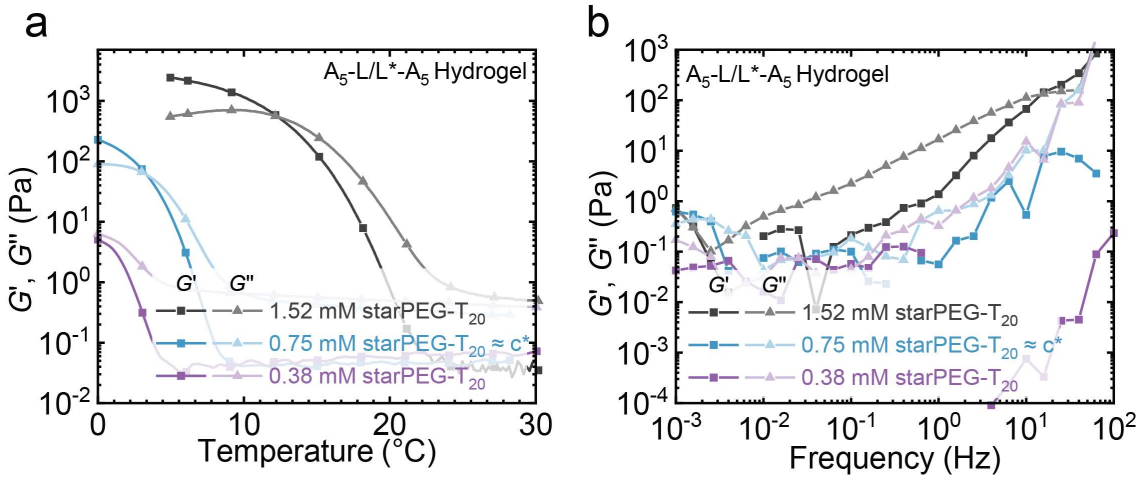

Figure 2.13. Linear viscoelastic behavior of A_5-L/L*-A_5 hydrogel below, above and at *c, 0 mM $MgCl_2$. (a)** Temperature sweep (f = 1 Hz, γ = 6%, from 30 °C to 0 °C, temperature rate = 0.4 °C/min) and **(b)** frequency sweep (f = 0.001 - 100 Hz, γ = 0.1%, 20 °C) of the hydrogels at different concentrations.

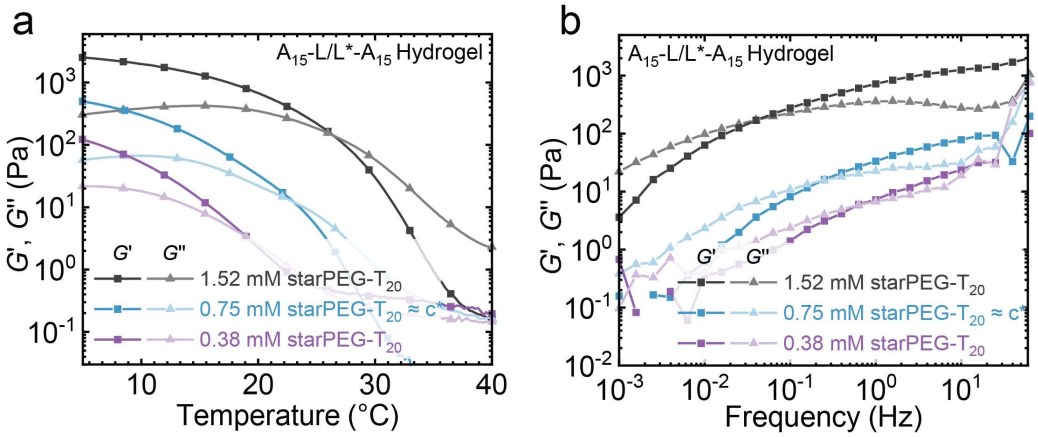

Figure 2.14. Linear viscoelastic behavior of A_{15}-L/L*-A_{15} hydrogel below, above and at *c, 0 mM $MgCl_2$. (a)** Temperature sweep (f = 1 Hz, γ = 6%, from 40 °C to 5 °C, temperature rate = 0.4 °C/min) and **(b)** frequency sweep (f = 0.001 - 100 Hz, γ = 0.1%, 20 °C) of the hydrogels at different concentrations.

Rheological characterization – Effect of duplex linker length, salt and polymer concentration on bond lifetime and T_{co} of the hydrogels

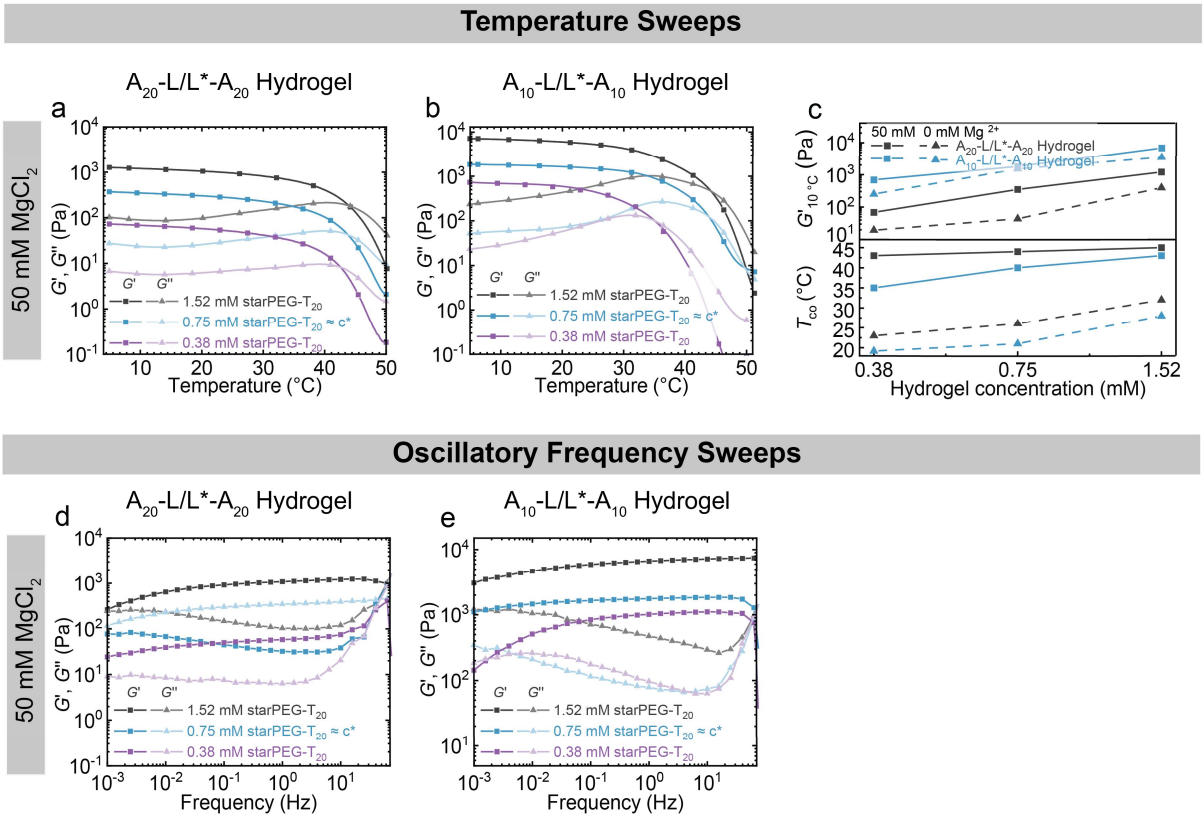

Figure 2.15. Influence of DNA linker rigidity and concentration on the mechanical properties of the hydrogel. The A_{20}-L/L*-A_{20} hydrogel and the A_{10}-L/L*-A_{10} hydrogels were formed at different starPEG-T_{20} concentrations, above, below and at c^* and at 50 mM $MgCl_2$ salt concentration. **(a)** Temperature sweep (f = 1 Hz, γ = 6%, from 50 °C to 5 °C, temperature rate = 0.4 °C/min) of the A_{20}-L/L*-A_{20} hydrogel and **(b)** of the A_{10}-L/L*-A_{10} hydrogel at 1.52 mM starPEG, 0.75 mM starPEG and 0.38 mM starPEG concentration. **(c)** Correlation of the storage moduli at 10 °C, $G'_{10\,°C}$ and the sol to gel cross over temperature, T_{co} of the A_{20}-L/L*-A_{20} hydrogel and the A_{10}-L/L*-A_{10} hydrogel at different starPEG concentrations. **(d)** Frequency sweep (f = 0.001 - 100 Hz, γ = 0.1%, 20 °C, 0 mM $MgCl_2$) of the A_{20}-hydrogel and **(e)** of the A_{10}-L/L*-A_{10} hydrogel at 1.52 mM starPEG, 0.75 mM starPEG and 0.38 mM starPEG concentration.

Birefringence in the A_{20}-L/L*-A_{20} hydrogel system

The A_{20}-L/L*-A_{20} hydrogel was carefully placed between two glass slides and imaged through crossed polarizers. Upon shearing, a slight birefringence occurs. Hydrogels formed at *c** show less birefringence than hydrogels above *c**.

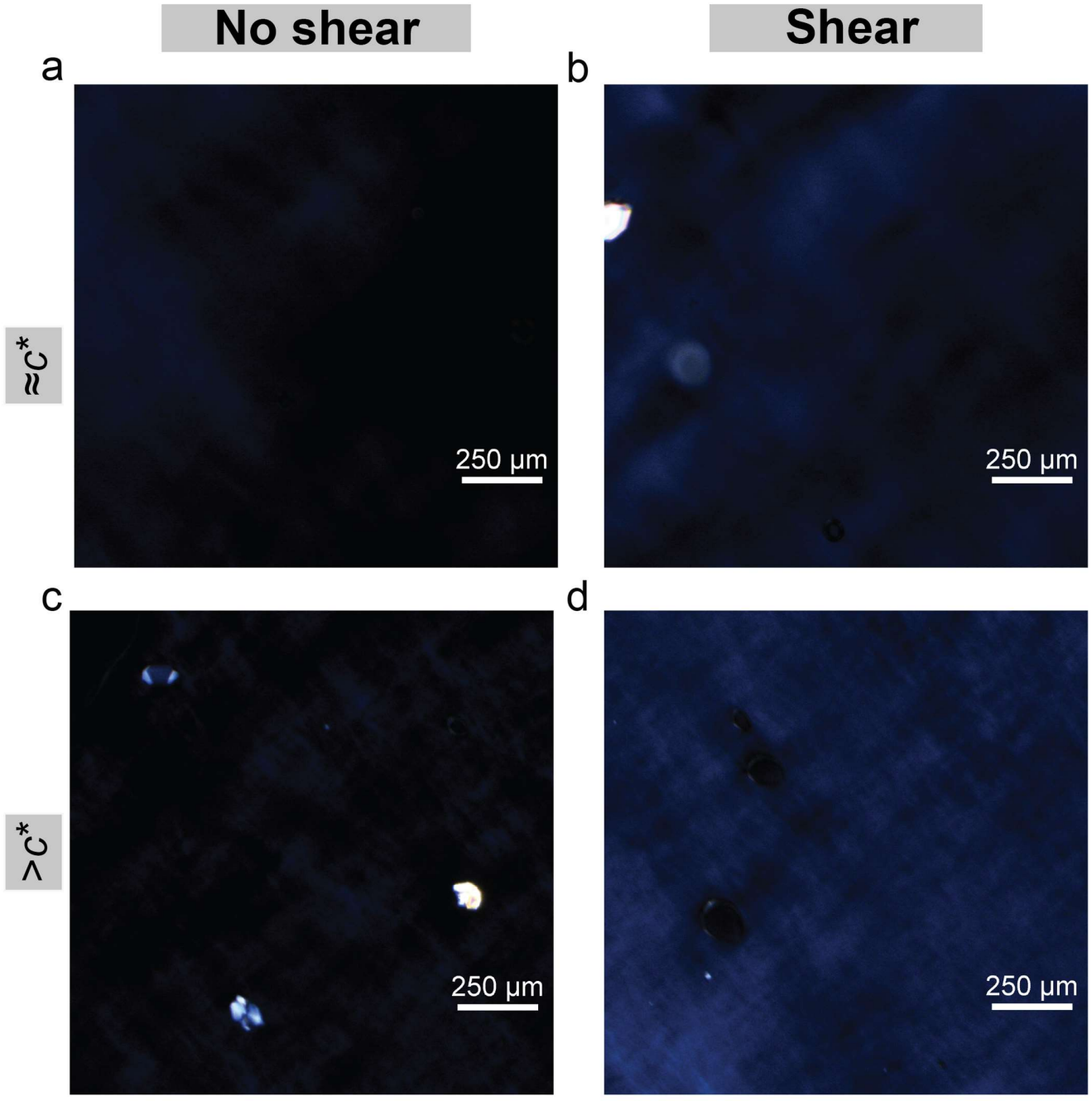

Figure 2.16. Polarized optical micrographs of the A_{20}-L/L*-A_{20} hydrogel. Sample at *c** starPEG-T_{20} concentration placed between two glass slides **(a)** without shearing and **(b)** with shearing. Sample above *c** starPEG-T_{20} concentration placed between two glass slides **(c)** without shearing and **(d)** with shearing.

Compression test of of A_{20}-L/L*-A_{20} hydrogel

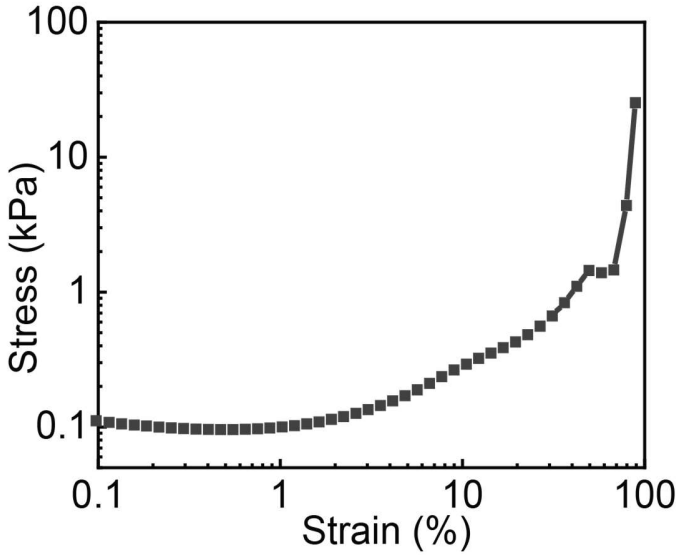

Figure 2.17. Compressive stress-strain curve of the hydrogel. The A_{20}-L/L*-A_{20} hydrogel was formed at *c** starPEG-T_{20} concentration and at 50 mM $MgCl_2$ salt concentration (*T* = 25 °C). Onset of fracture seems to occur at 60 – 70% compression.

2.7 References

(1) Richtering, W.; Saunders, B. R., Gel Architectures and Their Complexity. *Soft Matter* **2014,** *10* (21), 3695-3702.
(2) Hoare, T. R.; Kohane, D. S., Hydrogels in Drug Delivery: Progress and Challenges. *Polymer* **2008,** *49* (8), 1993-2007.
(3) Varaprasad, K.; Raghavendra, G. M.; Jayaramudu, T.; Yallapu, M. M.; Sadiku, R., A Mini Review on Hydrogels Classification and Recent Developments in Miscellaneous Applications. *Mater. Sci. Eng. C* **2017,** *79*, 958-971.
(4) Mondal, S.; Das, S.; Nandi, A. K., A Review on Recent Advances in Polymer and Peptide Hydrogels. *Soft Matter* **2020,** *16* (6), 1404-1454.
(5) Picchioni, F.; Muljana, H., Hydrogels Based on Dynamic Covalent and Non Covalent Bonds: A Chemistry Perspective. *Gels* **2018,** *4* (1), 21.
(6) Seiffert, S.; Sprakel, J., Physical Chemistry of Supramolecular Polymer Networks. *Chemical Society Reviews* **2012,** *41* (2), 909-930.
(7) Creusen, G.; Roshanasan, A.; Lopez, J. G.; Peneva, K.; Walther, A., Bottom-up Design of Model Network Elastomers and Hydrogels from Precise Star Polymers. *Polym. Chem.* **2019,** *10* (27), 3740-3750.
(8) Voorhaar, L.; Hoogenboom, R., Supramolecular Polymer Networks: Hydrogels and Bulk Materials. *Chemical Society Reviews* **2016,** *45* (14), 4013-4031.
(9) Ludwanowski, S.; Skarsetz, O.; Creusen, G.; Hoenders, D.; Straub, P.; Walther, A., Wavelength‐Gated Adaptation of Hydrogel Properties Via Photo‐Dynamic Multivalency in Associative Star Polymers. *Angewandte Chemie International Edition* **2021,** *60* (8), 4358-4367.
(10) Wu, J.; Li, P.; Dong, C.; Jiang, H.; Xue, B.; Gao, X.; Qin, M.; Wang, W.; Chen, B.; Cao, Y., Rationally Designed Synthetic Protein Hydrogels with Predictable Mechanical Properties. *Nat. Commun.* **2018,** *9* (1), 1-11.
(11) Gačanin, J.; Synatschke, C. V.; Weil, T., Biomedical Applications of DNA‐Based Hydrogels. *Advanced Functional Materials* **2020,** *30*, 1906253.
(12) Li, F.; Tang, J.; Geng, J.; Luo, D.; Yang, D., Polymeric DNA Hydrogel: Design, Synthesis and Applications. *Progress in Polymer Science* **2019,** *98*, 101163.
(13) Freeman, R.; Stephanopoulos, N.; Álvarez, Z.; Lewis, J. A.; Sur, S.; Serrano, C. M.; Boekhoven, J.; Lee, S. S.; Stupp, S. I., Instructing Cells with Programmable Peptide DNA Hybrids. *Nat. Commun.* **2017,** *8* (1), 1-11.
(14) Merindol, R.; Loescher, S.; Samanta, A.; Walther, A., Pathway-Controlled Formation of Mesostructured All-DNA Colloids and Superstructures. *Nat. Nanotechnol.* **2018,** *13* (8), 730-738.
(15) Fern, J.; Schulman, R., Modular DNA Strand-Displacement Controllers for Directing Material Expansion. *Nat. Commun.* **2018,** *9* (1), 3766.
(16) Madsen, M.; Gothelf, K. V., Chemistries for DNA Nanotechnology. *Chemical Reviews* **2019,** *119* (10), 6384-6458.
(17) Seeman, N. C.; Sleiman, H. F., DNA Nanotechnology. *Nat. Rev. Mater.* **2017,** *3* (1), 1-23.
(18) Xing, Y.; Cheng, E.; Yang, Y.; Chen, P.; Zhang, T.; Sun, Y.; Yang, Z.; Liu, D., Self-Assembled DNA Hydrogels with Designable Thermal and Enzymatic Responsiveness. *Advanced Materials* **2011,** *23* (9), 1117-1121.
(19) Wilner, O. I.; Weizmann, Y.; Gill, R.; Lioubashevski, O.; Freeman, R.; Willner, I., Enzyme Cascades Activated on Topologically Programmed DNA Scaffolds. *Nat. Nanotechnol.* **2009,** *4* (4), 249-254.
(20) Heinen, L.; Walther, A., Celebrating Soft Matter's 10th Anniversary: Approaches to Program the Time Domain of Self-Assemblies. *Soft Matter* **2015,** *11*, 7857-7866.
(21) Deng, J.; Walther, A., Fuel-Driven Transient DNA Strand Displacement Circuitry with Self-Resetting Function. *Journal of the American Chemical Society* **2020,** *142* (50), 21102-21109.
(22) Wang, S.; Yue, L.; Wulf, V.; Lilienthal, S.; Willner, I., Dissipative Constitutional Dynamic Networks for Tunable Transient Responses and Catalytic Functions. *Journal of the American Chemical Society* **2020,** *142* (41), 17480-17488.
(23) Simmel, F. C.; Schulman, R., Self-Organizing Materials Built with DNA. *MRS Bulletin* **2017,** *42* (12), 913-919.
(24) Hu, Y.; Wang, F.; Lu, C. H.; Girsh, J.; Golub, E.; Willner, I., Switchable Enzyme/Dnazyme Cascades by the Reconfiguration of DNA Nanostructures. *Chemistry- A European Journal* **2014,** *20* (49), 16203-16209.
(25) Zhao, Z.; Wang, C.; Yan, H.; Liu, Y., Soft Robotics Programmed with Double Crosslinking DNA Hydrogels. *Advanced Functional Materials* **2019,** *29* (45), 1905911.
(26) Shim, T. S.; Estephan, Z. G.; Qian, Z.; Prosser, J. H.; Lee, S. Y.; Chenoweth, D. M.; Lee, D.; Park, S.-J.; Crocker, J. C., Shape Changing Thin Films Powered by DNA Hybridization. *Nat. Nanotechnol.* **2017,** *12* (1), 41.

(27) Dorsey, P. J.; Rubanov, M.; Wang, W.; Schulman, R., Digital Maskless Photolithographic Patterning of DNA-Functionalized Poly (Ethylene Glycol) Diacrylate Hydrogels with Visible Light Enabling Photodirected Release of Oligonucleotides. *ACS Macro Letters* **2019,** *8*, 1133-1140.
(28) Kwon, P. S.; Ren, S.; Kwon, S. J.; Kizer, M. E.; Kuo, L.; Xie, M.; Zhu, D.; Zhou, F.; Zhang, F.; Kim, D.; Fraser, K.; Kramer, L. D.; Seeman, N. C.; Dordick, J. S.; Linhardt, R. J.; Chao, J.; Wang, X., Designer DNA Architecture Offers Precise and Multivalent Spatial Pattern-Recognition for Viral Sensing and Inhibition. *Nat. Chem.* **2020,** *12* (1), 26-35.
(29) Merindol, R.; Delechiave, G.; Heinen, L.; Catalani, L. H.; Walther, A., Modular Design of Programmable Mechanofluorescent DNA Hydrogels. *Nature communications* **2019,** *10*, 528.
(30) Woods, D.; Doty, D.; Myhrvold, C.; Hui, J.; Zhou, F.; Yin, P.; Winfree, E., Diverse and Robust Molecular Algorithms Using Reprogrammable DNA Self-Assembly. *Nature* **2019,** *567* (7748), 366-372.
(31) Xiong, X.; Wu, C.; Zhou, C.; Zhu, G.; Chen, Z.; Tan, W., Responsive DNA-Based Hydrogels and Their Applications. *Macromolecular Rapid Communications* **2013,** *34*, 1271-1283.
(32) Lee, J. B.; Peng, S.; Yang, D.; Roh, Y. H.; Funabashi, H.; Park, N.; Rice, E. J.; Chen, L.; Long, R.; Wu, M., A Mechanical Metamaterial Made from a DNA Hydrogel. *Nat. Nanotechnol.* **2012,** *7* (12), 816-820.
(33) Sakai, T.; Matsunaga, T.; Yamamoto, Y.; Ito, C.; Yoshida, R.; Suzuki, S.; Sasaki, N.; Shibayama, M.; Chung, U.-i., Design and Fabrication of a High-Strength Hydrogel with Ideally Homogeneous Network Structure from Tetrahedron-Like Macromonomers. *Macromolecules* **2008,** *41*, 5379-5384.
(34) Tanaka, S.; Yukami, S.; Hachiro, Y.; Ohya, Y.; Kuzuya, A., Application of DNA Quadruplex Hydrogels Prepared from Polyethylene Glycol-Oligodeoxynucleotide Conjugates to Cell Culture Media. *Polymers* **2019,** *11* (10).
(35) Hörner, M.; Raute, K.; Hummel, B.; Madl, J.; Creusen, G.; Thomas, O. S.; Christen, E. H.; Hotz, N.; Gübeli, R. J.; Engesser, R., Phytochrome ‐ Based Extracellular Matrix with Reversibly Tunable Mechanical Properties. *Advanced Materials* **2019,** *31* (12), 1806727.
(36) Shibayama, M.; Li, X.; Sakai, T., Precision Polymer Network Science with Tetra-Peg Gels—a Decade History and Future. *Colloid and Polymer Science* **2019,** *297* (1), 1-12.
(37) Sakai, T., Gelation Mechanism and Mechanical Properties of Tetra-Peg Gel. *Reactive and Functional Polymers* **2013,** *73*, 898–903.
(38) Apostolides, D. E.; Sakai, T.; Patrickios, C. S., Dynamic Covalent Star Poly (Ethylene Glycol) Model Hydrogels: A New Platform for Mechanically Robust, Multifunctional Materials. *Macromolecules* **2017,** *50* (5), 2155-2164.
(39) Du, C.; Hill, R. J., Complementary-DNA-Strand Cross-Linked Polyacrylamide Hydrogels. *Macromolecules* **2019,** *52*, 6683-6697.
(40) Fernandez-Castanon, J.; Bianchi, S.; Saglimbeni, F.; Di Leonardo, R.; Sciortino, F., Microrheology of DNA Hydrogel Gelling and Melting on Cooling. *Soft Matter* **2018,** *14* (31), 6431-6438.
(41) Conrad, N.; Kennedy, T.; Fygenson, D. K.; Saleh, O. A., Increasing Valence Pushes DNA Nanostar Networks to the Isostatic Point. *Proc. Nat. Acad. Sci.* **2019,** *116* (15), 7238-7243.
(42) Rovigatti, L.; Smallenburg, F.; Romano, F.; Sciortino, F., Gels of DNA Nanostars Never Crystallize. *ACS Nano* **2014,** *8*, 3567-3574.
(43) Tanaka, S.; Wakabayashi, K.; Fukushima, K.; Yukami, S.; Maezawa, R.; Takeda, Y.; Tatsumi, K.; Ohya, Y.; Kuzuya, A., Intelligent, Biodegradable, and Self-Healing Hydrogels Utilizing DNA Quadruplexes. *Chem. Asian J.* **2017,** *12* (18), 2388-2392.
(44) Creusen, G.; Akintayo, C. O.; Schumann, K.; Walther, A., Scalable One-Pot - Liquid-Phase Oligonucleotide Synthesis for Model Network Hydrogels. *Journal of the American Chemical Society* **2020,** *142* (39), 16610-16621.
(45) Zadeh, J. N.; Steenberg, C. D.; Bois, J. S.; Wolfe, B. R.; Pierce, M. B.; Khan, A. R.; Dirks, R. M.; Pierce, N. A., Nupack: Analysis and Design of Nucleic Acid Systems. *Journal of Computational Chemistry* **2011,** *32* (1), 170-173.
(46) Owczarzy, R.; Tataurov, A. V.; Wu, Y.; Manthey, J. A.; McQuisten, K. A.; Almabrazi, H. G.; Pedersen, K. F.; Lin, Y.; Garretson, J.; McEntaggart, N. O., Idt Scitools: A Suite for Analysis and Design of Nucleic Acid Oligomers. *Nucleic Acids Research* **2008,** *36* (suppl_2), W163-W169.
(47) Akagi, Y.; Gong, J. P.; Chung, U.-i.; Sakai, T., Transition between Phantom and Affine Network Model Observed in Polymer Gels with Controlled Network Structure. *Macromolecules* **2013,** *46* (3), 1035-1040.
(48) Parada, G. A.; Zhao, X., Ideal Reversible Polymer Networks. *Soft Matter* **2018,** *14*, 5186-5196.

(49) Owczarzy, R.; Moreira, B. G.; You, Y.; Behlke, M. A.; Walder, J. A., Predicting Stability of DNA Duplexes in Solutions Containing Magnesium and Monovalent Cations. *Biochemistry* **2008,** *47* (19), 5336-5353.
(50) Nakano, S.-i.; Fujimoto, M.; Hara, H.; Sugimoto, N., Nucleic Acid Duplex Stability: Influence of Base Composition on Cation Effects. *Nucleic Acids Research* **1999,** *27* (14), 2957-2965.
(51) Rubinstein, M.; Colby, R. H., *Polymer Physics*. Oxford: Oxford University Press: 2003.
(52) Xing, Z.; Caciagli, A.; Cao, T.; Stoev, I.; Zupkauskas, M.; O'Neill, T.; Wenzel, T.; Lamboll, R.; Liu, D.; Eiser, E., Microrheology of DNA Hydrogels. *Proc. Nat. Acad. Sci.* **2018**, 201722206.
(53) Bomboi, F.; Romano, F.; Leo, M.; Fernandez-Castanon, J.; Cerbino, R.; Bellini, T.; Bordi, F.; Filetici, P.; Sciortino, F., Re-Entrant DNA Gels. *Nat. Commun.* **2016,** *7*, 13191.
(54) Pan, W.; Wen, H.; Niu, L.; Su, C.; Liu, C.; Zhao, J.; Mao, C.; Liang, D., Effects of Chain Flexibility on the Properties of DNA Hydrogels. *Soft Matter* **2016,** *12* (25), 5537-41.
(55) Grimm, M.; Jeney, S.; Franosch, T., Brownian Motion in a Maxwell Fluid. *Soft Matter* **2011,** *7* (5), 2076-2084.
(56) Shao, Y.; Jia, H.; Cao, T.; Liu, D., Supramolecular Hydrogels Based on DNA Self-Assembly. *Accounts of chemical research* **2017,** *50*, 659-668.
(57) Li, C.; Chen, P.; Shao, Y.; Zhou, X.; Wu, Y.; Yang, Z.; Li, Z.; Weil, T.; Liu, D., A Writable Polypeptide–DNA Hydrogel with Rationally Designed Multi‐Modification Sites. *Small* **2015,** *11* (9-10), 1138-1143.
(58) Yue, L.; Wang, S.; Wulf, V.; Willner, I., Stiffness-Switchable DNA-Based Constitutional Dynamic Network Hydrogels for Self-Healing and Matrix-Guided Controlled Chemical Processes. *Nat. Commun.* **2019,** *10* (1), 1-10.
(59) Wang, C.; Fadeev, M.; Zhang, J.; Vázquez-González, M.; Davidson-Rozenfeld, G.; Tian, H.; Willner, I., Shape-Memory and Self-Healing Functions of DNA-Based Carboxymethyl Cellulose Hydrogels Driven by Chemical or Light Triggers. *Chem. Sci.* **2018,** *9* (35), 7145-7152.
(60) Holle, A. W.; Young, J. L.; Van Vliet, K. J.; Kamm, R. D.; Discher, D.; Janmey, P.; Spatz, J. P.; Saif, T., Cell–Extracellular Matrix Mechanobiology: Forceful Tools and Emerging Needs for Basic and Translational Research. *Nano Letters* **2018,** *18* (1), 1-8.
(61) Xia, Y.; Pfeifer, C. R.; Cho, S.; Discher, D. E.; Irianto, J., Nuclear Mechanosensing. *Emerg. Top Life Sci.* **2018,** *2* (5), 713-725.
(62) Özkale, B.; Sakar, M. S.; Mooney, D. J., Active Biomaterials for Mechanobiology. *Biomaterials* **2020**, 120497.

3 Hierarchical Mechanical Transduction of Precision-Engineered DNA Hydrogels with Sacrificial Bonds

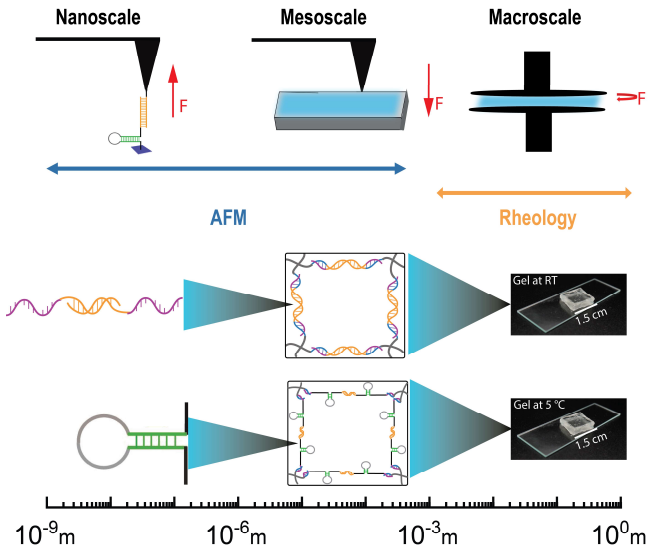

Figure 3.1. Table of contents graphic.

Preliminary note: This chapter is based on collaborative work conducted within the livMatS Cluster of Excellence, as published in the journal article "Hierarchical Mechanical Transduction of Precision-Engineered DNA Hydrogels with Sacrificial Bonds. *ACS Applied Materials & Interfaces*, **2023**, *15* (51), 59714-59721. DOI: 10.1021/acsami.3c15135" by Max Lallemang (ML)[†], **Cecilia Oluwadunsin Akintayo (COA)[†]**, Christiane Wenzel (CW), Weixiang Chen (WC), Lucca Sielaff (LS), Alexander Ripp (AP), Henning J. Jessen (HJJ), Bizan N. Balzer (BNB), Andreas Walther (AW)*, and Thorsten Hugel (TH)*. Minor changes in the text and formatting have been made to improve clarity and readability.

[†] These authors contributed equally to this work. *Corresponding author.

Author´s contributions: COA and ML contributed equally to this work. **COA** synthesized the DNA linkers and prepared the DNA based hydrogels. **COA** conducted the rheological characterizations while ML performed AFM imaging and analysis. CW, WC, LS, and AR provided support with secondary experimental measurements. COA, ML, BNB, HJJ, AW and TH designed the research and experiments. **COA** and ML wrote the manuscript and made the figures, which was revised by BNB, HJJ, AW and TH. All authors gave approval to the final version of the manuscript.

3.1 Abstract

Engineering the response to external signals in mechanically switchable hydrogels is important to promote smart materials applications. However, comparably little attention has focused on embedded precision mechanisms for autonomous nonlinear response in mechanical profiles in hydrogels, and we lack understanding of how the behavior from the molecular scale transduces to the macroscale. Here, we design a nonlinear stress-strain response into hydrogels by engineering sacrificial DNA hairpin loops into model network hydrogels formed from star-shaped building blocks. We characterize the force-extension response of single DNA hairpins and are able to describe how the specific topology influences the nonlinear mechanical behavior at different length scales. For this purpose, we utilize force spectroscopy as well as microscopic and macroscopic deformation tests. This study contributes to a better understanding of designing nonlinear strain-adaptive features into hydrogel materials.

3.2 Introduction

Responsiveness in soft matter materials is pivotal to the design of smart and switchable materials, but represents also an important aspect for the design of more life-like and self-adapting materials, wherein more complex energy landscapes need to be designed.[1] One important step in the field of mechanical materials is the design of non-linear responses.[1-2] Traditionally, there has been great success regarding shear-thinning or shear-thickening gels. More recently, these materials have been critically expanded by strain-stiffening hydrogels that mimic the behavior of biological tissues more closely, and which are important to engineer cell fate.[3-4] Additionally, sacrificial bonds, such as in metal-ion crosslinked hydrogels have been reported, mainly to toughen hydrogels.[5-7] However, often the underlying mechanisms are not fully understood from the microscale to the macroscale level, and their response is mostly based on inter-polymer interactions.[8-10]

To enable a better understanding and to obtain more complex responses, it is critical to integrate precise bottom-up construction strategies for the molecular effectors giving rise to the targeted behavior, as well as for the hydrogel topology which embeds these molecular effectors. The programmability of DNA motifs[11-15] enables to precision-engineer molecular effectors,[16-21] but those need to be combined with a defined hydrogel network to have a chance that the randomness of typical hydrogel networks, formed for instance by radical polymerization, as well as connectivity defects and topological defects of bulky DNA units outweigh all effects from the molecular engineering at large length scales. Formation of model network

hydrogels could be addressed by our recently discovered large scale synthesis for well-defined star-shaped poly(ethylene glycol)-DNA (starPEG) conjugates via liquid phase synthesis.[19, 22]

In contrast to more established DNA hydrogels, that use common single-stranded DNA to double-stranded DNA (ssDNA, dsDNA) transitions for engineering mechanical properties that are switchable by external triggers using temperature or pH,[12, 14, 23-27] we herein focus on the integration of a DNA hairpin loop motif with an intrinsically embedded non-linear mechanical response profile. Here, we use the term non-linear to describe a discontinuity in the force-extension curve in addition to the trivial discontinuity when the attachments rupture. How this non-linearity, which is well defined for a single molecule, translates into hydrogels is topic of this study. Our basic hydrogel consists of two building blocks. The first is a starPEG-DNA[19, 22] of molecular weight 66 kDa containing 20 adenine units as terminal blocks (starPEG-A_{20}). The second building block is a bivalent linker containing a palindromic segment and terminal parts of 20 thymine units (T_{20}). The formation of a starPEG-DNA hydrogel with a reasonably well controlled network structure occurs via T_{20}/A_{20} hybridization of the two different building blocks (**Figure 3.2a**, left).

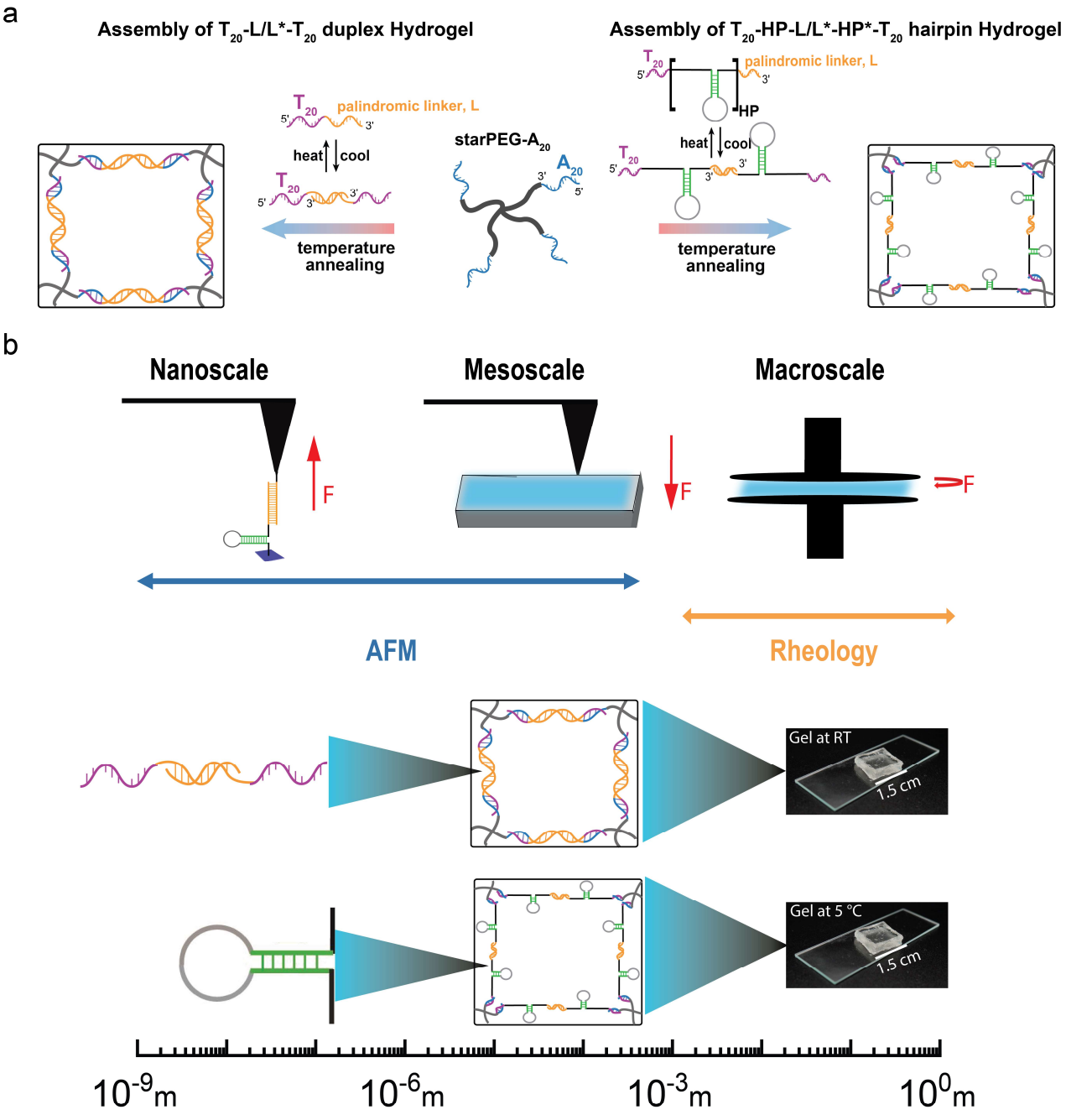

Figure 3.2. Hydrogel assembly and characterization methods across scales. (a) Schematic overview of starPEG-DNA hydrogel assembly. Following the synthesis of the starPEG-A_{20} building block, as we previously reported, the DNA duplex linker (left) and the DNA hairpin loop linker (right) building block are synthesized via automated solid phase oligonucleotide synthesis. The starPEG-DNA hydrogel formation is triggered by duplex hybridization of the A_{20} and T_{20} overhangs in the building blocks. **(b)** Top: Schematic depiction of the three different methods used to quantify the non-linear force-extension response of DNA hairpin loops and duplexes at the nanoscale with AFM (left), the mechanical properties at the mesoscale with AFM (middle) and the G-modulus at the macroscale with rheology (right). Bottom: Schematic images of the building blocks, ideal hydrogel structure and representative final hydrogels at the temperatures where self-standing gels are observed.

Here, we aim to implement a functional DNA linker with a non-linear stress-strain response into the hydrogels by replacing the bivalent linker with two DNA hairpin loops (**Figure 3.2a**, right). The DNA hairpin

loops are the programmable elements, which represent ideal candidates to study non-linear reversible extension behavior upon application of an external force. Such DNA hairpin loops form, when two complementary regions of the same ssDNA strand hybridize, resulting in a stem region with an unpaired DNA hairpin loop.[28] The length and the sequence of the stem region can be defined, and are the molecular programming elements to change both the unzipping force and unzipping work needed for opening. Together with the loop, a hidden length scale is provided, which has been characterized or implemented before in other systems.[29-33] Such hairpins give rise to a well-qualified molecular structure to study strain-adaptive behavior. Strain-adaptive materials are able to maintain structural integrity and endure a range of stiffness from small to large strains. Altogether, this creates a pathway towards overarching design principles from molecular-level folding motifs to a controlled network topology when incorporated into a hydrogel. In contrast to, e.g., strain-stiffening materials,[34-35] non-linear stress-strain response occurs via pulling of the DNA hairpin loop itself (intra-strand), but does not result from inter-strand interactions. Wherever appropriate, DNA hairpin loop samples are compared to control samples formed by simple palindromic linkers.

In the following, we characterize the occurring mechanical processes at different length scales. At the nanoscale (**Figure 3.2b**, left), the response and non-linear behavior of single polymers, DNA hairpin loops or DNA duplexes can be characterized by atomic force microscopy (AFM)-based single molecule force spectroscopy (SMFS) (see **Table 3.1** for the oligonucleotide sequence and **Table 3.3** for melting temperatures).[30, 36-43] At the mesoscale, AFM-based nanoindentation provides information about the mechanical properties of the material using contact mechanics (**Figure 3.2b**, middle).[44] Rheological analysis outlines the mechanical behavior of the hydrogels at the macroscopic scale. The response of the hydrogels to temperature (temperature sweep), to varying oscillation frequencies (frequency sweep) and oscillation amplitude (amplitude sweep) provides an understanding of various characteristic properties, such as sol/gel transition temperatures, bond relaxation times, yield strain and mesh size (**Figure 3.2b**, right). Here, we combine all these methods to compare the mechanical properties at different length scales and to create a bridge between nanoscopic, mesoscopic and macroscopic properties of such responsive materials.

3.3 Results and Discussion

For SMFS, we covalently attached the DNA hairpin loop to a SiO_x substrate via silane-PEG-NHS (5 kDa, NHS = *N*-Hydroxysuccinimide) linker and the complementary strand via silane-PEG-NHS (5 kDa) linker to an AFM cantilever tip. This arrangement ensures that the DNA hairpin loop is opened first via unzipping and subsequently, the DNA duplex opens via a shear mechanism (**Figure 3.3a**). It has already been shown that an unzipping force is lower than a shear force for similar DNA duplexes.[45] **Figure 3.3b** shows a typical force-extension trace for such an experiment. Successive force-extension curves (force mapping) allow to determine the unzipping force at room temperature as (70 ± 4) pN. The unzipping forces are in good agreement with previous studies [30-31, 46-48] considering the loading rate dependence of the unzipping force.

The length increment ΔL_{Cont} between the two consecutive stretches, where the first stretch accounts for the unzipping of the DNA loop and the second stretch for the rupture of the DNA duplex (**Figure 3.3b**), amounts to (41 ± 4) nm, which corresponds well with the expected change in contour length for 36 base pairs taking into account that a force of approx. 70 pN is applied to the construct. The length of one base pair in ssDNA in its B-form is approx. 0.67 nm at low force [49] and becomes longer by approx. a factor of 1.5 at approx. 35 pN (higher forces were not determined in this reference).[50] We obtain a factor of approx. 1.7 leading to a difference in the contour length of 41 nm, which is also consistent with previous AFM experiments.[51] The full mean contour length of 146 nm is also consistent with the used molecules as follows: We have two 5000 Da PEG, i.e., approximately 60 nm in total, which is extended to approx. 80 nm at higher force, taking into account that PEG is in its ttg conformation at low force of a few pN (0.28 nm/Monomer) and ttt conformation at high force of several tens of pN (0.36 nm/Monomer).[52] Together with the contour length of 41 nm of the hairpin and a few nm from the dsDNA regions this is almost 146 nm.

Altogether, our force-extension traces prove the successful formation of a surface-hairpin-DNA-cantilever construct.[53-55] In particular, the SMFS characterization clearly shows a non-linear force-extension response for the DNA hairpin loop building block. We assume that the non-linearity of the force-extension response is not affected by the temperature range used throughout this work. However, the degree of extension of the DNA chain at a certain force could vary in dependence on the temperature, as studied previously for PEG and PNiPAM.[37]

Next, we determine how this molecular non-linear force-extension response is transferred to the mesoscale using AFM indentation experiments (see **SI Table 3.2** for the oligonucleotide sequence and **Figure 3.4** for

the Nucleic acid Package (NUPACK) simulations to obtain the structure of the DNA linkers and their corresponding secondary structures). For a better understanding, we now compare the response of a DNA duplex hydrogel and a DNA hairpin hydrogel at a temperature of 5 °C (**Figure 3.3c,d**). We first quantify the approach curves by using the Hertz model (see Supporting Information for a detailed description). The elastic modulus, *E*, of the DNA hairpin hydrogel amounts to (1.1 ± 0.1) kPa, while the elastic modulus of the DNA duplex hydrogel is (6.5 ± 0.9) kPa (**SI Figure 3.5** shows exemplary curves with the Hertz model fit). This can be explained with the lower total amount of crosslinking units per volume element due the larger DNA construct used as a linker. The values are overall in a range reported for DNA-based hydrogels, namely 0.4 - 100 kPa.[56-58] In **SI Figure 3.6**, more force-extension curves for the DNA duplex and hairpin hydrogels are shown.

Next, we quantify the dissipated energy of the two hydrogels, defined as the area between the retract and approach force-extension curves. Critically, due to the adhesion between the AFM cantilever tip and hydrogel, it is possible to observe a non-linear response in the retraction curve. We find a comparable energy dissipation for the DNA duplex hydrogel of $(7.2 \pm 2.8) \cdot 10^{-16}$ J and the DNA hairpin hydrogel of $(6.4 \pm 1.9) \cdot 10^{-16}$ J.

The pronounced difference in the shape of the retraction curves stands out: In the case of the DNA duplex hydrogel, a relatively smooth curve with a high maximum force and short adhesive elongation is found that is similar to previously reported hydrogels.[59-61] In striking contrast, the DNA hairpin hydrogel shows prolonged adhesive interactions with sawtooth patterns, which indicate a continued opening of several DNA hairpin loops, as detailed in the following. The curve displays several small peaks usually with decreasing magnitude of the bond rupture peaks along the extension (**Figure 3.3d**). The lowest peak force (peak 1 in **Figure 3.3d**) has an average peak force of (59 ± 23) pN, followed by (125 ± 13) pN, (190 ± 25) pN, (288 ± 19) pN, (345 ± 16) pN, (408 ± 23) pN and finally (499 ± 33) pN for the higher peak forces (**Figure 3.3e**). Such a series of rupture peaks has previously been assigned to sacrificial bonds, e.g., in the bone matrix.[62] Moreover, the most likely explanation for the decreasing peak force at higher extensions is a decrease of the number of sacrificial bonds ruptured in parallel.[63] This actually fits very well with the expected structure of the DNA hairpin hydrogel, where several DNA hairpin loops (sacrificial bonds) can open in parallel. In particular, that suggests that not all loops in a plain open at the same time, because then the contour length gain should be doubled (two hairpins per chain) at similar forces, i.e., 82 nm, if the strain is in the direction of the unit cells. As that is very unlikely, a quantitative comparison of the length gains is not possible.

Nevertheless, the peaks in the extension trace show that there is some cooperativity in hairpin opening, i.e., some aligned nano- or microdomains. By contrast, in the case of full cooperativity, there would be only one rupture peak in the retract curve. Altogether, our data is best explained by domains of well oriented DNA structures in the hydrogel.

The mesoscale retraction trace even allows for a more quantitative evaluation by estimation of the number of DNA hairpin loops opening in parallel. The average work for opening of the DNA hairpin loop in the SMFS experiment (the area below the force-extension curves up to the first peak) amounts to approx. $9.3 \cdot 10^{-19}$ J. At the mesoscale (**Figure 3.3d**), the detachment peak (peak 1) shows a work of approx. $9.5 \cdot 10^{-18}$ J, which strongly hints towards the opening of around ten DNA hairpin loops in parallel (breaking of sacrificial bonds). Peak 2 shows a work of $1.6 \cdot 10^{-17}$ J, which would correspond to a simultaneous opening of 17 DNA hairpin loops. The work of the 3rd, 4th, 5th and 6th peak amounts to $2.0 \cdot 10^{-17}$ J, $1.9 \cdot 10^{-17}$ J, $3.3 \cdot 10^{-17}$ J and $3.9 \cdot 10^{-17}$ J, respectively. The highest force peaks (peak 7 and 8) correspond to about $4.7 \cdot 10^{-17}$ J, which indicate opening of around 50 DNA hairpin loops in parallel. Altogether, the nanoindentation data show that a non-linear response, programmed into single DNA polymers, translates to the local mesoscale elastic response in starPEG-DNA hydrogels. The response is not an 'all or nothing' one anymore, as found for single polymers in SMFS, but distinct steps can be locally retrieved. These steps (peaks) likely result from the opening of several DNA hairpin loops in parallel, i.e. some nano- or microdomains. Assuming a mesh size of 80 nm (see below), 50 hairpin loops would correspond to about 0.03 μm^3.

Next, we characterize the global mechanical properties of the hydrogels at the macroscale using plate/plate rheology (**Figure 3.3f,g**). The most important equivalent to the previous unidirectional mechanical tests is the deformation/strain sweep in **Figure 3.3h**, but in the interest of a comprehensive discussion, we also report temperature and frequency sweeps of both hydrogels. **Figure 3.3f** shows the rheological temperature sweeps of the hydrogels. The sol/gel transition temperature is defined by the G'/G'' crossover temperature, T_{co}, and is depicted by an arrow in the graph. The DNA duplex hydrogel shows a high T_{co} at 43 °C, while the DNA hairpin hydrogel shows T_{co} at 14 °C. While the DNA hairpin hydrogel corresponds to a very soft hydrogel that is barely self-supporting at room temperature the DNA duplex hydrogel is a stable self-supporting gel, without visible flow at room temperature. The temperature sweeps show a lower storage modulus for the hairpin hydrogels, G' at low temperatures ($G'_{10\,°C}$ = 300 Pa for the DNA duplex hydrogel; $G'_{10\,°C}$ = 7 Pa for the DNA hairpin hydrogel). Furthermore, frequency sweeps are conducted at 10 °C, to ensure a solid gel state for both materials, to investigate the dynamics of the DNA crosslinkers (**Figure 3.3g**). The DNA duplex

hydrogel does not relax within the measured frequency range, while the hairpin hydrogel shows a bond relaxation time at τ = 16.5 mins. Thus, overall the hairpin hydrogel is softer than the DNA duplex hydrogel. Note that the second crossover at high frequency for the DNA hairpin hydrogel indicates the onset of the transition regime before going into the elastically dominated/glassy part at very high frequency.

These differences are not surprising, because both hydrogels are made at the overlap concentration, c^*, of the starPEG-OH as an important constant parameter with two DNA constructs of significantly different size (**SI Figure 3.7**). The presence of a long DNA linker between each starPEG arm in the DNA hairpin system thus hinders the dynamic formation of a network topology and extensive coiling of the PEG chains in the DNA hairpin loop hydrogel network, which explains the lower mechanical consistency.

This can in fact be correlated with the mesh size ξ of the hydrogels which is calculated with the following equation:

$$\xi = \left(\frac{k_B T}{G'}\right)^{\frac{1}{3}} \tag{5}$$

with k_B being the Boltzmann constant, G' and T values are obtained during oscillatory temperature sweep. At T = 10 °C, the DNA duplex hydrogel has a mesh size of approx. 24 nm, while the DNA hairpin hydrogel has a mesh size of approx. 80 nm (**SI Figure 3.7c**). This is consistent with their expected structure, as the DNA duplex hydrogel contains 54 dsDNA nucleotides (nts) between each crosslink, while the DNA hairpin hydrogel contains 54 dsDNA nts and 56 ssDNA nts between crosslinks. The size of a nucleotide in ssDNA is approx. 0.67 nm, while dsDNA is approx. 0.34 nm,[64] resulting in a theoretical length of 18 nm for the DNA duplex hydrogel and 56 nm for the DNA hairpin hydrogel.

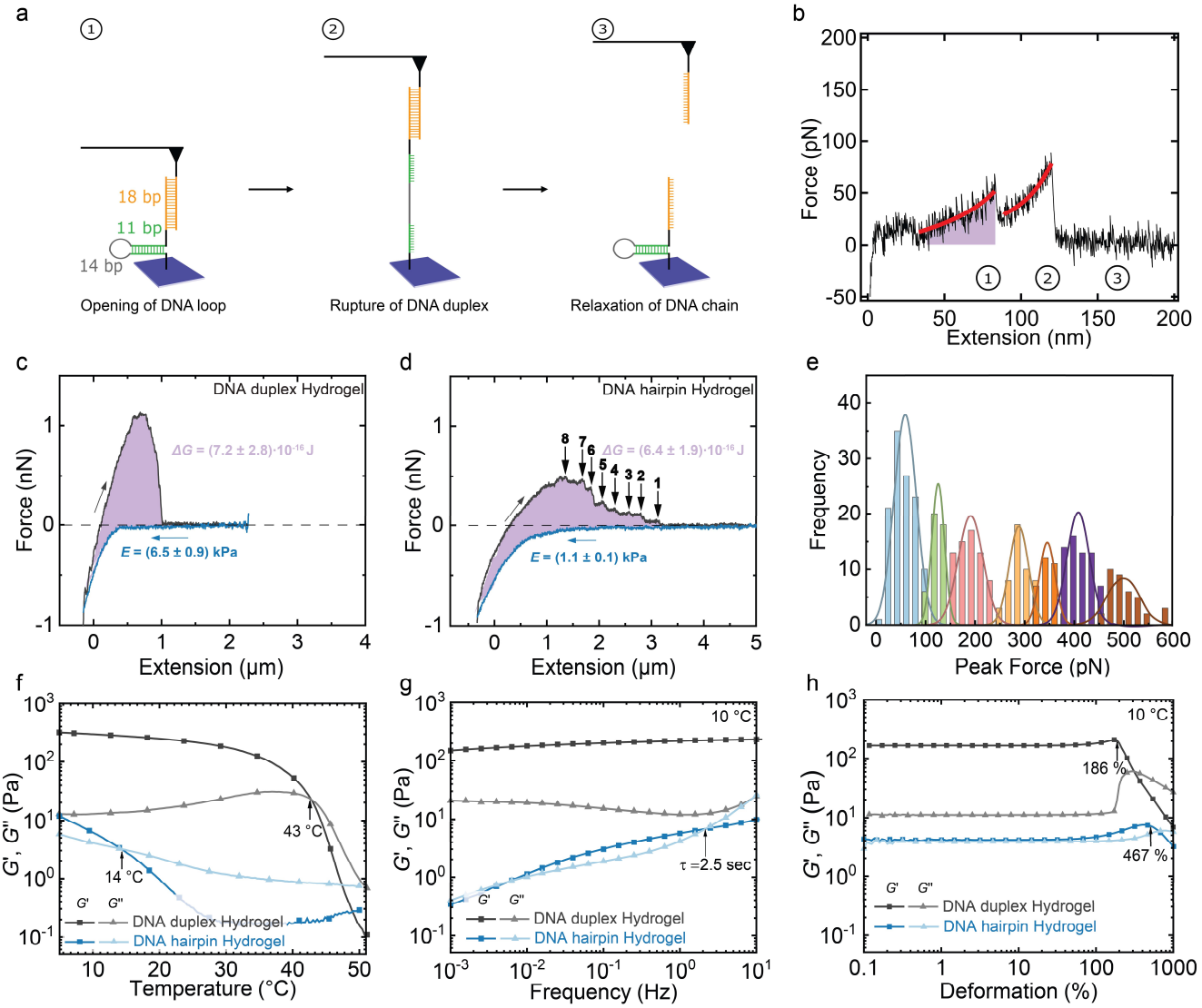

Figure 3.3. Quantification of the designed mechanical response across scales. (a) Schematics of the AFM-based force-extension experiment to characterize the DNA hairpin loop. **(b)** Exemplary force-extension trace showing the stretching of the complete construct with the opening of a DNA loop ①, rupture of the DNA duplex in shear geometry ② and relaxation of the DNA chain ③. The wormlike chain (WLC) model is used to fit the 1st and 2nd stretch of each force-extension curve (in red) in order to calculate the 1st and 2nd contour length to finally determine the difference in the contour length ΔL_{Cont}. The area under the first stretch (purple) indicates the work needed to open the DNA hairpin loop. **(c)** and **(d)**, approach (blue) and retract (black) force-extension curves are shown for the DNA duplex and hairpin hydrogels, respectively. The area between the curves (purple) indicates the dissipated energy. Most strikingly, the force-extension trace for the DNA hairpin hydrogel shows much larger extensions and several peaks, indicating the rupture of sacrificial bonds associated with the opening of the DNA hairpin loops. Out of all the peaks (sawtooth pattern), 8 are exemplary shown (indicated by the black arrows). **(e)** Distribution of the peak forces for the DNA hairpin hydrogel. **(f)** Temperature sweep of the DNA duplex hydrogel and DNA hairpin hydrogel (f = 1 Hz, γ = 6%, (5 - 50) °C, temperature rate = 0.4 °C/min; 25 mM $MgCl_2$, 150 mM NaCl). The sol-to-gel crossover temperature T_{co}, is indicated by the black arrows. **(g)** Frequency sweep of the hydrogels (f = (0.001 - 100) Hz, γ = 1%, 10 °C; 25 mM $MgCl_2$, 150 mM NaCl). While the bond relaxation time τ for the DNA hairpin hydrogel is depicted by an arrow (blue curve), the DNA duplex hydrogel does not relax within the measured frequency range (gray curve). **(h)** Amplitude sweep of DNA duplex hydrogel (gray curve) and DNA hairpin hydrogel (blue curve) (γ = (0.1 - 600)%, f = 1 Hz, 10 °C; 25 mM $MgCl_2$, 150 mM NaCl). The yield point is the value of G'_{yp} at the yield strain, γ_{yp}. γ_{yp} is the value of the shear strain at the limit of the linear viscoelastic region and depicted by an arrow.

As emphasized above, an important comparison to the molecular and mesoscale mechanical characterization comes from strain sweeps in oscillatory rheology (**Figure 3.3h**) to determine the onset of

flow and structural disruption. These measurements are also conducted at 10 °C to ensure a solid hydrogel structure. The yield strain, γ_{yp}, is the most appropriate parameter to describe the onset of non-linear viscoelastic behavior and is determined by the value of the shear strain at the limit of the linear viscoelastic region (LVE). The LVE region indicates the range in which the oscillatory strain sweep can be performed without destroying the sample structure. G' and G'' show a constant value to increasing strains within the LVE region. Strikingly, the γ_{yp} of the hairpin hydrogel is almost three times higher (ca. 467%) than that of the duplex hydrogel (ca. 186%). Hence, the hairpin hydrogel is visibly more stretchable than the duplex hydrogel. The hairpin building block is larger than the duplex building block and it contains flexible parts of ssDNA.

In order to gain a better understanding on the role of network structure in macroscale characterization via oscillatory rheology, we introduced deliberate defects into the DNA duplex network and measured the mechanical behavior of these hydrogels (**SI Figure 3.8**). The defects are introduced by adding a monovalent T_{20} dummy strand that blocks one of the arms of the starPEG-A_{20} and hinders arm-to-arm connections (**SI Figure 3.8a**). The hydrogels are termed D-$gel_{10\text{-}40}$ with the following defect amounts (D-gel_{10} = 10% defects; D-gel_{20} = 20% defects; D-gel_{30} = 30% defects; D-gel_{40} = 40% defects, **SI Figure 3.8b**). The temperature sweep in **SI Figure 3.8c** shows a slight decrease in the crossover Temperature, T_{co}, with increasing percentage of T_{20} dummy strand (defect). T_{co} is between 40 and 43 °C for all measured hydrogels with the exception of the hydrogel containing the highest number of defects, D-gel_{40} (T_{co} = 28 °C). This indicates that the dynamics of the crosslinks are quite similar for D-$gel_{10\text{-}30}$. Furthermore, a distinct decrease in G' with increasing defect content is observed. Hydrogels with more defects display a lower $G'_{10\ °C}$ (**SI Figure 3.8f**). Furthermore, the strain sweep (**SI Figure 3.8d**) shows an increase in the yield strain, γ_{yp}, and a decrease in the yield point, G'_{yp}, with increasing amount of defects. D-gel_{10} contains the lowest percentage of defects and displays a G'_{yp} of 110 Pa at 10 °C and γ_{yp} at 234%, while D-gel_{40} yields at γ_{yp} = 540% with G'_{yp} = 10 Pa at the same temperature (**SI Figure 3.8g**). Thus, we conclude that there is a relationship between the presence of a high number of defects and a high yield strain. Therefore, from the oscillatory rheology experiments, we can neither completely attribute stretchability/ high yield strain of the hairpin hydrogel to a high number of defects, nor to a property of hidden length scales of the DNA hairpin – it is likely a combination of both. Together with the insights from the nanoindentation experiments the most consistent explanation for our observations are a significant contribution from hidden length scales of the DNA hairpin beyond the introduction of defects.

3.4 Conclusion

In conclusion, this chapter has shown and quantified how properties of molecular building blocks can be transferred to macroscopic hydrogels. A designed DNA hairpin served as a programmable molecular building block, containing one or several sacrificial bonds leading to a non-linear mechanical response. We show that this feature can be transferred into the local response of a macroscopic hydrogel. The global response of the hydrogel shows evidence for the molecular building blocks in the form of sacrificial bonds, because the yield strain of the macroscopic hydrogel is increased. Altogether, we could show how the stretchability, relaxation times and energy dissipation in starPEG-DNA hydrogels are affected by the molecular building blocks. We anticipate that the concept of combining defined hydrogel geometries with programmable building blocks allows for the design of hydrogels with novel properties.

3.5 Experimental

3.5.1 Materials

The following reagents and solvents were used as received from the following suppliers: Ac-dC Synbase CPG 1000/110 (Link Technology), DMT-dA(bz) phosphoramidite, DMT-dG(dmf) phosphoramidite, DMT-dC(ac) phosphoramidite, DMT-dT phosphoramidite (Sigma-Aldrich, 99%, was dissolved 50mM in anhydrous acetonitrile), CAP A (Sigma Aldrich, tetrahydrofuran/pyridine/acetic anhydride, 8:1:1), CAP B (Sigma Aldrich, 10% methylimidazole in tetrahydrofuran), trichloroacetic acid Deblock (TCA Deblock, Sigma-Aldrich, 3% in DCM), 5-(Ethylthio)-1H tetrazole (ETT Activator, Sigma Aldrich, 0.25 M in ACN), oxidizer (Sigma Aldrich, Pyridine / Water / Iodine, 9:1:12.7), dichloromethane (DCM, Fischer Scientific U.K., CH_2Cl_2, analytical reagent grade), acetonitrile (ACN, Sigma-Aldrich, C_2H_3N), acetonitrile anhydrous (ACN, 99.8%, abcr GmbH), sodium chloride (NaCl, 99%, Sigma Aldrich), sodium hydroxide (NaOH, VWR), magnesium chloride ($MgCl_2$, 1M, Fischer Scientific), sodium dihydrogen phosphate (NaH_2PO_4, Sigma Aldrich), silicon oil (350cSt, Carl Roth GmbH), triethoxysilane-PEG-N-Hydroxysuccinimide ester (silane-PEG-NHS, NANOCS, M_w= 5 kDa), ultrapure water (H_2O, Purelab Chorus 1, Elga LabWater, Celle, 18.2 MΩcm), ammonia solution (NH_3, Roth, 28.0−30.0%), hydrogen peroxide (H_2O_2, Sigma-Aldrich, MO, ≥30%), toluene (Thermo Fisher Scientific), ethanol (Roth, ≥99.9%), borate buffer (50 mM, pH 8.5, Thermo Fisher Scientific), HEPES (Pan-Reac AppliChem) buffer (10 mM, 50 mM NaCl, pH 7.9), silicon oxide (SiO_x) wafers (Prime CZ-Si wafer, n-type (Phosphor) TTV<10 µm, MicroChemicals GmbH). StarPEG-A_{20} was synthesized as described in *Methods*.[22] The ssDNA for the AFM and SMFS experiments was purchased from IDT (Integrated DNA Technologies IDT), the ssDNA for substrate

functionalization was purchased from biomers.net GmbH. For the exact sequence see **Table 3.1**. The functionalizations are described in *Procedures and Synthesis*. All other DNA was synthesized as detailed in *Procedures and Synthesis.*

3.5.2 Instrumentation

High-performance liquid chromatography (HPLC) was performed on a Thermo Fischer Scientific Dionex Ultimate 3000 HPLC system. The sample was dissolved in Milli-Q water and measured using a gradient from 100% A to 90% B with solvent A being 0.1 M TEAA buffer (1/1) in 95/5 water/acetonitrile, and solvent B being acetonitrile.

UV-VIS measurements, used to determine the concentration of the DNA building blocks, were performed on an Analytik Jena ScanDrop 250 Spectrophotometer using a cuvette from Hellma with a path length of 3.0 mm.

Matrix-assisted laser-desorption-ionization time-of-flight mass spectrometry (MALDI-TOF MS) measurements were performed using 3-HPA (3-Hydroxypicolinic acid) and ammonium citrate di-basic as matrix. The measurements were conducted on an Autoflex III from Bruker.

Agarose gel electrophoresis (AGE): 2wt% Agarose solutions were prepared in tris-acetate EDTA buffer (TAE, containing 40 mM Tris, 20 mM acetic acid and 1 mM EDTA; pH 8.0) and the gel was stained with Roti-GelStain with a mixing ratio of 25 µL per 200 mL agarose solution. AGE was performed using a 20-sample gel chamber at a voltage of 105 V for 60 min. Images were captured with an Intas Chemostar ECL & Fluorescence Imager in UV transilluminator mode.

Rheological Characterization was performed on an Anton Paar Modular Compact Rheometer MCR 302 equipped with a 25 mm plate-plate geometry. Analysis of the data was done with the RheoCompass software. The storage, G', and loss moduli, G'', were measured in oscillation mode with a constant strain amplitude of 6%. This value was found to be in the linear viscoelastic range based on the results of an amplitude sweep at 1 Hz. Frequency sweeps were carried out on mixtures between 100 Hz and 0.001 Hz at a fixed strain of 1%. Temperature ramps were performed at a fixed frequency and strain of 1 Hz and 6%, respectively. The ramping rate of the temperature was 0.4 °C/min. Amplitude strain sweeps were performed at room temperature and a fixed frequency of 1 Hz. The gap between the plates was fixed at 0.2 mm and a thin layer of silicon oil was added around the measuring system to prevent evaporation.

SMFS measurements with the AFM. The SMFS measurements were performed on a MFP-3D-BIO (Asylum Research, an Oxford Instruments Company). Prior to the measurements, the inverse optical lever sensitivity, invOLS, was calculated by fitting a linear function to the indentation part of a force-extension curve. At least five different invOLS values were taken into account and averaged for each AFM cantilever used. As a next step, the cantilever was driven away from the substrate and the spring constant was determined using the thermal noise method.[65] First, a control cantilever (only silane-PEG-NHS tip functionalization) was measured on a control substrate. In a next step, a cantilever tip functionalized with silane-PEG-NHS and ssDNA was measured on the control substrate. Both steps are important, in order to guarantee a successful functionalization. Finally, the functionalized cantilevers were measured on the SiO_x substrate, which is functionalized with silane-PEG-NHS and the ssDNA hairpin loop. The following measurement parameters were used: velocity: 0.5 µm s^{-1}; contact force: 200-500 pN; sampling rate: ~3 kHz; dwell time towards substrate: 1-5 s; force distance: 1 µm. The force-extension curves were recorded in a grid-like manner comprising 10·10 points with a total area of 20·20 μm^2 (force maps). In case of a stretching event, the scan area was decreased around the area showing the event in order to increase the probability of hybridization of the complementary DNA ends. All measurements were performed in HEPES buffer at room temperature. At least two force maps were recorded at different spots on the respective substrate.

AFM Indentation Experiments. For nanoindentation experiments, an unfunctionalized silicon nitride AFM cantilever (MLCT-BIO-DC, Lever D, Bruker AFM probes) with a spring constant of approx. 0.03 Nm^{-1} has been used. All measurements were performed with a Cypher ES (Asylum Research, an Oxford Instruments company). Prior to the measurements, the invOLS was calibrated on a SiO_x substrate in HEPES buffer at 5 °C and the spring constant was calculated using the thermal noise method, as described above.[65] After the calibration of the cantilever, the substrate was exchanged and the measurement was continued on the DNA duplex hydrogel and DNA hairpin hydrogel in HEPES buffer at 5 °C. Due to the softness of the samples, the cantilever had to be driven manually towards the substrate. The following parameters were set for the indentation experiment: contact force: 0.5-0.1 nN; velocity: 10 µm s^{-1}; sampling rate: 5 kHz; dwell time towards substrate: 0 s. Approx. 1000 force-extension were recorded out of which 90 (~10%) showed molecular interaction events and were used for data evaluation. In total, 33 force-extension curves were obtained for the DNA hairpin hydrogel and 57 for the DNA duplex hydrogel.

3.5.3 Procedures and Synthesis

Synthesis and purification of oligonucleotide sequences

***Automated solid phase oligonucleotide synthesis*.** The oligonucleotides were synthesized on a H-8 custom LNA, DNA/RNA automatic synthesizer from K&A Laborgeräte at 10 µmol scale employing the standard solid phase β-cyanoethyl-phosphoramidite chemistry in trityl-on mode. The DNA phosphoramidites (DMT-dT, DMT-dA(bz), DMT-dG(dmf) and DMT-dC(ac)) were diluted to 50 mM with dry acetonitrile and synthesis occurred from the 3' towards the 5' end of the oligonucleotides on packed solid phase columns.

Deprotection and purification (general procedure for 10 µmol scale synthesis). Cleavage of the oligonucleotides from the solid support and base deprotection was achieved in one step to ensure optimal yields. The controlled pore glass (CPG) solid support was treated with 10 mL of a 50:50 wt% mixture of ethylenediamine:toluene for 2 h at room temperature. The deprotection solution was removed and the column was rinsed with 20 mL toluene to detach synthesized DNA from the support. The synthesized DNA sequence was then extracted with 5 mL Milli-Q water and purified by reverse phase-HPLC (RP-HPLC). The solvent was removed by freeze drying. After purification, the DMT group was cleaved by making a 2 wt% solution of the dry DNA in pH 4.0 (200 mM) NaOAc/HOAc buffer containing 200 mM NaCl and stirring at 50 °C for 1 h. Precipitation of the sample into a 5-fold excess of 2-propanol removed contaminants and exchanges counterions to sodium. The solvent was removed by freeze drying and the synthesized strands were stored at -20 °C until further use. The purity of the obtained oligonucleotides was confirmed with analytical HPLC and MALDI-TOF.

The ssDNA strands for the AFM cantilever tip and substrate are listed in **Table 3.1**.

Table 3.1. ssDNA linker data for the AFM cantilever tip and SiO_x substrate.

Linker	Full sequence 5' -> 3'	Molecular weight[a] / g mol^{-1}
Cantilever tip	5'-NH_2-TTC TAC TCA CCA TCT ATC CAC AAC TCT CAC ACA TCC TAC TAC GTC TAC TCA TCC TAC AGC CTA CAC TCA CCA TCT AAG TCA CGC TGC TGC CGA A-3'	28 541
Substrate	5'-NH_2-ATG TTG AAC CCG TAT AGG CGA CGA CCA AGC AGC AAA AAA AGG TCG TCG CCT CTA TCC TAA TTT TCG GCA GCA GCG TGA CT-3'	24 641

[a]The calculated molecular weights were determined with the oligo analyzer package from Integrated DNA Technologies (IDT).

Table 3.2. Overview of the synthesized linkers and its corresponding molecular weight.

Linker abbreviation	Full sequence 5' -> 3'	Molecular weight[a] / g mol^{-1}
T_{20}-L/L*-T_{20} duplex	5' TTT TTT TTT TTT TTT TTT TT GCA GCT GCA GCT GC	10348
T_{20}-HP-L/L*-HP*-T_{20} hairpin	5' TTT TTT TTT TTT TTT TTT TT ATG TTG AAC CCG TAT AGG CGA CGA CCA AGC AGC AAA AAA AGG TCG TCG CCT CTA TCC TAA TTG CAG CTG CAG CTG C	29474

[a]The calculated molecular weights were determined with the oligo analyzer package from Integrated DNA Technologies (IDT).

Table 3.3. Melting temperatures, T_m of the duplexes used in this work.

Nucleobase pair	T_m (°C)[a]
T_{20}/A_{20}	65.9
Hairpin stem	79.1
Palindromic linker, L/L*	81

[a] The melting points are determined with the Oligo Analyzer tool from Integrated DNA technologies (IDT). 1 mM DNA, 150 mM NaCl, 25 mM $MgCl_2$ concentration.

***Contour Length of the ssDNA*.** The ssDNA strand bound to the silane-PEG-NHS of the tip shows a contour length of ca. 63 nm (94bp), assuming a nucleotide length of 0.67 nm.[50] Accordingly, the ssDNA strand bound to the SiO_x substrate has a contour length of 54 nm (80bp). Both ssDNA strands comprise a 6C NH_2-linker in 5' in order to guarantee the successful reaction with the NHS ester of the PEG linker.

Hydrogel Preparation

***StarPEG-DNA hydrogel preparation*.** StarPEG-A_{20} and synthesized hairpin and duplex linker DNA were dissolved separately at desired concentration in a 25 mM Diphosphate EDTA buffer + 100 mM NaCl + 25 mM $MgCl_2$ (pH = 7.9) and the DNA concentration in the starPEG-A_{20} conjugate and in the linker DNA was determined by UV-Vis spectroscopy. StarPEG-DNA hydrogels were hybridized by mixing equimolar quantities of starPEG-A_{20} and linker-DNA in the same buffer. The sample was heated up to 75 °C for about 15 min and cooled to room temperature at about 1 °C/min. Samples were kept in the fridge at 4 °C until use. The oligonucleotide sequences of the bivalent DNA linkers are summarized in Table S2.

SMFS Experiments

***RCA cleaning*.** Prior to the atomic force microscopy (AFM) functionalization, the tweezers and glassware were incubated in a RCA 5:1:1 solution, i.e., H_2O, NH_3, H_2O_2, at 70 °C for 60 min. After the incubation, the glassware and tweezers were rinsed three times with H_2O, dried at 120 °C and stored at 120 °C until use.

***Cantilever tip functionalization*.** Silicon nitride AFM cantilevers (MLCT-BIO-DC, Bruker AFM probes, Camarillo, CA, USA) were used for all measurements. For the functionalization, the cantilevers were activated with oxygen plasma (40%, 0.1 mbar, 2 min, Diener Electronics) to obtain hydroxyl groups on the surface of the cantilever tips. As a next step, the 5 kDa silane-PEG-NHS linker was bound to the cantilever tip. To that aim, the cantilevers were incubated in a solution of silane-PEG-NHS in toluene at a concentration of 1.25 mg/mL for 2 h at 60 °C. Inactive PEGs act as a passivation layer to reduce undesirable interaction between the cantilever tip and the underlying substrate as well as between the single PEG polymer and the cantilever tip. The cantilevers were rinsed three times in toluene, twice in ethanol, one time in H_2O, one time in borate buffer and finally incubated for 1.5 h in a solution of ssDNA (100 nM, sequence in **Table 3.1**) in borate buffer at approx. 20 °C. Finally, the cantilevers were rinsed twice in borate buffer and once in HEPES buffer before storage in HEPES buffer at 4 °C. For every functionalization, control cantilevers were additionally prepared undergoing only the passivation step with silane-PEG-NHS.

***Substrate functionalization*.** For the functionalization of the substrate, SiO_x wafers with an approximate area of 0.25 cm^2 were used. The SiO_x wafers were sonicated (Elmasonic S15, Elma) for 10 min in ethanol. After sonication, the SiO_x wafers were treated with oxygen plasma (40%, 0.1 mbar, 2 min, Diener Electronics) to gain hydroxyl groups on the SiO_x substrate. Afterwards, the functionalization was done in two different ways: a) The wafers were incubated in a solution of 5 kDa silane-PEG-NHS linker (10 mg mL^{-1}) in toluene for 1.5-2 h at 60 °C and then rinsed three times in toluene, twice in ethanol, one time in H_2O and one time in borate buffer. The wafers were incubated in a solution of the ssDNA (6.25 µM, sequence in **Table 3.1**) in borate buffer at approx. 20 °C for 1-3 h (one wafer was incubated for 20 h). The wafers were rinsed twice in borate buffer and once in HEPES buffer before storage in HEPES buffer at 4 °C. b) The wafers were incubated in a solution of 5 kDa silane-PEG-NHS linker (25 mg mL^{-1}, the solution had to be heated to 60 °C for 1-2 min in order for the silane-PEG-NHS to fully dissolve in the toluene at this concentration) in toluene for 1.5-2 h at room temperature and then rinsed three times in toluene, twice in ethanol, one time in H_2O and one time in borate buffer. The wafers were incubated in a solution of ssDNA (6.25 µM, sequence in **Table 3.1**) in

borate buffer at approx. 20 °C for 1-3 h (one wafer was incubated for 20 h). The wafers were rinsed twice in borate buffer and once in HEPES buffer before storage in HEPES buffer at 4°C. For every functionalization, control wafers were additionally prepared undergoing only the passivation step with silane-PEG-NHS. Prior to the measurements, a high-resolution binding compound (101RF, Microset Products Ltd) was used to glue the wafer to an AFM fluid cell.

AFM Nanoindentation

***Sample preparation for AFM nanoindentation*.** The DNA duplex and DNA hairpin hydrogels were heated up to 65 °C and approx. 30 µL were deposited on a stainless steel clip (SPI Supplies) and cooled down to approx. 20 °C prior to the measurements.

Data Evaluation for the SMFS and Nanoindentation Experiments. A self-programmed software based on Igor Pro (Wavemetrics) has been used for correction and evaluation of the obtained SMFS force-extension curve, as described by Kolberg *et al.*[66] To calculate the contour length, a worm-like chain fit (WLC)[67] was used and calculated according to:

$$F = \frac{k_B T}{l_p}\left[\frac{z}{L_c} + \frac{1}{4\left(1-\frac{z}{L_c}\right)^2} - \frac{1}{4}\right] \tag{6}$$

where F is the force, z the extension, T the temperature, l_p the persistence length, L_c the contour length and finally k_B the Boltzmann constant.

For nanoindentation experiments, the approach force-extension curves were analyzed using Hertz model for contact mechanics (**SI Figure 3.5**).[68] For a pyramidal tip, the following equation has been used to calculate the elastic modulus, E:

$$E = \frac{F \cdot \sqrt{2} \cdot (1-\nu)^2}{\tan(\theta) \cdot \delta^2} \tag{7}$$

where F is the indentation force, ν the Poisson ratio (0.5), θ the semi-included angle of the tip (18.75°) and δ the indentation depth.[69]

For the calculation of the dissipated energy, the area between retract and approach force-extension curves was used.

To determine the peak force of the retract curve on the DNA hairpin hydrogel, a cursor was put on a local maximum of a stretch event or plateau before the force drops. Approx. 3-10 peak forces were obtained per retract curve.

3.6 Supplementary information

Nucleic Acid Package (Nupack) simulations of DNA strands

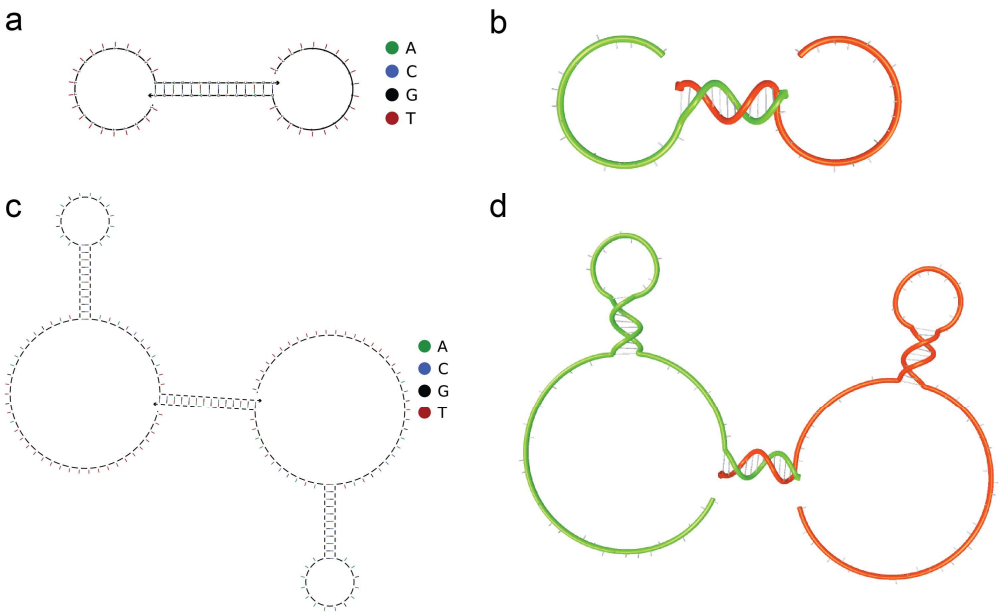

Figure 3.4. NUPACK Simulations showing (a) Minimum free energy, MFE structure of a DNA duplex linker at 25 °C. **(b)** Depiction of secondary structures with ideal helical geometry for stacked base pairs in a DNA duplex linker. **(c)** MFE structure of a DNA hairpin loop linker at 25 °C. **(d)** Depiction of secondary structures with ideal helical geometry for stacked base pairs in a DNA hairpin loop linker. Simulations were made using the NUPACK web server (accessible at http://www.nupack.org/).

Approach curves at the mesoscale

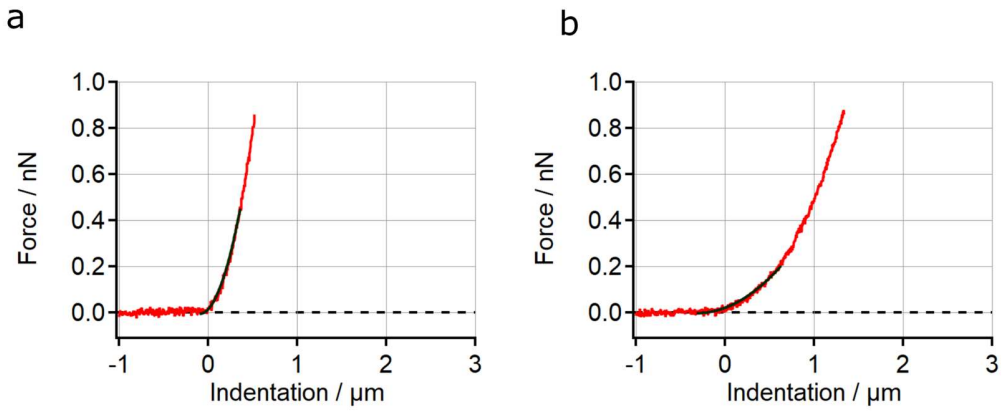

Figure 3.5. Approach curves (red) for (a) a DNA duplex hydrogel and **(b)** a DNA hairpin hydrogel measured in HEPES buffer at 5 °C. The black curve shows a Hertz model fit from which the elastic modulus was determined.

Additional force-extension curves for the DNA hairpin and duplex hydrogels

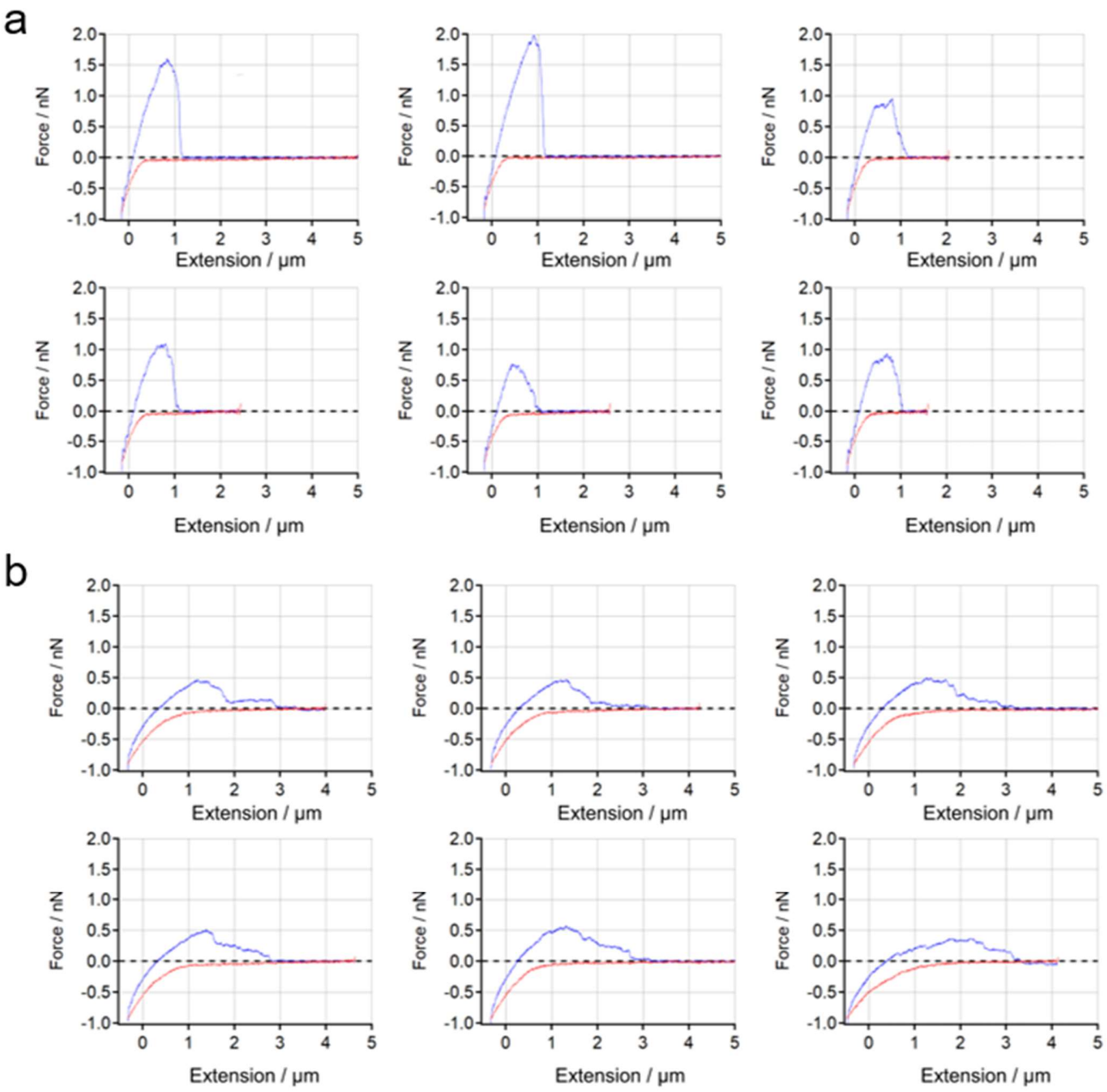

Figure 3.6. Additional force-extension curves on (a) a DNA duplex hydrogel and **(b)** a DNA hairpin hydrogel in HEPES buffer at 5 °C taken with an AFM.

Molecular weight determination and characterization of DNA linkers

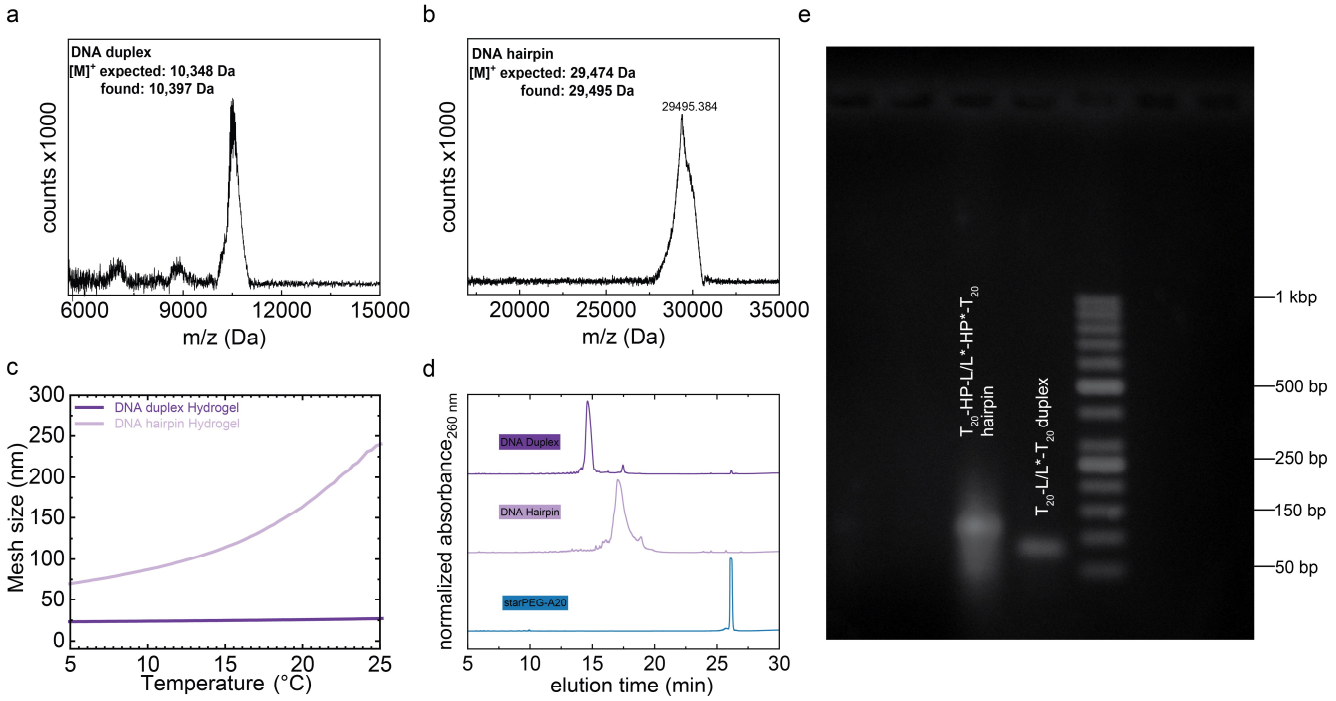

Figure 3.7. MALDI-TOF analysis of synthesized DNA linkers showing (a) a DNA duplex linker and **(b)** a DNA hairpin loop linker. **(c)** Plot showing changes in mesh size at different temperatures. **(d)** Analytical HPLC chromatograms of the purified DNA linker strands and starPEG-A_{20}. (e) AGE of the purified DNA linkers with 50 bp DNA ladder on both sides. The loaded 2 wt% agarose gel was stained with Roti-GelStain and separated at 105 V for 60 min. The AGE shows a single band for the duplex strand and a higher main band for the hairpin strand. The single band indicates that the hairpins assemble intramolecularly.

Rheological characterization of DNA duplex hydrogel with defects, D-gel

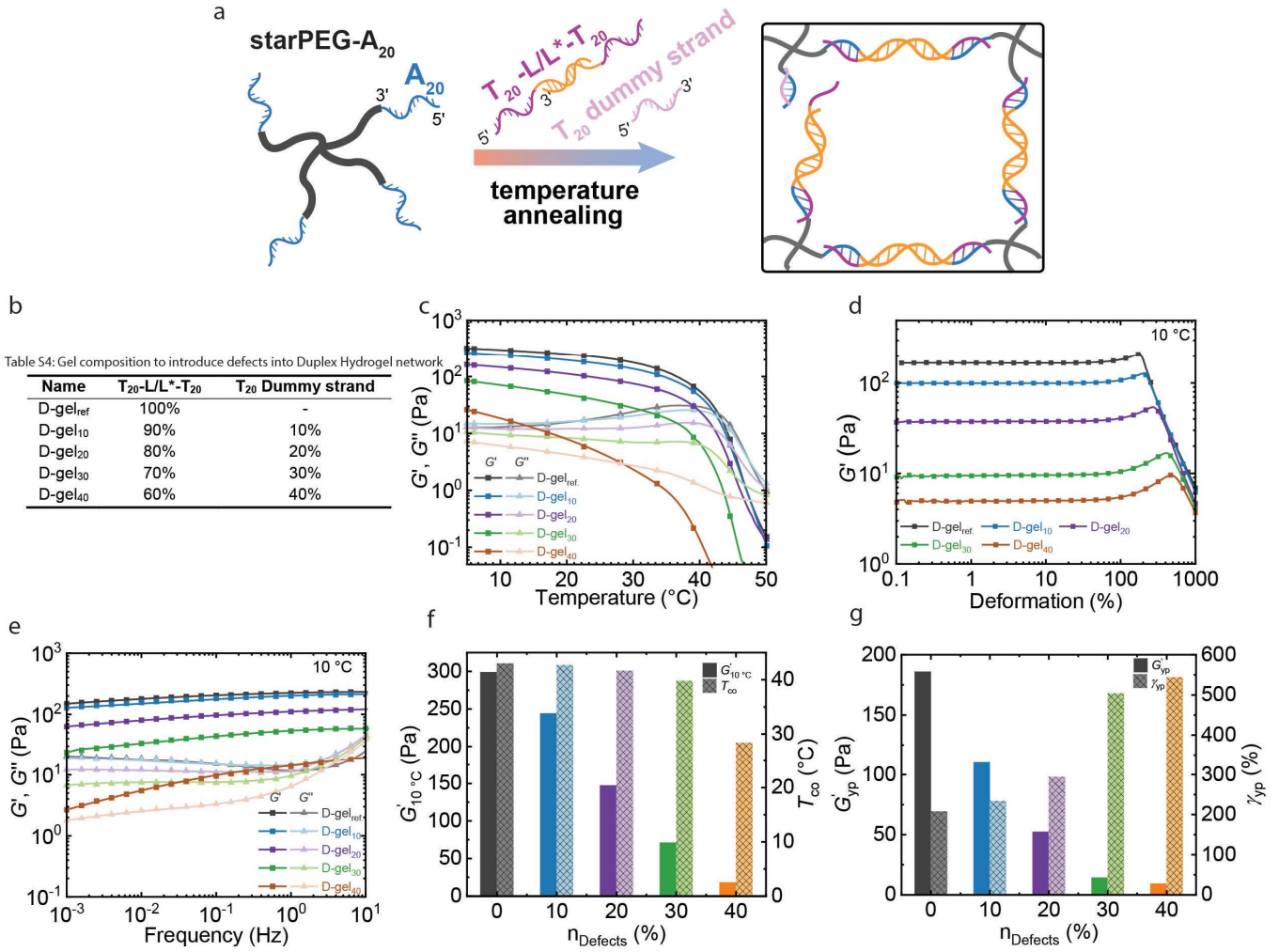

Table S4: Gel composition to introduce defects into Duplex Hydrogel network

Name	T_{20}-L/L*-T_{20}	T_{20} Dummy strand
D-gel_{ref}	100%	-
D-gel_{10}	90%	10%
D-gel_{20}	80%	20%
D-gel_{30}	70%	30%
D-gel_{40}	60%	40%

Figure 3.8. Duplex hydrogels containing defects. (a) General approach using dummy strands that block star/star coupling. **(b)** Table showing the defect hydrogel (D-gel) composition. **(c)** Temperature sweep of D-gels (f = 1 Hz, γ = 6%, (5 - 50) °C, temperature rate = 0.4 °C/min; 25 mM $MgCl_2$, 150 mM NaCl). **(d)** Amplitude sweep of D-gels (γ = (0.1 - 1000)%, f = 1 Hz, 10 °C; 25 mM $MgCl_2$, 150 mM NaCl). **(e)** Frequency sweep of the hydrogels (f = (0.001 - 100) Hz, γ = 1%, 10 °C; 25 mM $MgCl_2$, 150 mM NaCl). **(f)** Bar chart showing the evolution of the storage moduli at 10 °C, $G'_{10°C}$, and the G'/G'' crossover temperature (sol/gel transition temperature), T_{co} for the hydrogels with defects. **(g)** Bar chart showing the dependence of the yield point, G'_{yp}, and yield strain, γ_{yp}, on the number of defects.

3.7 References

(1) Walther, A., From Responsive to Adaptive and Interactive Materials and Materials Systems: A Roadmap. *Advanced Materials* **2020,** *32*, 1905111.

(2) Lehn, J. M., Perspectives in Chemistry—Aspects of Adaptive Chemistry and Materials. *Angewandte Chemie International Edition* **2015,** *54*, 3276-3289.

(3) Das, R. K.; Gocheva, V.; Hammink, R.; Zouani, O. F.; Rowan, A. E., Stress-Stiffening-Mediated Stem-Cell Commitment Switch in Soft Responsive Hydrogels. *Nature materials* **2016,** *15*, 318-325.

(4) Fernández-Castaño Romera, M.; Lou, X.; Schill, J.; Ter Huurne, G.; Fransen, P.-P. K.; Voets, I. K.; Storm, C.; Sijbesma, R. P., Strain-Stiffening in Dynamic Supramolecular Fiber Networks. *Journal of the American Chemical Society* **2018,** *140*, 17547-17555.

(5) Nakajima, T., Generalization of the Sacrificial Bond Principle for Gel and Elastomer Toughening. *Polymer Journal* **2017,** *49*, 477-485.

(6) Fukao, K.; Tanaka, K.; Kiyama, R.; Nonoyama, T.; Gong, J. P., Hydrogels Toughened by Biominerals Providing Energy-Dissipative Sacrificial Bonds. *Journal of materials chemistry B* **2020,** *8*, 5184-5188.

(7) Gong, J. P., Why Are Double Network Hydrogels So Tough? *Soft Matter* **2010,** *6*, 2583-2590.

(8) Guo, C.; Zeng, Z.; Yu, S.; Zhou, X.; Liu, Q.; Pei, D.; Lu, D.; Geng, Z., Highly Stretchable, Compressible, Adhesive Hydrogels with Double Network. *Journal of Polymer Research* **2021,** *28*, 1-9.

(9) Alam, K.; Iqbal, M.; Hasan, A.; Al-Maskari, N., Rheological Characterization of Biological Hydrogels in Aqueous State. *Journal of Applied Biotechnology Reports* **2020,** *7*, 171-175.

(10) Gharazi, S.; Zarket, B. C.; DeMella, K. C.; Raghavan, S. R., Nature-Inspired Hydrogels with Soft and Stiff Zones That Exhibit a 100-Fold Difference in Elastic Modulus. *ACS applied materials & interfaces* **2018,** *10*, 34664-34673.

(11) Merindol, R.; Loescher, S.; Samanta, A.; Walther, A., Pathway-Controlled Formation of Mesostructured All-DNA Colloids and Superstructures. *Nature nanotechnology* **2018,** *13*, 730-738.

(12) Fern, J.; Schulman, R., Modular DNA Strand-Displacement Controllers for Directing Material Expansion. *Nature communications* **2018,** *9*, 1-8.

(13) Seeman, N. C.; Sleiman, H. F., DNA Nanotechnology. *Nature Reviews Materials* **2017,** *3*, 1-23.

(14) Heinen, L.; Walther, A., Celebrating Soft Matter's 10th Anniversary: Approaches to Program the Time Domain of Self-Assemblies. *Soft Matter* **2015,** *11*, 7857-7866.

(15) Tabatabaei, S. K.; Pham, B.; Pan, C.; Liu, J.; Chandak, S.; Shorkey, S. A.; Hernandez, A. G.; Aksimentiev, A.; Chen, M.; Schroeder, C. M., Expanding the Molecular Alphabet of DNA-Based Data Storage Systems with Neural Network Nanopore Readout Processing. *Nano letters* **2022,** *22*, 1905-1914.

(16) Gačanin, J.; Synatschke, C. V.; Weil, T., Biomedical Applications of DNA‐Based Hydrogels. *Advanced Functional Materials* **2020,** *30*, 1906253.

(17) Li, F.; Tang, J.; Geng, J.; Luo, D.; Yang, D., Polymeric DNA Hydrogel: Design, Synthesis and Applications. *Progress in Polymer Science* **2019,** *98*, 101163.

(18) Freeman, R.; Stephanopoulos, N.; Álvarez, Z.; Lewis, J. A.; Sur, S.; Serrano, C. M.; Boekhoven, J.; Lee, S. S.; Stupp, S. I., Instructing Cells with Programmable Peptide DNA Hybrids. *Nature communications* **2017,** *8*, 1-11.

(19) Akintayo, C. O.; Creusen, G.; Straub, P.; Walther, A., Tunable and Large-Scale Model Network Starpeg-DNA Hydrogels. *Macromolecules* **2021,** *54*, 7125-7133.

(20) Merindol, R.; Delechiave, G.; Heinen, L.; Catalani, L. H.; Walther, A., Modular Design of Programmable Mechanofluorescent DNA Hydrogels. *Nature communications* **2019,** *10*, 528.

(21) Xiong, X.; Wu, C.; Zhou, C.; Zhu, G.; Chen, Z.; Tan, W., Responsive DNA-Based Hydrogels and Their Applications. *Macromolecular Rapid Communications* **2013,** *34*, 1271-1283.

(22) Creusen, G.; Akintayo, C. O.; Schumann, K.; Walther, A., Scalable One-Pot-Liquid-Phase Oligonucleotide Synthesis for Model Network Hydrogels. *Journal of the American Chemical Society* **2020,** *142*, 16610-16621.

(23) Dorsey, P. J.; Rubanov, M.; Wang, W.; Schulman, R., Digital Maskless Photolithographic Patterning of DNA-Functionalized Poly (Ethylene Glycol) Diacrylate Hydrogels with Visible Light Enabling Photodirected Release of Oligonucleotides. *ACS Macro Letters* **2019,** *8* (9), 1133-1140.

(24) Fernandez-Castanon, J.; Bianchi, S.; Saglimbeni, F.; Di Leonardo, R.; Sciortino, F., Microrheology of DNA Hydrogel Gelling and Melting on Cooling. *Soft Matter* **2018,** *14*, 6431-6438.

(25) Rovigatti, L.; Smallenburg, F.; Romano, F.; Sciortino, F., Gels of DNA Nanostars Never Crystallize. *ACS Nano* **2014,** *8*, 3567-3574.
(26) Tanaka, S.; Wakabayashi, K.; Fukushima, K.; Yukami, S.; Maezawa, R.; Takeda, Y.; Tatsumi, K.; Ohya, Y.; Kuzuya, A., Intelligent, Biodegradable, and Self‐Healing Hydrogels Utilizing DNA Quadruplexes. *Chemistry – An Asian Journal* **2017,** *12*, 2388-2392.
(27) Heinen, L.; Heuser, T.; Steinschulte, A.; Walther, A., Antagonistic Enzymes in a Biocatalytic Ph Feedback System Program Autonomous DNA Hydrogel Life Cycles. *Nano letters* **2017,** *17*, 4989-4995.
(28) Svoboda, P.; Cara, A. D., Hairpin Rna: A Secondary Structure of Primary Importance. *Cellular and Molecular Life Sciences* **2006,** *63*, 901-908.
(29) Woodside, M. T.; Behnke-Parks, W. M.; Larizadeh, K.; Travers, K.; Herschlag, D.; Block, S. M., Nanomechanical Measurements of the Sequence-Dependent Folding Landscapes of Single Nucleic Acid Hairpins. *Proceedings of the National Academy of Sciences* **2006,** *103*, 6190-6195.
(30) Zhang, T.-b.; Zhang, C.-l.; Dong, Z.-l.; Guan, Y.-f., Determination of Base Binding Strength and Base Stacking Interaction of DNA Duplex Using Atomic Force Microscope. *Scientific reports* **2015,** *5* (1), 1-7.
(31) Kurus, N.; Dultsev, F.; Shevelev, G. Y.; Lomzov, A.; Pyshnyi, D., Effect of the Relief on the Measurement of Bond Rupture Force with the Help of Afm: The Dynamics of Interaction and Optimization of the Procedure. *Analytical Methods* **2018,** *10*, 3498-3505.
(32) Chung, J.; Kushner, A. M.; Weisman, A. C.; Guan, Z., Direct Correlation of Single-Molecule Properties with Bulk Mechanical Performance for the Biomimetic Design of Polymers. *Nature materials* **2014,** *13*, 1055-1062.
(33) Wang, Z.; Zheng, X.; Ouchi, T.; Kouznetsova, T. B.; Beech, H. K.; Av-Ron, S.; Matsuda, T.; Bowser, B. H.; Wang, S.; Johnson, J. A., Toughening Hydrogels through Force-Triggered Chemical Reactions That Lengthen Polymer Strands. *Science* **2021,** *374*, 193-196.
(34) Bertula, K.; Martikainen, L.; Munne, P.; Hietala, S.; Klefström, J.; Ikkala, O.; Nonappa, Strain-Stiffening of Agarose Gels. *ACS Macro Letters* **2019,** *8*, 670-675.
(35) Wang, Y.; Xu, Z.; Lovrak, M.; le Sage, V. A.; Zhang, K.; Guo, X.; Eelkema, R.; Mendes, E.; van Esch, J. H., Biomimetic Strain‐Stiffening Self‐Assembled Hydrogels. *Angewandte Chemie* **2020,** *132*, 4860-4864.
(36) Grandbois, M.; Beyer, M.; Rief, M.; Clausen-Schaumann, H.; Gaub, H. E., How Strong Is a Covalent Bond? *Science* **1999,** *283*, 1727-1730.
(37) Kolberg, A.; Wenzel, C.; Hackenstrass, K.; Schwarzl, R.; Rüttiger, C.; Hugel, T.; Gallei, M.; Netz, R. R.; Balzer, B. N., Opposing Temperature Dependence of the Stretching Response of Single Peg and Pnipam Polymers. *Journal of the American Chemical Society* **2019,** *141*, 11603-11613.
(38) Bano, F.; Sluysmans, D.; Wislez, A.; Duwez, A.-S., Unraveling the Complexity of the Interactions of DNA Nucleotides with Gold by Single Molecule Force Spectroscopy. *Nanoscale* **2015,** *7*, 19528-19533.
(39) Walder, R.; Van Patten, W. J.; Ritchie, D. B.; Montange, R. K.; Miller, T. W.; Woodside, M. T.; Perkins, T. T., High-Precision Single-Molecule Characterization of the Folding of an Hiv Rna Hairpin by Atomic Force Microscopy. *Nano letters* **2018,** *18*, 6318-6325.
(40) Balzer, B. N.; Gallei, M.; Hauf, M. V.; Stallhofer, M.; Wiegleb, L.; Holleitner, A.; Rehahn, M.; Hugel, T., Nanoscale Friction Mechanisms at Solid–Liquid Interfaces. *Angewandte Chemie International Edition* **2013,** *52*, 6541-6544.
(41) Bertz, M.; Kunfermann, A.; Rief, M., Navigating the Folding Energy Landscape of Green Fluorescent Protein. *Angewandte Chemie International Edition* **2008,** *47*, 8192-8195.
(42) Xue, Y.; Li, X.; Li, H.; Zhang, W., Quantifying Thiol–Gold Interactions Towards the Efficient Strength Control. *Nature communications* **2014,** *5*, 1-9.
(43) Sharma, D.; Cao, Y.; Li, H., Engineering Proteins with Novel Mechanical Properties by Recombination of Protein Fragments. *Angewandte Chemie International Edition* **2006,** *45*, 5633-5638.
(44) Hertz, H., Ueber Die Berührung Fester Elastischer Körper. **1882**.
(45) Kufer, S.; Puchner, E.; Gumpp, H.; Liedl, T.; Gaub, H., Single-Molecule Cut-and-Paste Surface Assembly. *Science* **2008,** *319*, 594-596.
(46) Strunz, T.; Oroszlan, K.; Schäfer, R.; Güntherodt, H.-J., Dynamic Force Spectroscopy of Single DNA Molecules. *Proceedings of the National Academy of Sciences* **1999,** *96*, 11277-11282.

(47) Morfill, J.; Kühner, F.; Blank, K.; Lugmaier, R. A.; Sedlmair, J.; Gaub, H. E., Bs Transition in Short Oligonucleotides. *Biophysical journal* **2007,** *93*, 2400-2409.
(48) Krautbauer, R.; Rief, M.; Gaub, H. E., Unzipping DNA Oligomers. *Nano letters* **2003,** *3*, 493-496.
(49) Chi, Q.; Wang, G.; Jiang, J., The Persistence Length and Length Per Base of Single-Stranded DNA Obtained from Fluorescence Correlation Spectroscopy Measurements Using Mean Field Theory. *Physica A: Statistical Mechanics and its Applications* **2013,** *392*, 1072-1079.
(50) Zhang, Y.; Zhou, H.; Ou-Yang, Z.-C., Stretching Single-Stranded DNA: Interplay of Electrostatic, Base-Pairing, and Base-Pair Stacking Interactions. *Biophysical journal* **2001,** *81* (2), 1133-1143.
(51) Rief, M.; Clausen-Schaumann, H.; Gaub, H. E., Sequence-Dependent Mechanics of Single DNA Molecules. *Nature structural biology* **1999,** *6*, 346-349.
(52) Oesterhelt, F.; Rief, M.; Gaub, H., Single Molecule Force Spectroscopy by Afm Indicates Helical Structure of Poly (Ethylene-Glycol) in Water. *New Journal of Physics* **1999,** *1*, 6.
(53) Cai, W.; Lu, S.; Wei, J.; Cui, S., Single-Chain Polymer Models Incorporating the Effects of Side Groups: An Approach to General Polymer Models. *Macromolecules* **2019,** *52*, 7324-7330.
(54) Cui, S.; Albrecht, C.; Kühner, F.; Gaub, H. E., Weakly Bound Water Molecules Shorten Single-Stranded DNA. *Journal of the American Chemical Society* **2006,** *128*, 6636-6639.
(55) Dumont, S.; Cheng, W.; Serebrov, V.; Beran, R. K.; Tinoco, I.; Pyle, A. M.; Bustamante, C., Rna Translocation and Unwinding Mechanism of Hcv Ns3 Helicase and Its Coordination by Atp. *Nature* **2006,** *439*, 105-108.
(56) Castilho, M.; Hochleitner, G.; Wilson, W.; van Rietbergen, B.; Dalton, P. D.; Groll, J.; Malda, J.; Ito, K., Mechanical Behavior of a Soft Hydrogel Reinforced with Three-Dimensional Printed Microfibre Scaffolds. *Scientific reports* **2018,** *8*, 1-10.
(57) McBane, J. E.; Vulesevic, B.; Padavan, D. T.; McEwan, K. A.; Korbutt, G. S.; Suuronen, E. J., Evaluation of a Collagen-Chitosan Hydrogel for Potential Use as a Pro-Angiogenic Site for Islet Transplantation. *PloS one* **2013,** *8*, e77538.
(58) Zeng, L.; Song, M.; Gu, J.; Xu, Z.; Xue, B.; Li, Y.; Cao, Y., A Highly Stretchable, Tough, Fast Self-Healing Hydrogel Based on Peptide–Metal Ion Coordination. *Biomimetics* **2019,** *4*, 36.
(59) Baniasadi, M.; Minary-Jolandan, M., Alginate-Collagen Fibril Composite Hydrogel. *Materials* **2015,** *8*, 799-814.
(60) Nalam, P. C.; Gosvami, N. N.; Caporizzo, M. A.; Composto, R. J.; Carpick, R. W., Nano-Rheology of Hydrogels Using Direct Drive Force Modulation Atomic Force Microscopy. *Soft Matter* **2015,** *11*, 8165-8178.
(61) Xue, B.; Tang, D.; Wu, X.; Xu, Z.; Gu, J.; Han, Y.; Zhu, Z.; Qin, M.; Zou, X.; Wang, W., Engineering Hydrogels with Homogeneous Mechanical Properties for Controlling Stem Cell Lineage Specification. *Proceedings of the National Academy of Sciences* **2021,** *118*.
(62) Fantner, G. E.; Hassenkam, T.; Kindt, J. H.; Weaver, J. C.; Birkedal, H.; Pechenik, L.; Cutroni, J. A.; Cidade, G. A.; Stucky, G. D.; Morse, D. E., Sacrificial Bonds and Hidden Length Dissipate Energy as Mineralized Fibrils Separate During Bone Fracture. *Nature materials* **2005,** *4*, 612-616.
(63) Fantner, G. E.; Oroudjev, E.; Schitter, G.; Golde, L. S.; Thurner, P.; Finch, M. M.; Turner, P.; Gutsmann, T.; Morse, D. E.; Hansma, H., Sacrificial Bonds and Hidden Length: Unraveling Molecular Mesostructures in Tough Materials. *Biophysical journal* **2006,** *90*, 1411-1418.
(64) Schakenraad, K.; Biebricher, A. S.; Sebregts, M.; Ten Bensel, B.; Peterman, E. J.; Wuite, G. J.; Heller, I.; Storm, C.; Van Der Schoot, P., Hyperstretching DNA. *Nature communications* **2017,** *8*, 1-7.
(65) Hutter, J. L.; Bechhoefer, J., Calibration of Atomic‐Force Microscope Tips. *Review of scientific instruments* **1993,** *64*, 1868-1873.
(66) Kolberg, A.; Wenzel, C.; Hugel, T.; Gallei, M.; Balzer, B. N., Covalent Attachment of Single Molecules for Afm-Based Force Spectroscopy. *JoVE (Journal of Visualized Experiments)* **2020,** (157), e60934.
(67) Marko, J. F.; Siggia, E. D., Stretching Dna. *Macromolecules* **1995,** *28*, 8759-8770.
(68) Hertz, H., Ueber Die Berührung Fester Elastischer Körper. *Journal für die reine und angewandte Mathematik* **1882,** *92*, 156-171.
(69) Rico, F.; Roca-Cusachs, P.; Gavara, N.; Farré, R.; Rotger, M.; Navajas, D., Probing Mechanical Properties of Living Cells by Atomic Force Microscopy with Blunted Pyramidal Cantilever Tips. *Physical Review E* **2005,** *72*, 021914.

4 Enhancing DNA Hydrogels Complexity via A Light Responsive Moiety

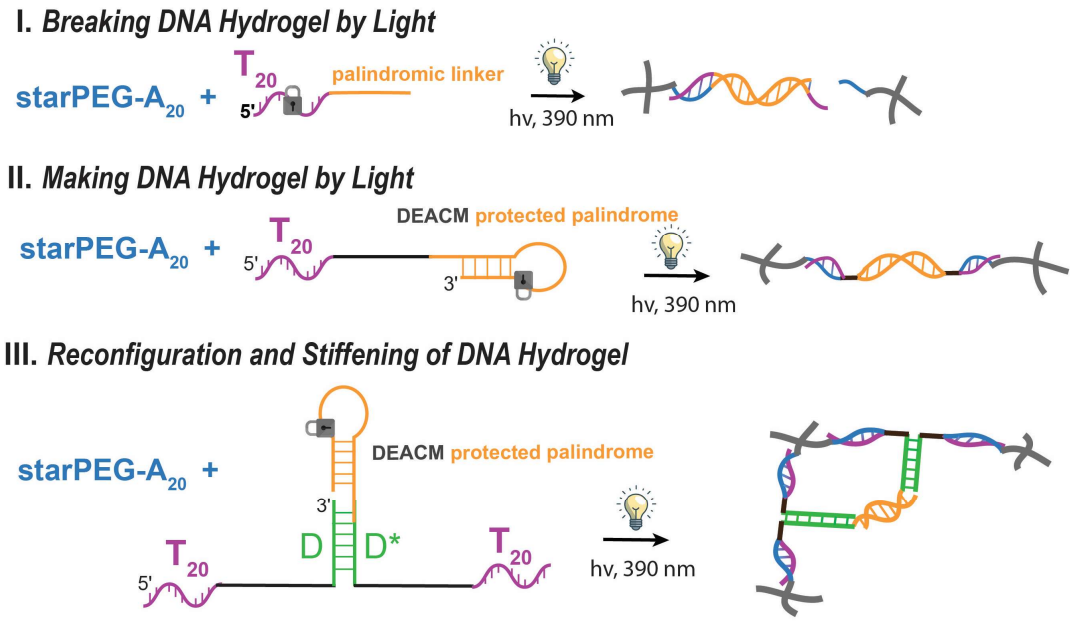

Figure 4.1. Table of contents graphic.

Preliminary note: This chapter is based on a manuscript draft prepared by **Cecilia Oluwadunsin Akintayo (COA)**, Alexander Ripp (AR), Aritra Sakar (AS), Henning J. Jessen (HJJ) and Andreas Walther (AW). The manuscript is not yet submitted for publication.

Author Contributions: COA and AW conceptualized the project. **COA** designed and performed the experiments and analyzed the data. AR and HJJ developed and synthesized the DEACM phosphoramidite. AS performed MALDI-TOF measurements. COA wrote the draft, which was revised by AR and AW.

4.1 Abstract

Smart soft materials such as DNA crosslinked hydrogels provide a versatile approach in the design of materials with tunable and programmable properties and have gained attention for applications in various fields such as biomedicine and nanotechnology. In particular, light provides a superior external stimulus for these systems, granting high spatiotemporal resolution and non-invasive control. Research in the area of light-responsive DNA materials has however been hindered by various factors such as the complexity involved in their design and synthesis, photodegradation and the need for high-intensity or prolonged light exposure to achieve desired responses. We address these limitations by incorporating a light-responsive moiety in DNA crosslinker strands, DEACM (7-(Diethylamino)-4-(Hydroxymethyl)-Coumarin), to enhance the structural and functional complexity of DNA hydrogels. Our approach is based on model network hydrogels formed from star-shaped building blocks and we leverage the photouncaging properties of DEACM to achieve precise control over hydrogel disassembly, assembly and strengthening within minutes of irradiation. Rheological characterization confirms that light activation triggers significant changes in the hydrogel structural and mechanical properties and we gain insights into the efficiency of the photouncaging reaction via high-performance liquid chromatography. Our approach highlights the potential of light-responsive DNA hydrogels for advanced applications requiring programmable material behavior.

4.2 Introduction

The functional and structural traits of biological materials have inspired many scientist to integrate such advanced concepts into synthetic systems.[1-3] However, achieving synthetic materials with intricate features, such as active dynamics through fuel conversion, information processing, and communication, remains challenging due to both synthetic and conceptual hurdles.[4-7] Responsive or “smart” materials that replicate lower-complexity features including self-healing and external switches are achieved based on diverse strategies.[8-10] Stimulus responsive materials, whose material properties can be altered on external trigger, such as pH change,[11-13] small molecules,[14-15] enzymes,[16-17] temperature[18-19] or light,[20-21] have garnered significant attention in recent years.[22] Especially, light offers here significant advantages as it is non-invasive and enables precise spatial and temporal control, with the flexibility to tune the intensity, exposure time and wavelength of the light as needed.[23-25] To construct such externally regulated materials, DNA is an ideal platform, because the crosslinking connectivities can be specifically addressed and it can interact with biological systems. Therefore, incorporating photosensitive chemical groups into nucleic acids has emerged as a promising avenue for controlling DNA based nanostructures[26] and triggering a broad range of biological

and nano-technological processes that rely on DNA assembly/disassembly.[9, 27-29] Photoresponsive DNA nanomaterials have been used in well-known applications including nano-tweezers,[30] drug delivery systems[31] and light-modulated tetrahedral structures.[32-33]

To date, light-responsive DNA materials have largely relied on two strategies: reversible photoswitching and irreversible photouncaging. Reversible approaches frequently utilize azobenzene derivatives that modulate DNA hybridization via cis-trans isomerization.[24, 34] These system however often require specific, narrow wavelengths for efficient switching, operate only in very specific temperature windows, and can suffer from incomplete reversibility. Photocages alternatively provide a irreversible "on" switch. The most commonly used photocage is the o-nitrobenzyl (o-NB) group. However, o-NB groups typically possess low quantum yields and require activation with high-energy Ultraviolet (UV) light, which is prone to scattering in tissues and can be phototoxic to biological samples. Furthermore, the uncaging byproducts of NB groups can interact unfavorably with sensitive biomolecules.[35] To overcome the limitations of UV-dependent NB cages, coumarin-based photocages like DEACM offer a superior alternative because they feature a red-shifted absorption profile that allows for activation with visible blue light, significantly reducing potential photodamage.[36-38] Additionally, DEACM possesses high molar absorption coefficients, faster release kinetics compared to NB derivatives[35, 39] and a well understood uncaging mechanism[40] dating back to its identification as a phosphate releasing group by Givens and Matuszewski in 1984.[41]

Herein, we used a DEACM-based photocage, to demonstrate light-induced engineering of starPEG-DNA hydrogels. Unlike previous reports that incorporate light-sensitive elements primarily to prevent assembly,[32, 42] we utilize DEACM to modulate the mechanical properties of our star poly(ethylene glycol)-DNA (starPEG-DNA) hydrogel by inducing both stiffening and softening. By leveraging the superior photophysical properties of DEACM over traditional NB cages, specifically its biocompatibility and efficiency under milder light conditions, we present a strategy for the precise, non-invasive tuning of material properties without compromising biological activity.

We build on the unique properties of DEACM and integrate it into our previously developed large scale starPEG-DNA hydrogel system.[43] Our previous work established a foundation for large-scale polymer/DNA hybrid material synthesis[43] and mechanical characterization of these tunable and scalable starPEG-DNA hydrogels.[44] More recently, we quantified how properties of molecular building blocks can be transferred to macroscopic hydrogels and introduce nonlinear stress−strain response into the hydrogels by incorporating a DNA hairpin.[45] We herein present a platform to investigate the incorporation of the

photocleavable DEACM group to regulate DNA hydrogel response to light. DEACM undergoes cleavage in the high UV region, around 400 nm[46] and the DEACM based phosphoramidite photocage is integrated at an internal position of a DNA during standard DNA solid-phase synthesis. Upon irradiation, the phosphate ester bond of the DNA backbone next to the DEACM moiety is cleaved. We investigate the impact of the photocage on hybridization behavior and the mechanical properties of our starPEG-DNA hydrogel. We demonstrate that hydrogel formation, breakage and stiffening can be controlled within minutes of irradiation. This showcases a viable path to the design of tunable photoresponsive DNA hydrogels to fully harness their potential application in various fields.

4.3 Results and Discussion

Our main goal of modulating starPEG-DNA hydrogels by light is divided into three objectives. (1) Softening a DNA hydrogel by light, (2) assembly of a DNA hydrogel by light and (3) reconfiguration and stiffening of a DNA hydrogel by light. To achieve these objectives as outlined in **Figure 4.2**, we designed systems that feature two primary components. The first is a starPEG-A_{20} (M_n = 66 kDa) containing four terminal 20-mer adenine blocks and the second is an all-DNA bivalent linker containing a DEACM protected segment and terminal parts of 20-mer thymine blocks to hybridize with the starPEG-A_{20} component. The all-DNA linker is crucial in our design, leveraging the versatility of DNA to fit our objectives. We altered the sequence of the second building block to achieve our three goals. For the 1st objective, DEACM is used to introduce a defined "fracture point" within the hydrogel network. In Linker-1, the photocage is inserted directly into the phosphodiester backbone, positioning it centrally between the terminal binding domains. Although the photocage interrupts the continuous sequence, it maintains the structural integrity required for initial hydrogel formation upon mixing the A_{20} and T_{20}. However, exposure to UV light triggers the photo-uncaging process, cleaving the linker strand. This scission destroys the connectivity between the polymer arms, subsequently leading to hydrogel softening. Linker-2 features a single stranded oligo-T_{20} overhang and a self-protected palindromic segment in the 2nd objective. DEACM is used to activate the protected DNA palindrome, resulting in light-trigged hydrogel assembly in this instance. Finally, the photocage protected palindrome, Linker-3, is used to reconfigure the topology of the hydrogel network by increasing the crosslink density to achieve the 3rd objective.

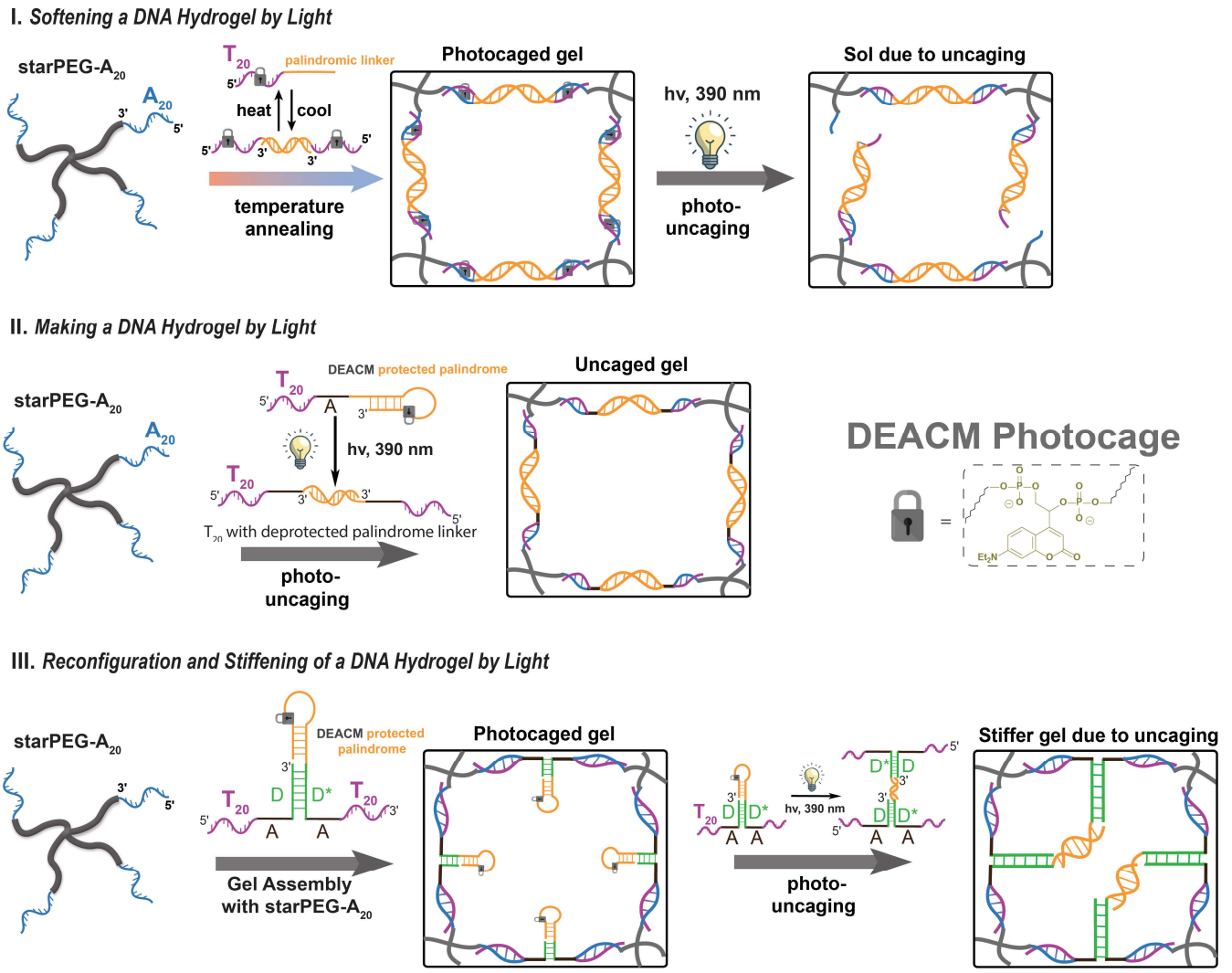

Figure 4.2. Schematic Overview of Light-Modulated Control of DNA Hydrogels. The first building block starPEG-A_{20} is synthesized in an OP-LPOS, one-pot liquid-phase oligonucleotide synthesis, as we previously reported.[43] This is followed by synthesis of the second all-DNA linker building blocks via automated SPOS, solid-phase oligonucleotide synthesis. **(I)** Hydrogel Softening: A DEACM "fracture point" is incorporated into the DNA linker that upon light exposure, cleaves the hydrogel network and reduces stiffness. **(II)** Hydrogel Assembly: DEACM-protected palindromic sequence is used to trigger network formation and gelation upon irradiation. **(III)** Hydrogel Stiffening. Light-induced network reconfiguration and increased crosslink density, results in mechanical reinforcement of the hydrogel.

The required DEACM phosphoramidite was synthesized according to publication of Weyel *et al.*[47] However, by changing the substrates of a Wittig olefination we could reduce the overall step count from 8 to 6 steps, depicted in **SI Figure 4.8**. All linkers were synthesized via automated SPOS and are listed in **SI Table 4.1**. **SI Figure 4.10** summarizes the characterization of the linker strands via high-performance liquid chromatography, HPLC, and matrix-assisted laser-desorption-ionization time-of-flight mass spectrometry, MALDI-TOF. Analytical HPLC chromatogram shows single bands and the molecular weights of the synthesized linkers closely match the theoretical molecular weights of the strands, thus confirming that the synthesized linker strands are present in high purity. All hydrogels were prepared by mixing the starPEG-A_{20}

at overlap concentration,[44] c^*, and the respective linkers at stoichiometric ratios in a phosphate buffer solution containing 150 mM Na^+ and 25 mM Mg^{2+}. After gel formation, we employed rheology to monitor and analyze the effects of light exposure on the mechanical properties of the hydrogels.

We firstly examined one of the fundamental light-triggered reactions to manipulate the properties of our starPEG-DNA hydrogel by facilitating the controlled disassembly of the DNA hydrogel network. Following gel assembly, we assessed the rheological properties of the hydrogel both before and after light exposure. These experiments were conducted using our rheo-UV setup, which allowed for simultaneous irradiation of the hydrogel sample while it was placed in the rheometer. **Figure 4.3** shows the mechanical analysis of the hydrogel before, during and after light activation. Examination of the sol-gel transition temperature, as defined by the crossover temperature, T_{co}, of the storage modulus, G' and the loss modulus, G'' reveals a T_{co} of 42 °C prior to light activation (**Figure 4.3a,** grey curve). This corresponds to a gel that exhibits solid-like behavior without visible flow at room temperature, RT. Oscillatory frequency sweeps conducted at 25 °C provides insights into the dynamic properties of the hydrogel, revealing the crossover frequency, f_c, and bond relaxation time, τ, of the hydrogel. These two parameters offer a deeper understanding of the viscoelastic properties and are directly related. While f_c is the point at which G'/G'' intersect and indicates an elastic to viscous transition zone, τ as derived from f_c reflects the timescale over which the hydrogel network bonds reorganize or relax. **Figure 4.3b** (grey curve) shows that the hydrogel does not relax within the measured frequency range before DEACM uncaging, thereby preserving its solid-like property. This temperature- and frequency-dependent behavior suggests that the gel remains stable and retains its structural integrity at RT.

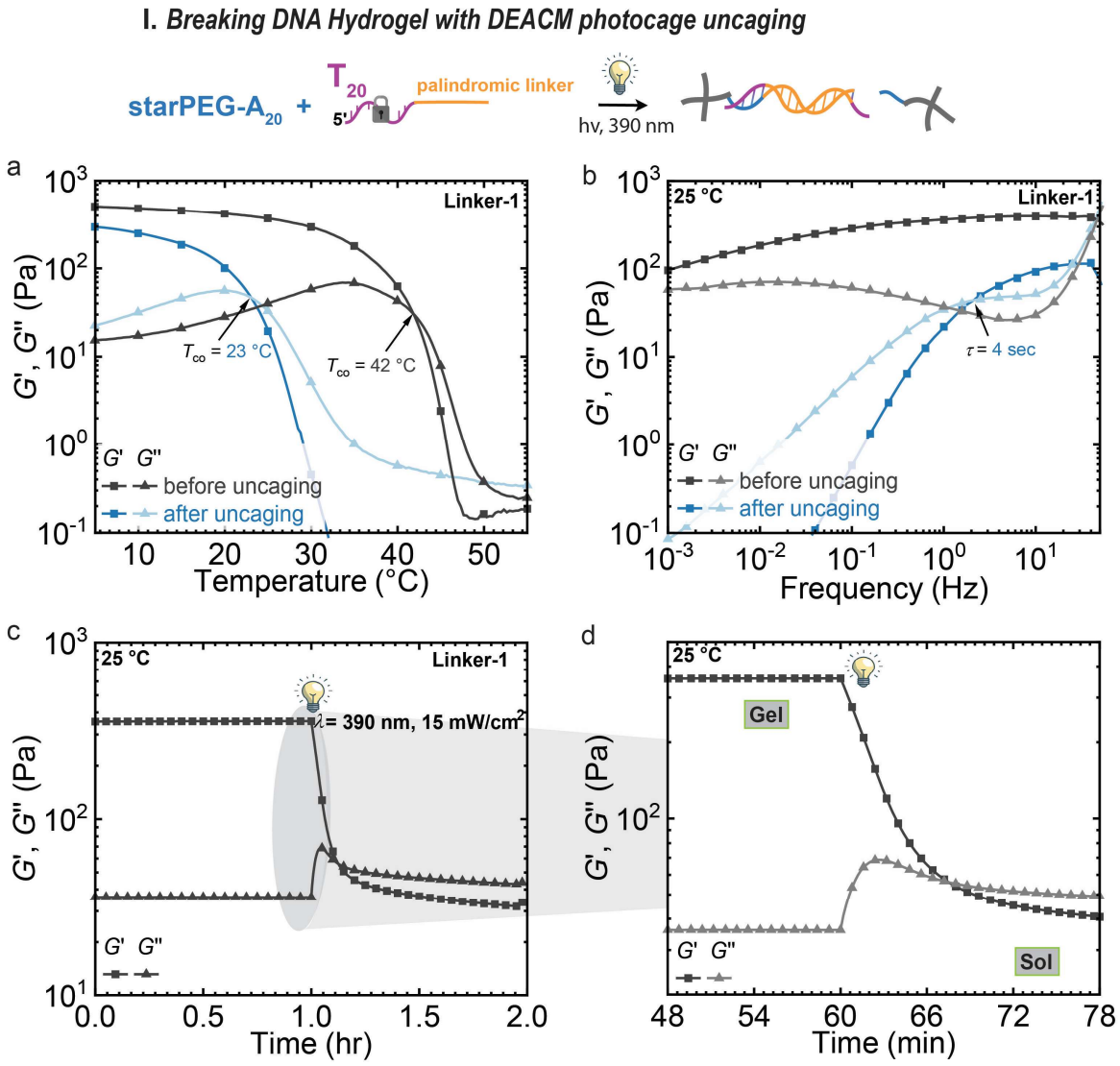

Figure 4.3: Light-induced softening of a DNA hydrogel. (a) Temperature sweep of the hydrogel before and after photouncaging (f = 1 Hz, γ = 6%, from 55 °C to 5 °C, temperature rate = 0.4 °C/min). T_{co} is denoted with arrows in the graph. **(b)** Frequency sweep of the hydrogel before and after uncaging (f = 0.001 - 100 Hz, γ = 0.1%, 10 °C). Before uncaging, the hydrogel does not relax within the measured frequency range (gray curve). While after uncaging, τ is depicted by the arrow in the graph (blue curve). **(c)** Trend of G' and G'' over time at 25 °C. **(d)** Zoomed in image of the time dependent G' and G'' showing the time between 48 – 78 minutes. Crossover from Gel to Sol is observed upon DEACM uncaging.

The impact of light activation in Linker-1 and its effect on the mechanical properties on the DNA hydrogel network is depicted in **Figure 4.3c**, with **Figure 4.3d** providing a zoomed in view of the circled out section of **Figure 4.3c**. Linker-1 is monitored for an hour prior to light activation at a wavelength of 390 nm. Upon exposure to light with a power of 15 mW/cm^2, DEACM is uncaged and a noticeable decrease in G' accompanied by a slight increase in G'' is observed. This shift in the mechanical property of the hydrogel is

followed by a G'/G'' crossover within a few minutes, transitioning the hydrogel from a gel-like to a sol-like state. This shift reveals the impact of light on the structural integrity of the Linker-1 hydrogel.

In order to confirm successful disassembly of the Linker-1 hydrogel network triggered by light and assess the extent of mechanical property change induced by light exposure, we performed rheology on the gels post-uncaging and compared it with the gels pre-uncaging. A pronounced change in $G'_{10\,°C}$ and T_{co} is observed post-uncaging (**Figure 4.3a**). T_{co} reduces drastically from an initial value of 42 °C to 23 °C while $G'_{10\,°C}$ reduces by half from 490 Pa before light activation to 250 Pa after light activation. The post-uncaging Linker-1 system also has a shorter bond lifetime and fast bond relaxation within 4 seconds at RT (**Figure 4.3b**). The T_{co} value of Linker-1 after light exposure, indicates that the system exhibits a more fluid-like behavior at RT. Repeated temperature sweeps of the Linker-1 hydrogel pre- and post-uncaging show a similar trend and indicate that the thermal response is stable and reproducible across multiple cycles (**SI Figure 4.11a, b**). Subsequent frequency-dependent sweeps of the post-uncaging hydrogel at different temperatures also reveal shorter relaxation times as the temperature increases (**SI Figure 4.11d**). As expected, DEACM uncaging significantly reduced the mechanical integrity of Linker-1 hydrogel and caused a shift from a solid-like gel state to a more dynamic, liquid-like sol state. This response is however not an 'all-or-nothing' dissociation. DEACM breaks the T_{20} bridging domains into shorter segments which retain residual binding affinity for the starPEG-A_{20} cores at lower temperatures. The network connectivity is therefore not abolished but rather thermally destabilized.

In contrast to this softening approach, we next explore the potential of light to induce the assembly of a DNA hydrogel with Linker-2. In the Linker-2 hydrogel, we leverage the photouncaging of a protected DNA palindrome sequence to trigger formation of the DNA hydrogel and aim to facilitate the transition from a sol-like to a gel-like state upon uncaging. Mixing our Linker-2 building blocks together results in a free flowing solution, as anticipated in its sol-like state. This behavior is confirmed by the rheological temperature sweep of the system (**Figure 4.4a**, black curve). Absence of any T_{co} for the hydrogel within the measured temperature range (5 - 50 °C) and a clearly higher G'' over G' confirm the sol state before light activation. Repeated temperature sweep cycles (**SI Figure 4.12a**) confirm robustness. We did not examine the frequency-dependent behavior of the system before light activation because it does not exhibit the required structural integrity. Analysis of Linker-2 hydrogels mechanical properties under light exposure, at RT (**Figure 4.4b**) shows a clear transition from a liquid-like to a more solid-like state within minutes of illumination, as

seen by the rapid increase of *G*'. Further inspection of the highlighted area (**Figure 4.4c**) reveals that this transition occurs rapidly and is completed within 4 minutes of light exposure.

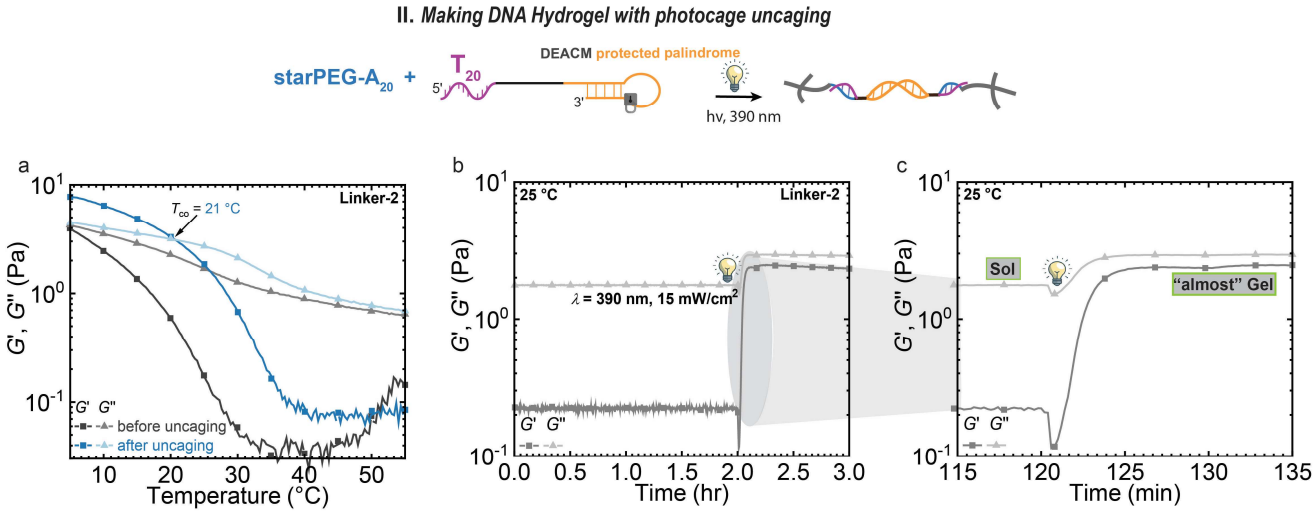

Figure 4.4. Light-Induced assembly of a DNA Hydrogel. (a) Temperature sweep of the hydrogel before and after photocage uncaging (f = 1 Hz, γ = 6%, from 55 °C to 5 °C, temperature rate = 0.4 °C/min). T_{co} is denoted with arrow in the graph. **(b)** Trend of *G*′ and *G*″ over time at 25 °C. **(c)** Zoomed in image of the time dependent *G*′ and *G*″ showing the time between 115 – 135 minutes. Crossover from Sol to "Gel" is observed upon DEACM uncaging.

Notably, the hydrogel remains in a sol state at RT (*G*' > *G*''). The post-uncaging temperature sweep however reveals a T_{co} at 21 °C (**Figure 4.4a**, blue curve), significantly higher than the pre-uncaging value (T_{co} = < 5°C). This shift confirms that the DNA system successfully undergoes assembly in response to DEACM uncaging, and our results confirm that light exposure to the Linker-2 network induces crosslinking and enables the gel assembly.

Building on this, we attempt to further enhance the robustness of light-activated assembly in our Linker-3 hydrogel system. Here we aimed to increase the density of crosslinks in the hydrogel and strengthen the DNA hydrogel network upon light activation (**Figure 4.5**). We targeted this by uncaging a DEACM protected palindrome within a formed hydrogel network, whereby the palindrome makes additional crosslinks. The temperature sweep (**Figure 4.5a**, black curve) and the frequency sweep (**Figure 4.5b**, black curve) respectively show that the uncaged hydrogel exhibits self-supporting properties at RT. With a T_{co} of 31 °C and τ = 6.5 mins at 25 °C, the hydrogel demonstrates robustness and does not flow at ambient temperatures. We monitored DEACM uncaging over time and it is evident that light activation triggers a rapid increase in *G*' by 100 Pa within minutes of irradiation (**Figure 4.5c, d**). This significant increase in *G*' highlights the light induced strengthening of the hydrogel.

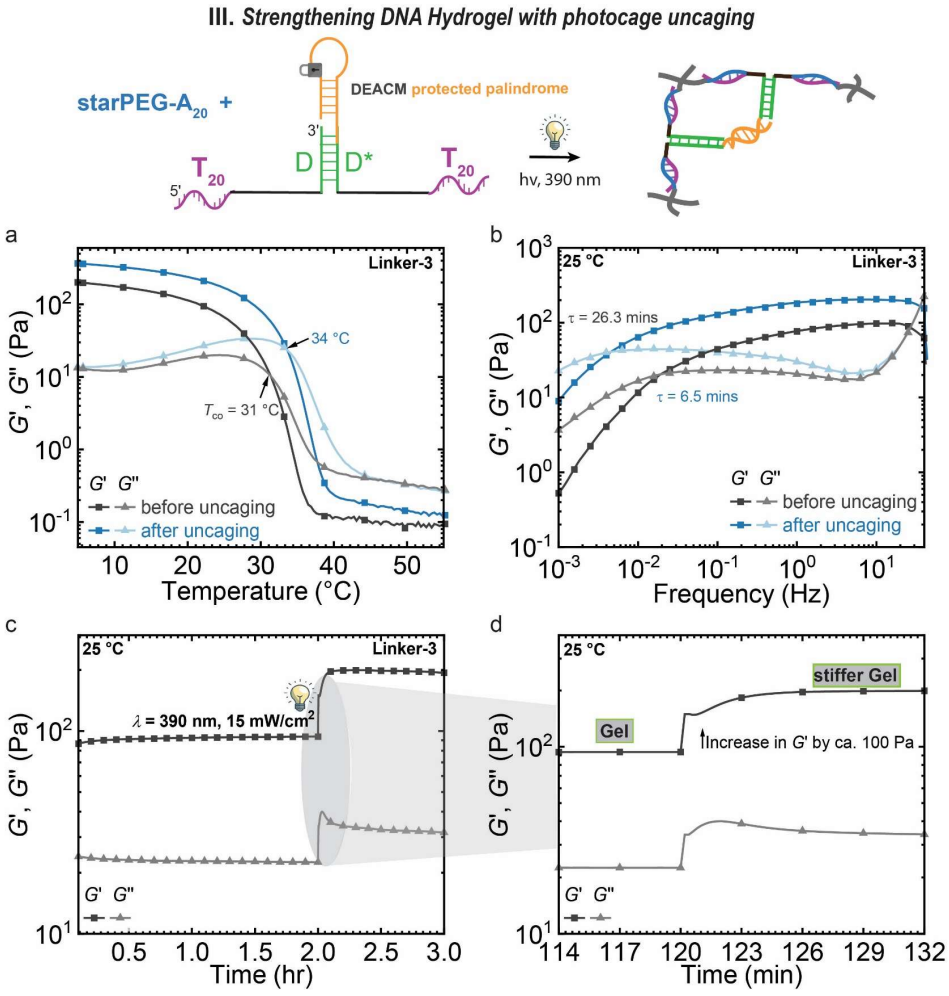

Figure 4.5. Light-Induced strengthening of a DNA Hydrogel. (a) Temperature sweep of the hydrogel before and after photocage uncaging (f = 1 Hz, γ = 6%, from 55 °C to 5 °C, temperature rate = 0.4 °C/min). T_{co} is denoted with arrows in the graph. **(b)** Frequency sweep of the hydrogel before and after uncaging (f = 0.001 - 100 Hz, γ = 0.1%, 10 °C). τ is depicted by the arrows in the graph. **(c)** Trend of G' and G'' over time at 25 °C. **(d)** Zoomed in image of the time dependent G' and G'' showing the time between 114 – 132 minutes.

To confirm the enhanced mechanical properties of the hydrogel, we repeated the temperature and frequency sweeps (**Figure 4.5a** and **Figure 4.5b** respectively, blue curves) of the hydrogel after uncaging. The temperature sweeps of the uncaged hydrogel shows a higher T_{co}, increasing by 3 °C, and a higher G', rising from 177 Pa to 333 Pa at 10 °C ($G'_{10\,°C}$ = 177 Pa before uncaging; $G'_{10\,°C}$ = 333 Pa after uncaging). This indicates a stronger, thermally stable hydrogel structure with improved rigidity. The strengthening of the gel after light activation is further proven by the increase in τ from 6.5 mins to 26.3 min, signifying an enhancement in the dynamics of the hydrogel structure and greater crosslink stability. Furthermore, the thermal responsiveness of the Linker-3 hydrogel demonstrates reproducibility across multiple cycles. This is observed in the repeated temperature sweeps before and after uncaging (**SI Figure 4.13a, b**). Frequency-dependent sweeps of the post-uncaging hydrogel at different temperatures reveal no crossover within the

measured frequency range at temperatures below 25 °C. The post-uncaging hydrogel shows overall improvement in mechanical strength/stiffness and confirms that DEACM uncaging in Linker-3 enhances the mechanical coherence of the DNA hydrogel.

These findings, along our demonstrations of DEACM-mediated disassembly and assembly highlights the versatility of the DEACM photocage in modulating DNA hydrogel behavior. The three objectives of our study, which includes the disassembly, assembly and strengthening of DNA hydrogels were all successfully achieved within minutes of light irradiation.

To assess the reaction kinetics, we monitored the uncaging process using analytical HPLC with dual-wavelength detection. We recorded the absorbance at 260 nm to track the concentration of DNA strands, while simultaneously monitoring at 400 nm to detect the DEACM photocage moiety. This spectral monitoring allowed us to independently quantify the depletion of the caged species and the accumulation of the uncaged product over time (**Figure 4.6**). **Figure 4.6a** illustrates the time-dependent DEACM uncaging efficiency observed with in situ irradiation during a typical rheological experiment. Uncaging was firstly monitored by measuring the UV absorbance of DNA samples at 260 nm. It is important to state that although starPEG also absorbs at 260 nm, it elutes later than DNA and does not interfere with the DNA sample signal. The starPEG signal is not considered in the analysis uncaging efficiency, which we calculate by integrating the area under each DNA Peak (**Figure 4.6b**).

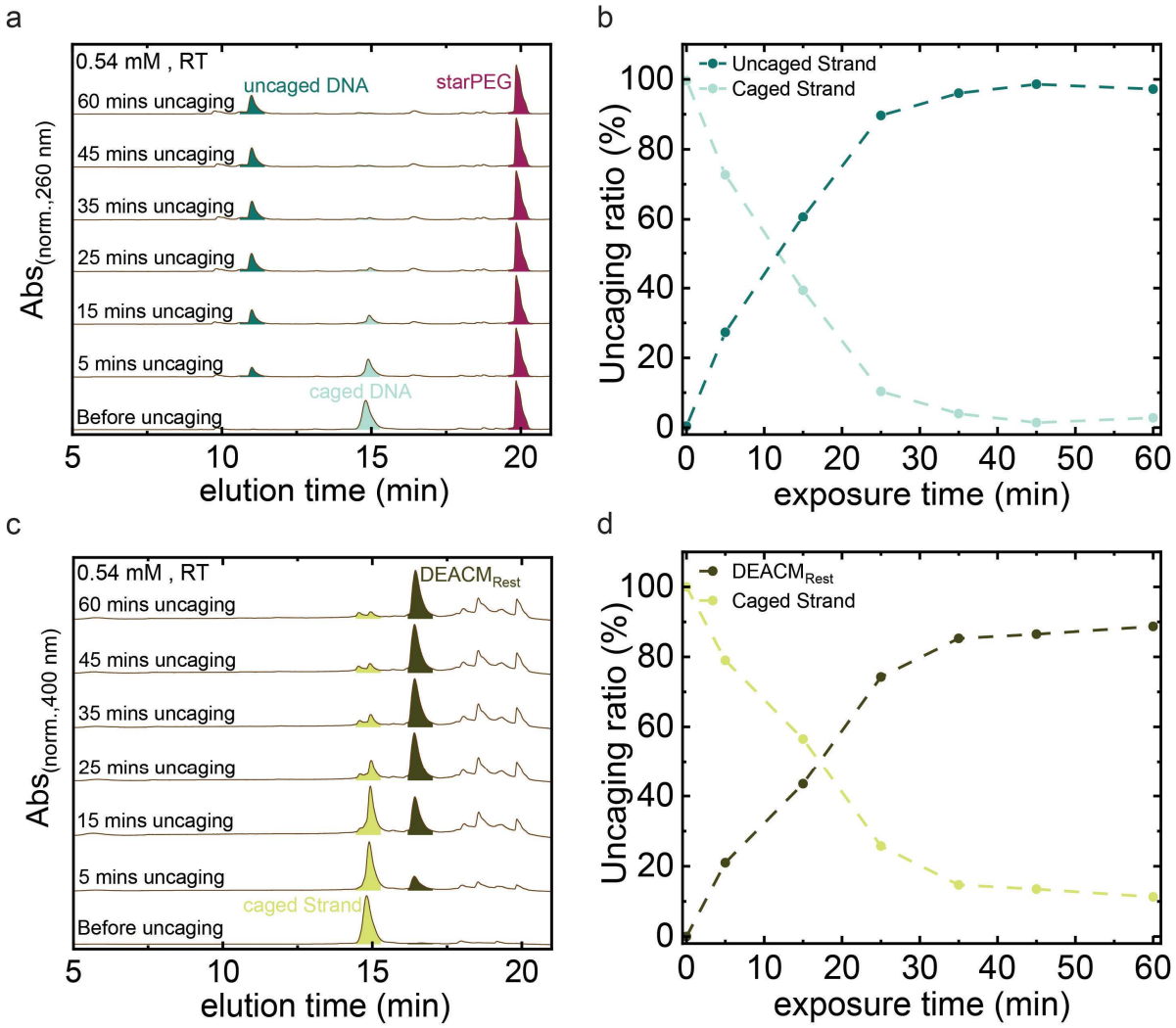

Figure 4.6. Time-dependent evaluation of DEACM hydrogel uncaging via HPLC monitored at 260 nm (DNA) and at 400 nm (DEACM). The kinetics of the uncaging process is analyzed via **(a)** Analytical HPLC chromatograms of DNA hydrogels at varying light exposure times with a detection wavelength of 260 nm. **(b)** Corresponding uncaging ratio of DEACM-modified DNA hydrogels indicates rapid uncaging that plateaus at 28 minutes. **(c)** Analytical HPLC chromatograms of DNA hydrogels at varying light exposure times with a detection wavelength of 400 nm, highlighting the decrease of the DEACM containing strand and increase in free photocage over time. **(d)** Uncaging ratio of DEACM-modified DNA hydrogels as a function of light exposure time.

Uncaging begins immediately upon irradiation, with the amount of uncaged strand increasing steadily until it reaches a maximum after about 28 minutes. At this stage, the system contains the highest level of uncaged strand and only a negligible amount of caged DNA strand remains. This trend aligns with uncaging efficiency measurements detected by UV absorbance at 400 nm, the optimal absorbance wavelength for DEACM (**Figure 4.6c, d**). At 400 nm, only samples containing DEACM are detected and a gradual decline in the caged strand peak, accompanied by a corresponding increase in the residual DEACM photocage peak is observed over time. Similar to the HPLC with a detection wavelength of 260 nm, this process reaches a plateau at

approximately 28 minutes, beyond which no further significant changes are observed. While this consistent result offers a detailed view on the kinetics involved in DEACM uncaging and how long it takes to fully uncage the photocage during a rheology experiment, our findings from rheology also demonstrate that complete DEACM uncaging is not essential for observing significant changes in the hydrogel mechanical properties. Notably, the mechanical properties of all our tested hydrogels reached their peak within the first 5 minutes of irradiation. Further exposure to light did not lead to further substantial change in the hydrogel´s mechanical properties. This confirms that even partial uncaging is sufficient to trigger desired mechanical transformations, highlighting the efficiency of the DEACM photocage.

4.4 Conclusion

In this chapter, we demonstrated the potential of light-responsive modulation of DNA hydrogels by leveraging on the photouncaging properties of the DEACM moiety. Through the incorporation of DEACM into various DNA linker topologies, we achieved precise and efficient control over hydrogel assembly, disassembly and mechanical strengthening, all within minutes of light activation (=DEACM uncaging). Rheological characterization confirmed that these macroscopic property changes, spanning from complete sol-gel transitions to tunable modulus adjustments, occur rapidly and under mild irradiation conditions. These results validate that DEACM-based photouncaging offers a versatile and efficient platform for engineering the mechanical properties of starPEG-DNA hydrogels without compromising the biological compatibility of the system.

HPLC offered detailed insights into the kinetics and efficiency of the photouncaging reaction at 260 nm (wavelength for DNA absorbance) and 400 nm (wavelength for DEACM absorbance) and reveals that uncaging begins immediately upon irradiation and reaches a plateau after about 28 minutes. The photouncaging process is rapid and steadily modulates the structural and mechanical properties of the DNA hydrogel. Our system presents an efficient synthesis process for achieving light-triggered control over hydrogel properties while maintaining critical attributes such as biocompatibility and stability. This work not only broadens the understanding of light-responsive DNA hydrogels, it also establishes new pathways for their use and paves the ways for further exploration in the development of programmable smart materials.

4.5 Experimental

4.5.1 Materials

The following reagents and solvents were used as received from the following suppliers: Ac-dC Synbase CPG 1000, dT Synbase CPG 1000, dA Synbase CPG 1000 (Link Technology), DMT-dA(bz) phosphoramidite, DMT-dG(dmf) phosphoramidite, DMTdC(ac) phosphoramidite, DMT-dT phosphoramidite (Sigma-Aldrich, 99%, was dissolved 50mM in anhydrous acetonitrile), CAP A (Sigma Aldrich, tetrahydrofuran/pyridine/acetic anhydride, 8:1:1), CAP B (Sigma Aldrich, 10% methylimidazole in tetrahydrofuran), trichloroacetic acid Deblock (TCA Deblock, Sigma-Aldrich, 3% in DCM), 5-(Ethylthio)-1H tetrazole (ETT Activator, Sigma Aldrich, 0.25 M in ACN), oxidizer (Sigma Aldrich, Pyridine/Water/Iodine, 9:1:12.7), dichloromethane (DCM, Fischer Scientific U.K., CH_2Cl_2, analytical reagent grade), acetonitrile (ACN, Sigma-Aldrich, C_2H_3N), acetonitrile anhydrous (ACN, 99.8%, abcr GmbH), sodium chloride (NaCl, 99%, Sigma Aldrich), sodium hydroxide (NaOH, VWR), magnesium chloride ($MgCl_2$, 1M, Fischer Scientific), sodium dihydrogen phosphate (NaH_2PO_4, Sigma Aldrich), ammonia solution (NH_3, Roth, 28.0−30.0%), 2-propanol (analytical grade), acetic acid (100%) (Merck Millipore), silicon oil (350cSt, Carl Roth GmbH).

StarPEG-A_{20} was synthesized as described previously in detail.[43]

4.5.2 Instrumentation

High-performance liquid chromatography (HPLC) was performed on a Thermo Fischer Scientific Dionex Ultimate 3000 HPLC system. The sample was dissolved in Milli-Q water and measured using a gradient from 100% A to 90% B with solvent A being 0.1 M TEAA buffer (1/1) in 95/5 water/acetonitrile, and solvent B being acetonitrile.

Ultraviolet–visible spectrophotometry (UV-VIS) measurements, used to determine the concentration of the starPEG-DNA and Amine-DNA building blocks, were performed on an Analytik Jena ScanDrop 250 Spectrophotometer using a cuvette from Hellma with a path length of 3.0 mm.

Matrix-assisted laser-desorption-ionization time-of-flight mass spectrometry (MALDI-TOF MS) measurements were performed using 3-HPA (3-Hydroxypicolinic acid) and ammonium citrate di-basic as matrix. The measurements were conducted on an Autoflex III from Bruker.

Rheological Characterization was performed on an Anton Paar Modular Compact Rheometer MCR 302 equipped with a 25 mm plate-plate geometry. Analysis of the data was done with the RheoCompass

software. The storage, *G*', and loss moduli, *G*'', were measured in oscillation mode with a constant strain amplitude of 6%. This value was found to be in the linear viscoelastic range based on the results of an amplitude sweep at 1 Hz. Frequency sweeps were carried out between 100 Hz and 0.001 Hz at a fixed strain of 6%. Temperature ramps were performed at a fixed frequency and strain of 1 Hz and 6%, respectively. The ramping rate of the temperature was 0.3 °C/min. The gap between the plates was fixed at 0.2 mm and a thin layer of silicon oil was added around the measuring system to prevent evaporation.

4.5.3 Procedures and Synthesis

DNA sequence, synthesis and characterization

Automated solid phase oligonucleotide synthesis

The oligonucleotides were synthesized on a H-8 custom LNA, DNA/RNA automatic synthesizer from K&A Laborgeräte at 10 µmol scale employing the standard solid phase β-cyanoethyl-phosphoramidite chemistry in trityl-on mode. The DNA phosphoramidites (DMT-dT, DMT-dA(bz), DMT-dG(dmf) and DMTdC(ac)) were diluted to 50 mM with dry acetonitrile and synthesis occurred from the 3' towards the 5' end of the oligonucleotides on packed solid phase columns.

Deprotection and purification (general procedure for 10 µmol scale synthesis)

Cleavage of the oligonucleotides from the solid support and base deprotection was achieved in one step to ensure optimal yields. The controlled pore glass (CPG) solid support was treated with 10 mL of a 50:50 wt% mixture of ethylenediamine:toluene for 2 h at room temperature. The deprotection solution was removed and the column was rinsed with 20 mL toluene to detach synthesized DNA from the support. The synthesized DNA sequence was then extracted with 5 mL Milli-Q water and purified by reverse phase-HPLC (RP-HPLC). The solvent was removed by freeze-drying. After purification, the DMT group was cleaved by making a 2 wt% solution of the dry DNA in pH 4.0 (200 mM) NaOAc/HOAc buffer containing 200 mM NaCl and stirring at 50 °C for 1 h. Precipitation of the sample into a 5-fold excess of 2-propanol removed contaminants and exchanges counterions to sodium. The solvent was removed by freeze drying and the synthesized strands were stored at -20 °C until further use. The purity of the obtained oligonucleotides was confirmed with analytical HPLC and MALDI-TOF.

Table 4.1. Overview of synthesized oligonuclotides

ID	DNA Sequence	$MW_{calc.}$ (g/mol)[a]
Linker-1	5' TTT TTT TTT T /PC/ TTT TTT TTT T TAG CTA TAG CTA 3'	10132.58
Linker-2	5' TTT TTT TTT TTT TTT TTT TT CCC GTA TAG CTA TAG CTA A /PC/ TAG CTA TAC 3'	15019.68
Linker-3	S1 - 5' TTT TTT TTT TTT TTT TTT TT CCC GTA GAC GAC 3' S2 - 5' TC GAT /PC/ A ATC GAT ATC GAT GTC GTC ATG CCC TTT TTT TTT TTT TTT TTT TT 3'	S1 – 9699.3 S2 – 15645.1

[a]The calculated molecular weights are determined with the Oligo Analyzer package from Integrated DNA technologies (IDT).

Phosphoramidite synthesis

Synthesis of coumarin-linker phosphoramidite (05)

The synthesis of the coumarin-linker phosphoramidite (**05**) was modified compared to the already published procedure by Weyel.[47]

Instead of starting from DEACM, we decided to start from 7-(diethylamino)-2-oxo-2H-chromene-4-carbaldehyde (**01**) which was obtained according to a reported procedure by Weinrich.[48]

Using methyl-triphenylphosphoniumbromid, **01** was transformed into 7-(diethylamino)-4-vinyl-2H-chromen-2-one (**02**). With **02** in hand, the subsequent synthesis, apart from minor changes, was performed identical to the already published procedure by Weyel.[47]

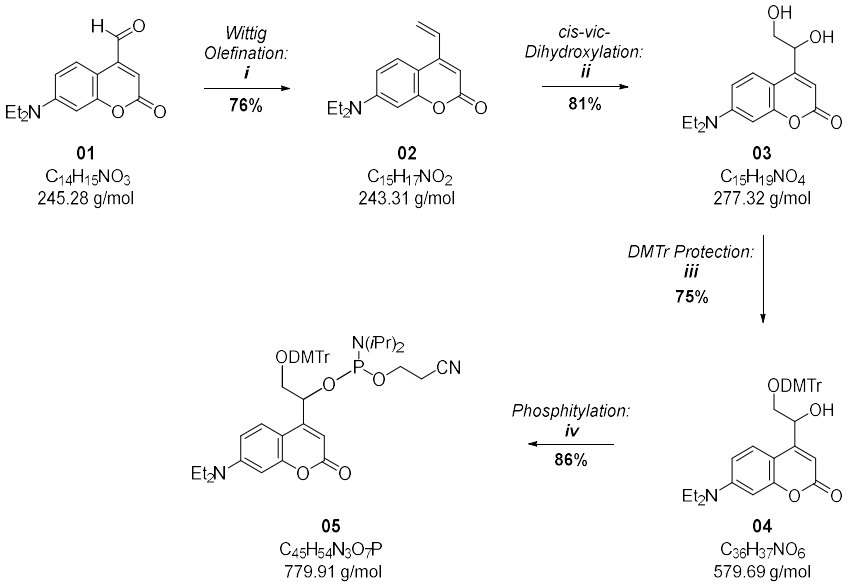

Figure 4.7. Synthesis of 2-(bis(4-methoxyphenyl)(phenyl)methoxy)-1-(7-(diethylamino)-2-oxo-2H-chromen-4-yl)ethyl (2-cyanoethyl) diisopropylphosphoramidite (05). **i.)** KOtBu, Ph_3PMeBr, THF, r.t., overnight; **ii.)** $K_2Os_4*2H_2O$, NMO, in $tBuOH/H_2O$, r.t., overnight; **iii.)** DMT-Cl, in pyridine, 24 h; **iv.)** $CEO(iPr_2)NPCl$, DIPEA, in DCM, r.t., 2 h.

7-(diethylamino)-4-vinyl-2H-chromen-2-one (02)

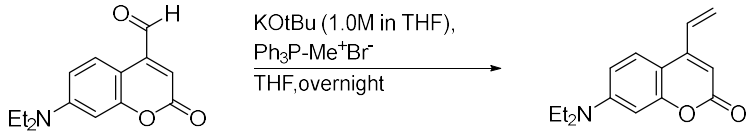

01
$C_{14}H_{15}NO_3$
245.28 g/mol

02
$C_{15}H_{17}NO_2$
243.31 g/mol

The reaction was performed under inert conditions.

Methyltriphenylphosphonium bromide (4.37 g, 12.2 mmol, 1.0 eq.) was suspended in dry THF (90 mL) and stirred for 1 h. KOtBu (1 M in THF, 13.4 mL, 13.4 mmol, 1.1 eq.) was added dropwise at 0 °C and the mixture was stirred first at 0 °C for 30 min then at room temperature for 1 h. A premixed solution of **01** (3.00 g, 12.2 mmol, 1.0 eq.) in dry THF (12 mL) was added dropwise over ca. 1.5 h at −78 °C using a transferring cannula. The reaction mixture was stirred first at −78 °C for 4 h, then allowing to reach room temperature slowly overnight. After the solvent was removed under reduced pressure, the residue was suspended in DCM (100 mL) and aq. sat. $NaHCO_3$ (75 mL). After phase separation, the aqueous layer was extracted with DCM (3 × 100 mL), the combined organic layers were dried over Na_2SO_4 and concentrated under recued pressure. The residue was purified by flash chromatography (silica-gel, dry load, CH:EA 5:1) to obtain the title compound **02** (2.27 g, 9.33 mmol, 76 %) as a brown oil.

Analytical data are consistent with those reported in the literature.[47]

Note: The cooling towards -78 °C is crucial for this reaction.

R_f = 0.35 (silica-gel, CH:EA = 5:1)

^{1}H-NMR (300 MHz, DMSO-d_6, δ/ppm): 7.63 (d, *J* = 9.1 Hz, 1H), 7.13 (ddd, *J* = 17.2, 11.1, 0.7 Hz, 1H), 6.69 (dd, *J* = 9.1, 2.6 Hz, 1H), 6.53 (d, J = 2.6 Hz, 1H), 6.15 (s, 1H), 6.12 (dd, *J* = 17.5, 1.1 Hz, 1H), 5.70 (dd, *J* = 11.0, 1.1 Hz, 1H), 3.43 (q, *J* = 7.0 Hz, 4H), 1.12 (t, *J* = 6.9 Hz, 6H).

2-(bis(4-methoxyphenyl)(phenyl)methoxy)-1-(7-(diethylamino)-2-oxo-2H-chromen-4-yl)ethyl (2-cyanoethyl) diisopropylphosphoramidite (05)

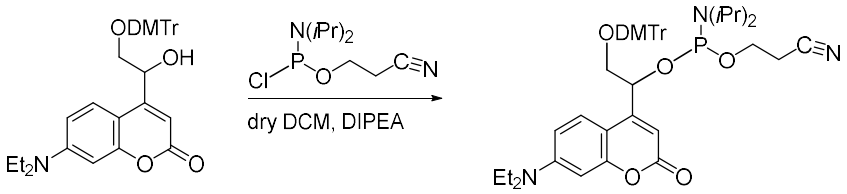

04
$C_{36}H_{37}NO_6$
579.69 g/mol

05
$C_{45}H_{54}N_3O_7P$
779.91 g/mol

Similar to a reported procedure from Weyel.[47]

The reaction was performed under inert conditions.

Dry DIPEA (0.19 mL, 145 mg, 1.1 mmol, 2.6 eq.) was added to a solution of **04** (250 mg, 0.43 mmol, 1.0 eq.) in dry DCM (6 mL). Afterwards, CEO(iPr_2)NPCl (0.13 mL, 142 mg, 0.60 mmol, 1.4 eq.) was added and it was stirred at r.t. for 2 h. The solvent was removed under reduced pressure and the resulting residue was directly purified by flash chromatography (silica-gel, dry load, CH:EA = 2:1). The title compound was obtained as a yellow foam (**05**, 292 mg, 0.37 mmol, 86%). LC-MS- and NMR-analysis revealed the formation of both diastereomers.

R_f = 0.42 (diastereomer 1) and 0.31 (diastereomer 2) (silica gel, CH:EA = 2:1)

^{1}H-NMR (400 MHz, $CDCl_3$,**Figure 4.8**, δ/ppm): 7.46 – 7.35 (m, 2H), 7.34 – 7.12 (m, 8H), 6.82 – 6.70 (m, 4H), 6.51 – 6.40 (m, 2H), 6.23 – 6.14 (m, 1H), 5.16 (ddd, J = 17.2, 8.8, 4.8 Hz, 1H), 3.98 – 3.80 (m, 1H), 3.80 – 3.75 (m, 6H), 3.72 – 3.53 (m, 3H), 3.48 (m_c, 1H), 3.44 – 3.35 (m, 4H), 3.30 (m_c, 1H), 2.55 (td, J = 6.5, 1.6 Hz, 1H), 2.47 (td, J = 6.5, 2.3 Hz, 1H), 1.23 – 1.15 (m, 15H), 1.03 (m_c, 3H). **^{31}P-NMR** (162 MHz, $CDCl_3$,**Figure 4.9**, δ/ppm): 150.1 (1P), 149.9 (1P).

HRMS (ESI$^+$) m/z for $[C_{45}H_{55}O_7N_3P]^+$: calcd. 780.3772, found 780.3771.

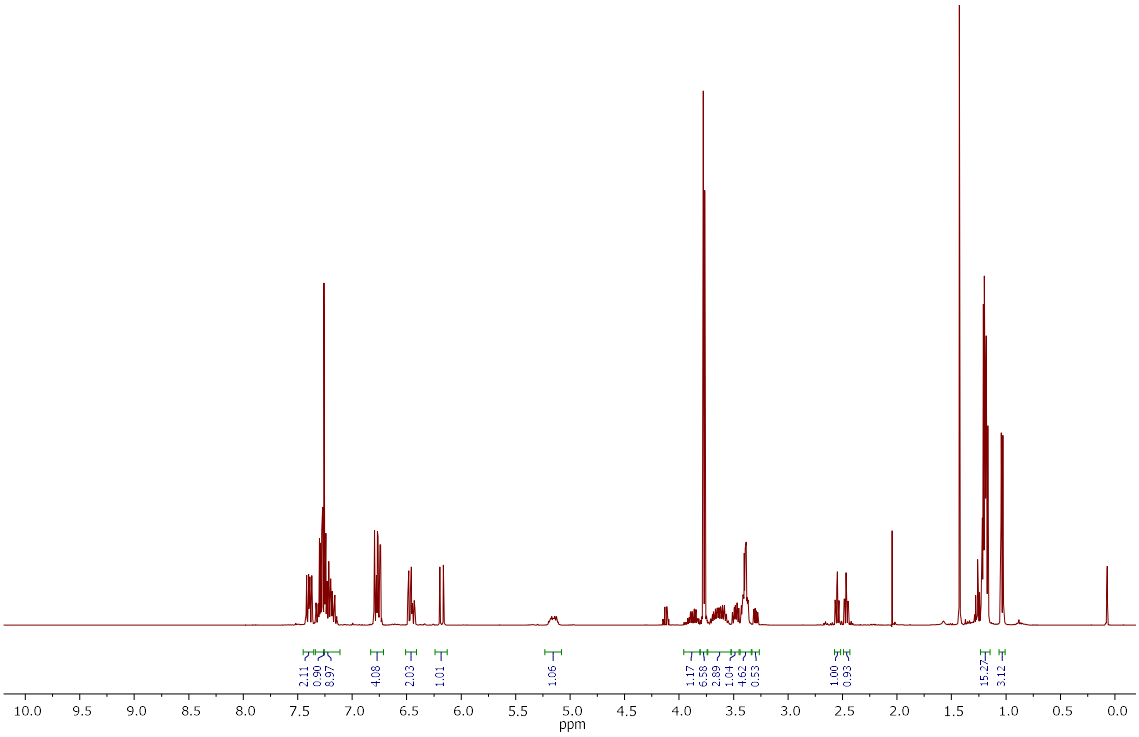

Figure 4.8. **^{1}H-NMR-spectrum** (400 MHz) of compound **05**, measured in $CDCl_3$ at 298 K.

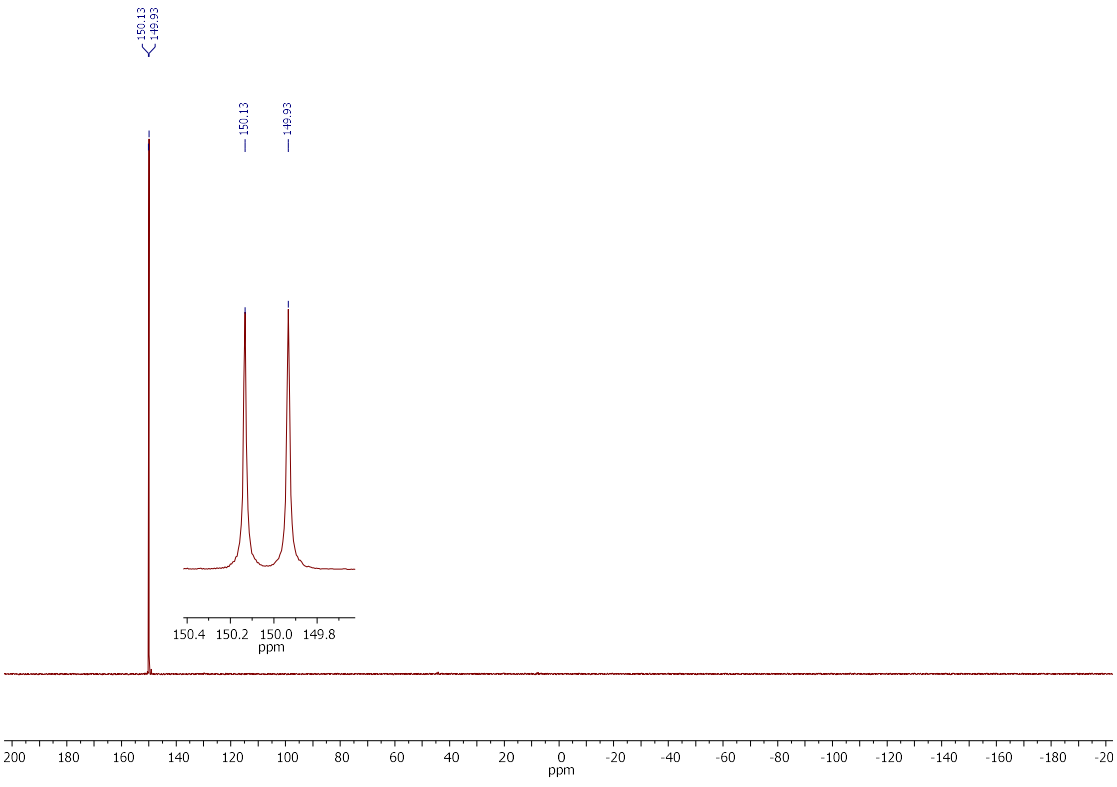

Figure 4.9. **^{31}P-NMR-spectrum** (162 MHz) of compound **05**, measured in $CDCl_3$ at 298 K.

StarPEG-DNA hydrogel preparation

StarPEG-A_{20} and synthesized hairpin and linker-DNA were dissolved separately at desired concentration in a 25 mM Diphosphate EDTA buffer + 100 mM NaCl + 25 mM MgCl2 (pH = 7.9). The DNA concentration in the starPEG-A_{20} conjugate and in the linker DNA was determined by UV-Vis spectroscopy. StarPEG-DNA hydrogels were hybridized by mixing equimolar quantities of starPEG-A_{20} and linker-DNA in the same buffer. The sample was heated up to 70 °C for about 15 min and cooled to room temperature at about 1 °C/min. Samples were kept in the fridge at 4 °C until use. The oligonucleotide sequences of the DNA Linkers are in **Table 4.1**.

4.6 Supplementary information

DNA Linkers

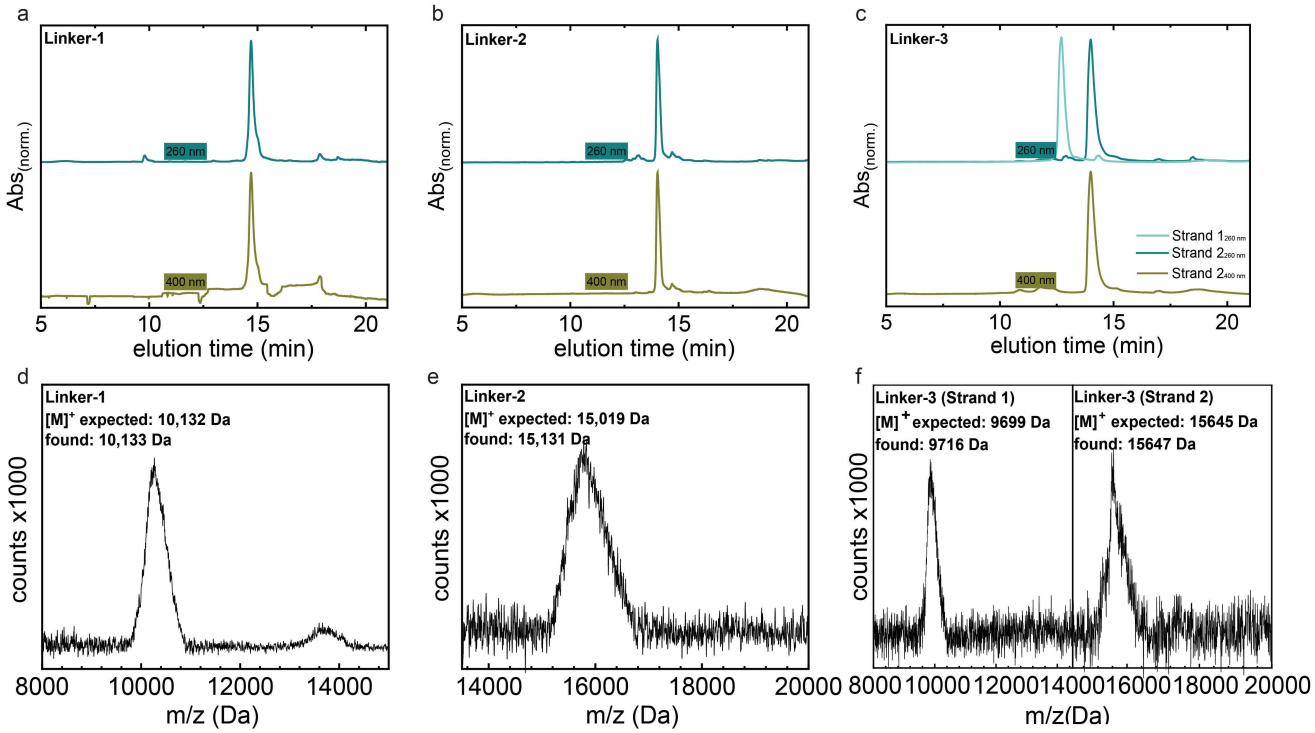

Figure 4.10. Ananlysis of snythesized DNA linkers. (a - c) Analytical HPLC chromatograms of the DNA linker strands after deprotection and preparative HPLC purification. DNA specific absorbance at 260nm (top) and DEACM specific absrobance at 400 nm (botoom). **(d – f)** MALDI-TOF analysis of synthesized DNA linkers.

Rheological characterization of Linker-1

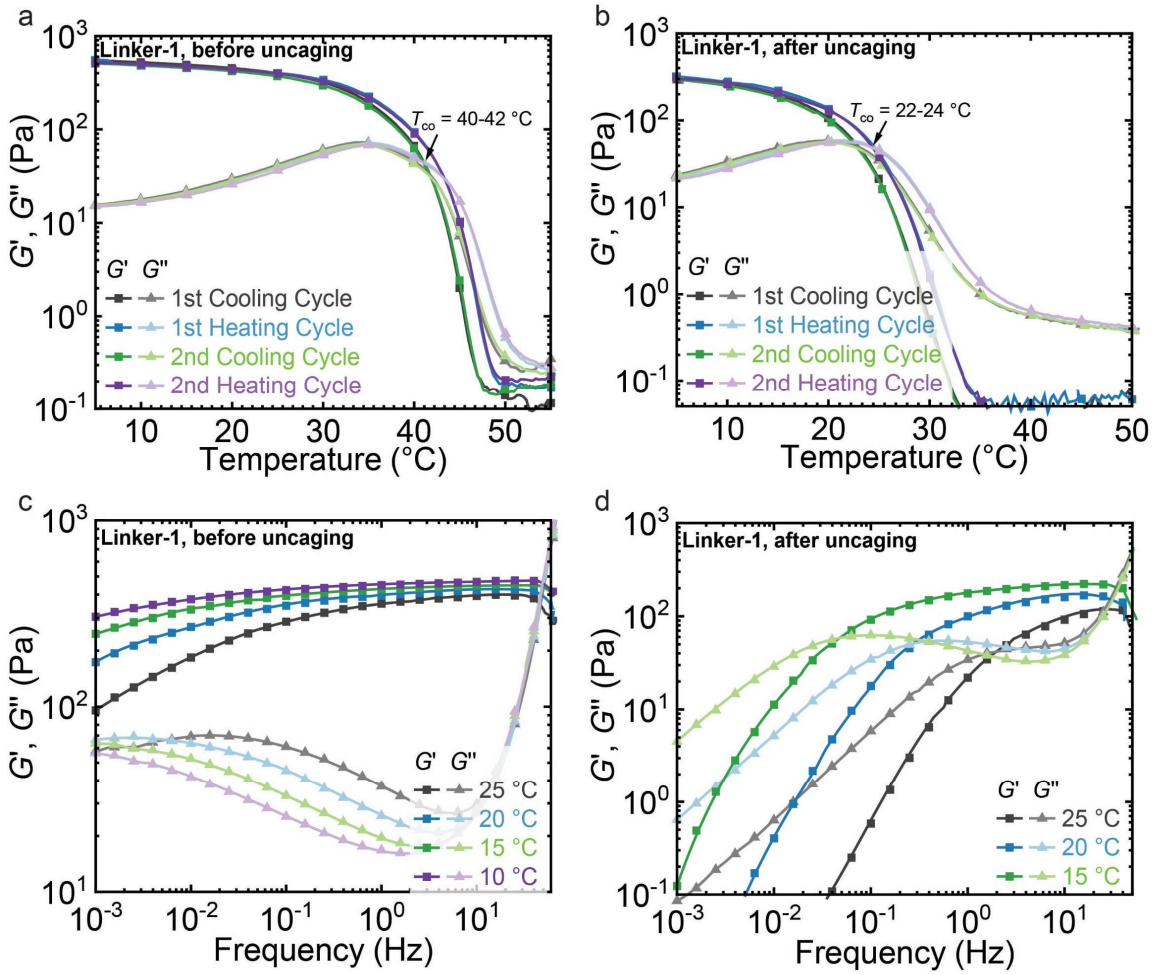

Figure 4.11. Rheological characterization of Linker-1. Repeated Temperature sweep cycles (f = 1 Hz, γ = 6%, 5-50 °C) of Linker-1 (a) Before uncaging and **(b)** After uncaging. **Frequency sweeps (f = 0.001-100 Hz, γ = 1%) of Linker-1 at different temperatures. (c)** Before uncaging and **(d)** After uncaging.

Rheological characterization of Linker-2

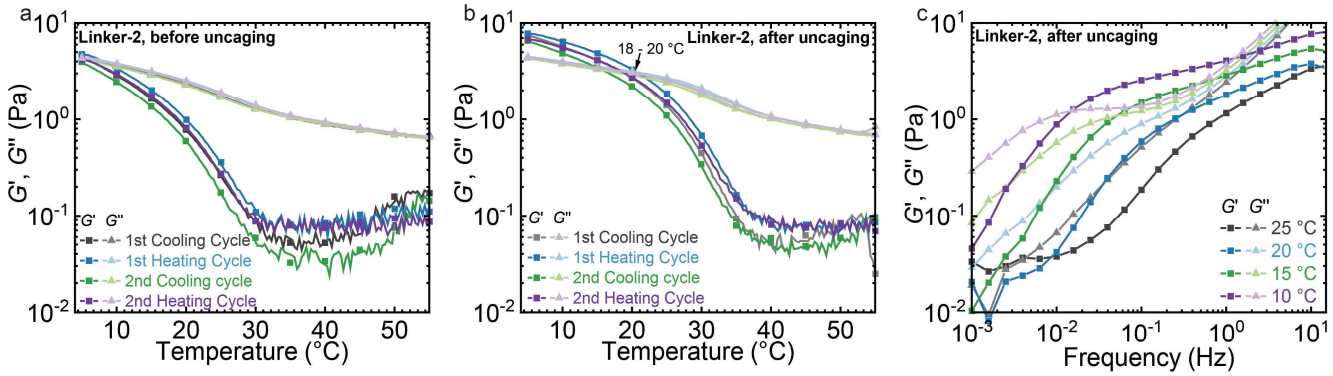

Figure 4.12. Rheological characterization of Linker-2. Repeated Temperature sweep cycles (*f* = 1 Hz, *γ* = 6%, (5-50) °C) of Linker-2 (a) Before uncaging and **(b)** After uncaging. **Frequency sweeps (*f* = (0.001-100) Hz, *γ* = 1%) of Linker-2 at different temperatures. (c)** After uncaging.

Rheological characterization of Linker-3

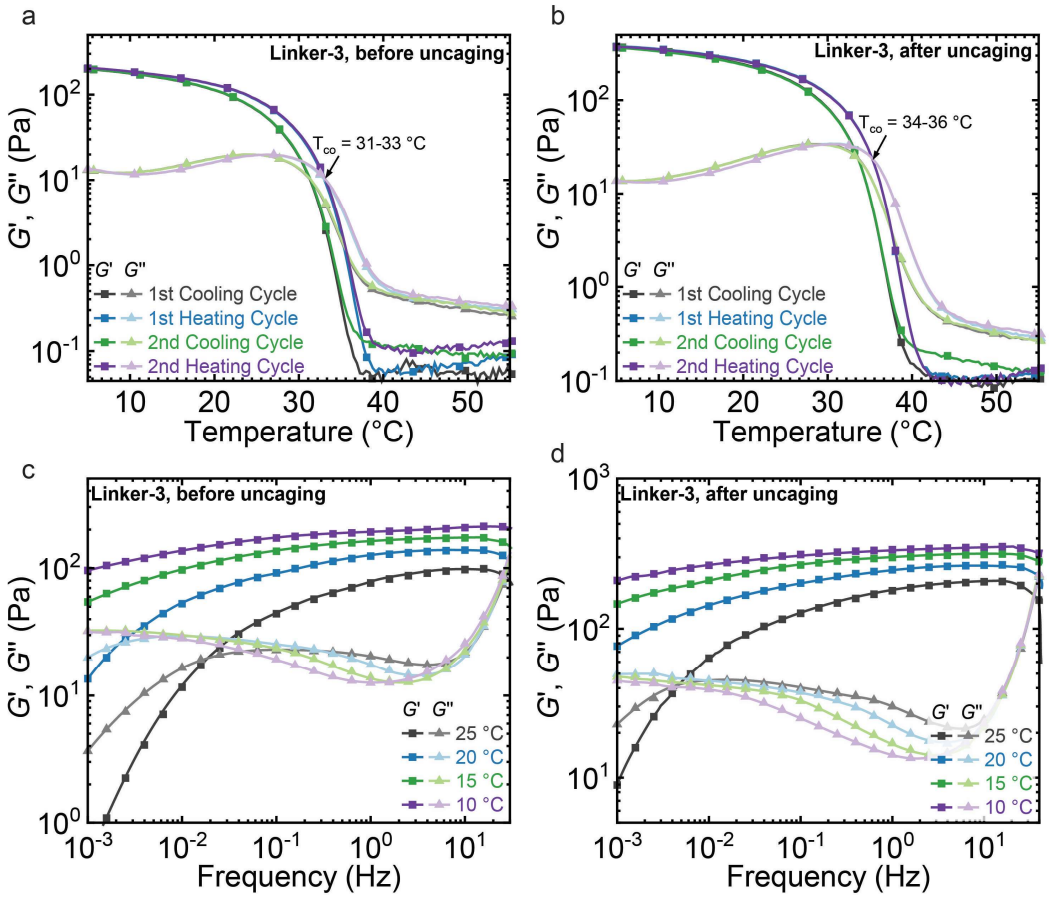

Figure 4.13. Rheological characterization of Linker-3. Repeated Temperature sweep cycles (*f* = 1 Hz, *γ* = 6%, (5-55) °C) of Linker-3 (a) Before uncaging and **(b)** After uncaging. **Frequency sweeps (*f* = (0.001-100) Hz, *γ* = 1%) of Linker-1 at different temperatures. (c)** Before uncaging and **(d)** After uncaging.

4.7 References

(1) Merindol, R.; Walther, A., Materials Learning from Life: Concepts for Active, Adaptive and Autonomous Molecular Systems. *Chemical Society Reviews* **2017,** *46*, 5588-5619.
(2) Walther, A., From Responsive to Adaptive and Interactive Materials and Materials Systems: A Roadmap. *Advanced Materials* **2020,** *32*, 1905111.
(3) Kostiainen, M. A.; Priimagi, A.; Timonen, J. V.; Ras, R. H.; Sammalkorpi, M.; Penttilä, M.; Ikkala, O.; Linder, M. B., Materials Inspired by Living Functions. *Advanced Functional Materials* **2024**, 2402097.
(4) He, X.; Aizenberg, M.; Kuksenok, O.; Zarzar, L. D.; Shastri, A.; Balazs, A. C.; Aizenberg, J., Synthetic Homeostatic Materials with Chemo-Mechano-Chemical Self-Regulation. *Nature* **2012,** *487*, 214-218.
(5) Giuseppone, N., Toward Self-Constructing Materials: A Systems Chemistry Approach. *Accounts of chemical research* **2012,** *45*, 2178-2188.
(6) Tang, T.-C.; An, B.; Huang, Y.; Vasikaran, S.; Wang, Y.; Jiang, X.; Lu, T. K.; Zhong, C., Materials Design by Synthetic Biology. *Nature Reviews Materials* **2021,** *6*, 332-350.
(7) Wagner, H. J.; Engesser, R.; Ermes, K.; Geraths, C.; Timmer, J.; Weber, W., Synthetic Biology-Inspired Design of Signal-Amplifying Materials Systems. *Materials Today* **2019,** *22*, 25-34.
(8) Stuart, M. A. C.; Huck, W. T.; Genzer, J.; Müller, M.; Ober, C.; Stamm, M.; Sukhorukov, G. B.; Szleifer, I.; Tsukruk, V. V.; Urban, M., Emerging Applications of Stimuli-Responsive Polymer Materials. *Nature materials* **2010,** *9*, 101-113.
(9) Bril, M.; Fredrich, S.; Kurniawan, N. A., Stimuli-Responsive Materials: A Smart Way to Study Dynamic Cell Responses. *Smart Materials in Medicine* **2022,** *3*, 257-273.
(10) Campanella, A.; Döhler, D.; Binder, W. H., Self‐Healing in Supramolecular Polymers. *Macromolecular Rapid Communications* **2018,** *39*, 1700739.
(11) Modi, S.; MG, S.; Goswami, D.; Gupta, G. D.; Mayor, S.; Krishnan, Y., A DNA Nanomachine That Maps Spatial and Temporal Ph Changes inside Living Cells. *Nature nanotechnology* **2009,** *4*, 325-330.
(12) Yan, Y.; Ding, H., Ph-Responsive Nanoparticles for Cancer Immunotherapy: A Brief Review. *Nanomaterials* **2020,** *10*, 1613.
(13) Heuser, T.; Weyandt, E.; Walther, A., Biocatalytic Feedback-Driven Temporal Programming of Self-Regulating Peptide Hydrogels (Angew. Chem. Int. Ed. 45/2015). *Angewandte Chemie International Edition* **2015,** *54*.
(14) Chen, H.; Zhang, H.; Pan, J.; Cha, T.-G.; Li, S.; Andréasson, J.; Choi, J. H., Dynamic and Progressive Control of DNA Origami Conformation by Modulating DNA Helicity with Chemical Adducts. *ACS Nano* **2016,** *10*, 4989-4996.
(15) Banerjee, A.; Bhatia, D.; Saminathan, A.; Chakraborty, S.; Kar, S.; Krishnan, Y., Controlled Release of Encapsulated Cargo from a DNA Icosahedron Using a Chemical Trigger. *Angew. Chem. Int. Ed* **2013,** *52*, 6854-6857.
(16) Xu, W.; Deng, R.; Wang, L.; Li, J., Multiresponsive Rolling Circle Amplification for DNA Logic Gates Mediated by Endonuclease. *Analytical chemistry* **2014,** *86*, 7813-7818.
(17) Billah, S. M. R.; Mondal, M. I. H.; Somoal, S. H.; Pervez, M. N.; Haque, M. O., Enzyme-Responsive Hydrogels. *Cellulose-Based Superabsorbent Hydrogels. Polymers and Polymeric Composites: A Reference Series* **2018**.
(18) Gerling, T.; Wagenbauer, K. F.; Neuner, A. M.; Dietz, H., Dynamic DNA Devices and Assemblies Formed by Shape-Complementary, Non–Base Pairing 3d Components. *Science* **2015,** *347*, 1446-1452.
(19) Yu, Z.; Li, N.; Zheng, P.; Pan, W.; Tang, B., Temperature-Responsive DNA-Gated Nanocarriers for Intracellular Controlled Release. *Chemical communications* **2014,** *50*, 3494-3497.
(20) Lubbe, A. S.; Szymanski, W.; Feringa, B. L., Recent Developments in Reversible Photoregulation of Oligonucleotide Structure and Function. *Chemical Society Reviews* **2017,** *46*, 1052-1079.
(21) Phillips, J. A.; Liu, H.; O'Donoghue, M. B.; Xiong, X.; Wang, R.; You, M.; Sefah, K.; Tan, W., Using Azobenzene Incorporated DNA Aptamers to Probe Molecular Binding Interactions. *Bioconjugate chemistry* **2011,** *22*, 282-288.
(22) Khizar, S.; Zine, N.; Errachid, A.; Elaissari, A., Introduction to Stimuli-Responsive Materials and Their Biomedical Applications. *Stimuli-Responsive Materials for Biomedical Applications* **2023**, 1-30.
(23) Szymanski, W.; Beierle, J. M.; Kistemaker, H. A.; Velema, W. A.; Feringa, B. L., Reversible Photocontrol of Biological Systems by the Incorporation of Molecular Photoswitches. *Chemical reviews* **2013,** *113*, 6114-6178.
(24) Brieke, C.; Rohrbach, F.; Gottschalk, A.; Mayer, G.; Heckel, A., Light‐Controlled Tools. *Angewandte Chemie International Edition* **2012,** *51*, 8446-8476.

(25) Major, G. S.; Joukhdar, H.; Choi, Y. S.; Rnjak-Kovacina, J.; Wise, S. G.; Ju, L. A.; Cox, T. R.; Xu, C.; Yeo, G. C.; Young, J. L., Photochemistry as a Tool for Dynamic Modulation of Hydrogel Mechanics. *Cell Reports Physical Science* **2025,** *6*.
(26) Xavier, P. L.; Chandrasekaran, A. R., DNA-Based Construction at the Nanoscale: Emerging Trends and Applications. *Nanotechnology* **2018,** *29*, 062001.
(27) Liu, J.; Ding, B., Stimuli-Responsive DNA Nanostructures for Biomedical Applications. *Handbook of Chemical Biology of Nucleic Acids* **2022**, 1-28.
(28) Lubbe, A. S.; Liu, Q.; Smith, S. J.; De Vries, J. W.; Kistemaker, J. C.; De Vries, A. H.; Faustino, I.; Meng, Z.; Szymanski, W.; Herrmann, A., Photoswitching of DNA Hybridization Using a Molecular Motor. *Journal of the American Chemical Society* **2018,** *140*, 5069-5076.
(29) Suzuki, Y.; Endo, M.; Yang, Y.; Sugiyama, H., Dynamic Assembly/Disassembly Processes of Photoresponsive DNA Origami Nanostructures Directly Visualized on a Lipid Membrane Surface. *Journal of the American Chemical Society* **2014,** *136*, 1714-1717.
(30) Liang, X.; Nishioka, H.; Takenaka, N.; Asanuma, H., A DNA Nanomachine Powered by Light Irradiation. *ChemBioChem* **2008,** *9* (5), 702-705.
(31) Wang, C.; Fadeev, M.; Zhang, J.; Vázquez-González, M.; Davidson-Rozenfeld, G.; Tian, H.; Willner, I., Shape-Memory and Self-Healing Functions of DNA-Based Carboxymethyl Cellulose Hydrogels Driven by Chemical or Light Triggers. *Chemical science* **2018,** *9*, 7145-7152.
(32) Tam, D. Y.; Zhuang, X.; Wong, S. W.; Lo, P. K., Photoresponsive Self‐Assembled DNA Nanomaterials: Design, Working Principles, and Applications. *Small* **2019,** *15*, 1805481.
(33) Huang, F.; Chen, M.; Zhou, Z.; Duan, R.; Xia, F.; Willner, I., Spatiotemporal Patterning of Photoresponsive DNA-Based Hydrogels to Tune Local Cell Responses. *Nature communications* **2021,** *12*, 2364.
(34) Goulet‐Hanssens, A.; Eisenreich, F.; Hecht, S., Enlightening Materials with Photoswitches. *Advanced Materials* **2020,** *32*, 1905966.
(35) Klán, P.; Solomek, T.; Bochet, C. G.; Blanc, A.; Givens, R.; Rubina, M.; Popik, V.; Kostikov, A.; Wirz, J., Photoremovable Protecting Groups in Chemistry and Biology: Reaction Mechanisms and Efficacy. *Chemical reviews* **2013,** *113*, 119-191.
(36) Josa-Culleré, L.; Llebaria, A., In the Search for Photocages Cleavable with Visible Light: An Overview of Recent Advances and Chemical Strategies. . *ChemPhotoChem* **2021,** *5*, 296–314.
(37) Givens, R. S.; Rubina, M.; Wirz, J., Applications of P-Hydroxyphenacyl (P Hp) and Coumarin-4-Ylmethyl Photoremovable Protecting Groups. *Photochemical & Photobiological Sciences* **2012,** *11*, 472-488.
(38) Van Wilderen, L.; Neumann, C.; Rodrigues-Correia, A.; Kern-Michler, D.; Mielke, N.; Reinfelds, M.; Heckel, A.; Bredenbeck, J., Picosecond Activation of the Deacm Photocage Unravelled by Vis-Pump-Ir-Probe Spectroscopy. *Physical Chemistry Chemical Physics* **2017,** *19*, 6487-6496.
(39) Mayer, G.; Heckel, A., Biologically Active Molecules with a "Light Switch". *Angewandte Chemie International Edition* **2006,** *45*, 4900-4921.
(40) Schmidt, R.; Geissler, D.; Hagen, V.; Bendig, J., Mechanism of Photocleavage of (Coumarin-4-Yl) Methyl Esters. *The Journal of Physical Chemistry A* **2007,** *111*, 5768-5774.
(41) Givens, R. S.; Matuszewski, B., Photochemistry of Phosphate Esters: An Efficient Method for the Generation of Electrophiles. *Journal of the American Chemical Society* **1984,** *106*, 6860-6861.
(42) Wang, C.; O'Hagan, M. P.; Li, Z.; Zhang, J.; Ma, X.; Tian, H.; Willner, I., Photoresponsive DNA Materials and Their Applications. *Chemical Society Reviews* **2022,** *51*, 720-760.
(43) Creusen, G.; Akintayo, C. O.; Schumann, K.; Walther, A., Scalable One-Pot-Liquid-Phase Oligonucleotide Synthesis for Model Network Hydrogels. *Journal of the American Chemical Society* **2020,** *142*, 16610-16621.
(44) Akintayo, C. O.; Creusen, G.; Straub, P.; Walther, A., Tunable and Large-Scale Model Network Starpeg-DNA Hydrogels. *Macromolecules* **2021,** *54*, 7125-7133.
(45) Lallemang, M.; Akintayo, C. O.; Wenzel, C.; Chen, W.; Sielaff, L.; Ripp, A.; Jessen, H. J.; Balzer, B. N.; Walther, A.; Hugel, T., Hierarchical Mechanical Transduction of Precision-Engineered DNA Hydrogels with Sacrificial Bonds. *ACS applied materials & interfaces* **2023,** *15*, 59714-59721.
(46) Menge, C.; Heckel, A., Coumarin-Caged Dg for Improved Wavelength-Selective Uncaging of DNA. *Organic letters* **2011,** *13*, 4620-4623.

(47) Weyel, X. M.; Fichte, M. A.; Heckel, A., A Two-Photon-Photocleavable Linker for Triggering Light-Induced Strand Breaks in Oligonucleotides. *ACS chemical biology* **2017,** *12*, 2183-2190.
(48) Weinrich, T.; Gränz, M.; Grünewald, C.; Prisner, T. F.; Göbel, M. W., Synthesis of a Cytidine Phosphoramidite with Protected Nitroxide Spin Label for Epr Experiments with Rna. *European Journal of Organic Chemistry* **2017,** *2017*, 491-496.

5 Synopsis

5.1 Summary and Conclusion

The overarching goal of this thesis was to understand how molecular network connectivity translates to and influences the macroscopic mechanical properties of hydrogels. This work builds primarily on two building blocks: the model starPEG, a synthetic polymer with a defined architecture, and DNA connecting motifs. While pure DNA-based hydrogels are known for their interesting range of properties and promising applications, their use is often limited by challenges in scalability. By combining the dynamic nature of DNA hybridization with starPEG, we created hybrid hydrogels that harness the strengths of both building blocks and demonstrated the correlation between the properties of the DNA connecting motifs and macroscale hydrogel mechanics. The three projects outlined in this thesis show different strategies to expand the design space of starPEG-DNA hydrogels.

Chapter **2** presents a comprehensive investigation into the synthesis and mechanical characterization of starPEG-DNA hydrogels. These hydrogels were synthesized to form quasi-ideal networks with minimal topological defects, crosslinked by divalent DNA linkers. This modular design enabled precise control over crosslinking density and connectivity through programmable Watson-Crick base pairing, overcoming the limitations inherent to randomly crosslinked or heterogeneously structured polymer hydrogels. Consequently, this approach offers a robust strategy for engineering hydrogels with well-defined and reproducible mechanical properties. Furthermore, the OP-LPOS synthesis strategy used to synthesize our starPEG building block allows for the multigram-scale synthesis of these starPEG-DNA hydrogels, directly addressing challenges of scalability and batch consistency. Through the variation of molecular parameters, this chapter establishes a quantitative structure–property relationship that bridges molecular design and macroscopic mechanics. Rheological characterization revealed that the resulting hydrogels exhibit tunable elastic moduli spanning three orders of magnitude, from the low-Pascal to the kilopascal regime, encompassing stiffness ranges relevant to biological mechanosensing. The hydrogels exhibited excellent thermal and mechanical resilience, maintaining their integrity through repeated heating and cooling cycles. After mechanical disruption, they demonstrated rapid self-healing behavior, fully restoring their structure and mechanical properties within approximately four minutes. Moreover, the starPEG-DNA hydrogels

displayed reversible viscoelastic behavior with programmable bond relaxation dynamics and adjustable sol–gel transition temperatures governed by duplex stability and environmental conditions.

Chapter **3** focuses on understanding how precisely engineered molecular mechanisms translate into programmable mechanical responses. Through the strategic use of DNA hairpin loops as sacrificial bonds within the network architecture, these molecular motifs act as force-responsive actuators that unzip under stress, enabling tunable nonlinear viscoelastic behavior across multiple length scales. By combining SMFS with macroscopic rheological characterization, we established a direct quantitative correlation between molecular-level mechanics and the bulk material response. Using AFM-based force extension experiments, the unzipping and rupture forces of individual DNA hairpins were measured, revealing characteristic force thresholds determined by sequence composition and stem length. These data were directly linked to macroscopic observations obtained from oscillatory rheology and uniaxial deformation experiments, demonstrating that parameters such as energy dissipation and yield strain can be systematically modulated through variations in DNA hairpin topology. The resulting hydrogel network is able to withstand large deformations and recover its structure after strain release. This nonlinear mechanical adaptation reflects the presence of hidden internal length scales that contribute to complex, multi-well energy landscapes governing the material's macroscopic resilience.

In Chapter **4** the goal was to enable the rapid and efficient modulation of starPEG-DNA hydrogel properties via light-triggered photo-uncaging. This was achieved by integrating the DEACM photocage into the DNA linker. Upon irradiation, the hydrogels underwent controlled disassembly, softening and stiffening as confirmed by rheological measurements showing distinct shifts in G' and T_{co} within minutes of irradiation. HPLC analysis at 260 nm and 400 nm further confirmed the reproducible kinetics of the photo-uncaging process, which reached completion within approximately 28 minutes. This approach effectively overcomes common limitations in light-responsive DNA materials, such as complex synthesis, photodegradation, and the need for high-intensity light. It provides a straightforward and biocompatible platform for the optical modulation of hydrogel mechanics. The ability to tune network architecture and mechanical strength via a noninvasive external stimulus represents a significant advancement in the development of smart soft materials.

5.2 Outlook

This thesis established a molecularly defined framework for designing programmable starPEG-DNA hydrogels with tunable network connectivity, nonlinear mechanical behavior, and light-responsive control. The findings demonstrate how the intrinsic programmability of DNA can be translated into macroscopic material properties, bridging the gap between bottom-up molecular engineering and functional material performance.

The modular starPEG-DNA platform offers precise control over network topology and mechanical properties, providing a foundation for developing next-generation hydrogels with hierarchical and multi-responsive architectures. Additionally, the successful embedding of DNA hairpin loops as sacrificial bonds verifies the effective transduction of nanoscale molecular unfolding events into macroscopic nonlinear mechanics. Expanding on this principle, future studies should investigate the thermodynamic and kinetic reversibility of these mechanisms under cyclic loading and environmental fluctuations (e.g., temperature, ionic strength, or pH). Furthermore, employing strategies that promote refolding and self-repair would lead to materials that autonomously adapt their stiffness or dissipate energy on demand. Finally, integrating various DNA motifs with differentiated force thresholds could enable the engineering of hydrogels exhibiting graded mechanical responses, optimizing them for sophisticated applications in soft robotics and biomimetic scaffolds.

The integration of DEACM-caged linkers provides a pathway for precise, spatiotemporal control of hydrogel mechanics using light as an external trigger. Future developments should focus on extending activation into visible or near-infrared wavelengths to enhance biocompatibility and allow for deeper tissue penetration. The implementation of reversible photoswitching moieties could unlock further advanced functionalities, particularly for dynamic applications in biosensing and diagnostics.

Overall, this thesis lays the fundamental groundwork for rationally designed, mechano-adaptive soft materials that merge the programmability of DNA with the structural versatility of synthetic polymers. Future research integrating multi-stimuli responsiveness, hierarchical organization, and biological functionality will advance the field toward autonomous materials that emulate Nature.

6 List of Publications

1. Max Lallemang[†] (equal), **Cecilia Oluwadunsin Akintayo[†]** (equal), Christiane Wenzel, Weixiang Chen, Lucca Sielaff, Alexander Ripp, Henning J. Jessen, Bizan N. Balzer, Andreas Walther*, and Thorsten Hugel*, Hierarchical Mechanical Transduction of Precision-Engineered DNA Hydrogels with Sacrificial Bonds. *ACS Applied Materials & Interfaces*, **2023**. DOI: doi.org/10.1021/acsami.3c15135

2. Wei Liu, Avik Samanta, Jie Deng, **Cecilia Oluwadunsin Akintayo**, Andreas Walther*, Mechanistic insights into the phase separation behavior and pathway-directed information exchange in all-DNA droplets. *Angewandte Chemie International Edition,* **2022**. DOI: doi.org/10.1002/ange.202208951

3. **Cecilia Oluwadunsin Akintayo**, Guido Creusen, Paula Straub, and Andreas Walther*, Tunable and large-scale model network starPEG-DNA hydrogels. *Macromolecules*, **2021**. DOI: doi.org/10.1021/acs.macromol.1c00600

4. Guido Creusen, **Cecilia Oluwadunsin Akintayo**, Katja Schumann, and Andreas Walther*, Scalable one-pot-liquid-phase oligonucleotide synthesis for model network hydrogels. *Journal of the American Chemical Society*, **2020**. DOI: doi.org/10.1021/jacs.0c05488

[†]These authors contributed equally. *Corresponding author(s)

7 Acknowledgments

This content has been redacted in accordance with data protection regulations.

8 Statement on AI Use

Large language models (ChatGPT-5) were used for purposes of text improvement, never for text generation.